



University of Kentucky  
UKnowledge

---

University of Kentucky Master's Theses

Graduate School

---

2005

## A FULL SYSTEM CHARACTERIZATION OF THE MEASUREMENT UNCERTAINTY OF A CONDUCTED EMISSIONS MEASUREMENT SYSTEM

Robert A. Menke

*University of Kentucky*, [robertmenke33@yahoo.com](mailto:robertmenke33@yahoo.com)

[Right click to open a feedback form in a new tab to let us know how this document benefits you.](#)

---

### Recommended Citation

Menke, Robert A., "A FULL SYSTEM CHARACTERIZATION OF THE MEASUREMENT UNCERTAINTY OF A CONDUCTED EMISSIONS MEASUREMENT SYSTEM" (2005). *University of Kentucky Master's Theses*. 264. [https://uknowledge.uky.edu/gradschool\\_theses/264](https://uknowledge.uky.edu/gradschool_theses/264)

This Thesis is brought to you for free and open access by the Graduate School at UKnowledge. It has been accepted for inclusion in University of Kentucky Master's Theses by an authorized administrator of UKnowledge. For more information, please contact [UKnowledge@lsv.uky.edu](mailto:UKnowledge@lsv.uky.edu).

## ABSTRACT OF THESIS

### A FULL SYSTEM CHARACTERIZATION OF THE MEASUREMENT UNCERTAINTY OF A CONDUCTED EMISSIONS MEASUREMENT SYSTEM

Electromagnetic compatibility (EMC) standards for an accredited test laboratory require that the measurement uncertainty of the measuring instruments be characterized. The CISPR 16-4 standard gives guidance to the magnitude of this uncertainty, but no method of characterization. This thesis describes a method to perform this characterization on a conducted emissions measurement system, taking advantage of full system analysis techniques to reduce the uncertainty to exceptionally low levels. In addition, a framework is introduced whereby uncertainty can be decomposed into its constituent parts such that the laboratory operator can identify methods to improve the system's performance.

**KEYWORDS:** Electromagnetic Compatibility (EMC), Measurement Uncertainty, Conducted Emissions, Line Impedance Stabilization Network (LISN), CISPR 16-4

Robert A. Menke

November 29<sup>th</sup>, 2005

© Robert A. Menke 2005

A FULL SYSTEM CHARACTERIZATION OF THE MEASUREMENT  
UNCERTAINTY OF A CONDUCTED EMISSIONS MEASUREMENT SYSTEM

By

Robert A. Menke

Dr. William T. Smith

**Director of Thesis**

Dr. YuMing Zhang

**Director of Graduate Studies**

November 29<sup>th</sup>, 2005

## RULES FOR THE USE OF THESES

Unpublished theses submitted for the Master's degree and deposited in the University of Kentucky Library are as a rule open for inspection, but are to be used only with due regard to the rights of the authors. Bibliographical references may be noted, but quotations or summaries of parts may be published only with the permission of the author, and with the usual scholarly acknowledgments.

Extensive copying or publication of the thesis in whole or in part also requires the consent of the Dean of the Graduate School of the University of Kentucky.

A library that borrows this thesis for use by its patrons is expected to secure the signature of each user.

**THESIS**

**Robert A. Menke**

**The Graduate School  
University of Kentucky  
2005**

A FULL SYSTEM CHARACTERIZATION OF THE MEASUREMENT  
UNCERTAINTY OF A CONDUCTED EMISSIONS MEASUREMENT SYSTEM

---

THESIS

---

A thesis submitted in partial fulfillment of the  
requirements for the degree of Master of Science in the  
College of Business and Economics  
at the University of Kentucky

By

Robert A. Menke

Lexington, Kentucky

Director: Dr. William T. Smith, Professor of Electrical Engineering

Lexington, Kentucky

2005

© Robert A. Menke 2005

## ACKNOWLEDGMENTS

The author would like to thank Dr. Keith Hardin of Lexmark International, (Lexington, Kentucky) for his mentorship and technical guidance. The entire staff of the Lexmark International EMC department is also thanked for their training, technical skill, and access to their world-class facilities.

The thesis advisor for this project is Dr. William Smith, University of Kentucky (Lexington, Kentucky). Thanks are given to Dr. Smith for his guidance on this project.

Finally, thanks are due to the author's spouse, Bethany Menke, for making this process possible, and for her continued love and support.

## TABLE OF CONTENTS

TABLE OF CONTENTS .....	iv
LIST OF TABLES.....	vi
LIST OF FIGURES .....	vii
CHAPTER 1: INTRODUCTION .....	1
1.1 Introduction to EMC and Conducted Emissions Testing.....	1
1.2 Requirements for Measurement Uncertainty in EMC Standards .....	2
1.3 The Need for a Well-Defined Method for Determining Conducted Emissions Measurement Uncertainty .....	3
CHAPTER 2: BACKGROUND .....	5
2.1 Conducted Emissions Measurement Setup.....	5
2.2 Artificial Mains Network (AMN) Characteristics .....	9
2.3 Calibration of an AMN .....	13
2.4 Uncertainty Characterizations of EMC Measurements .....	16
2.5 Systematic Error and Corrections of EMC Measurements .....	18
2.6 Determination of Systematic Error, Corrections, and Uncertainty for a Conducted Emissions Measurement System .....	20
CHAPTER 3: LISN CALIBRATION METHOD REFINEMENT .....	25
3.1 Selection of Calibration Method and Circuit Model.....	25
3.2 Low Frequency Calibration Errors .....	26
3.3 High Frequency Calibration Errors .....	28
3.4 Correction for LISN Calibration Systematic Errors .....	41



CHAPTER 4: TEST SETUP FOR TYPE A UNCERTAINTY MEASUREMENT OF A LISN.....	46
4.1 Measurement Setup .....	46
4.2 Coupling Box Design Requirements.....	48
4.3 Simulated and Measured Coupling Box Characteristics.....	52
4.4 Coupling Box Interface with LISN.....	57
CHAPTER 5. UNCERTAINTY MEASUREMENTS .....	60
5.1 Measurement Test Setup .....	60
5.2 Measured Data.....	67
5.3 Computation of Measurement Uncertainty .....	77
5.3.1 Uncertainty of Sinusoidal and Pulsed Signal Sources.....	79
5.3.2 Uncertainty Due to Measuring Instrument Noise Floor.....	81
5.3.3 Uncertainty Due to LISN Input Impedance Mismatch.....	83
5.3.4 Final Calculated Measurement Uncertainty Values.....	85
CHAPTER 6: ANALYSIS AND CONCLUSIONS.....	86
6.1 Dominant Uncertainty Factors.....	86
6.2 Effectiveness of LISN Correction Factors.....	90
6.3 Conclusions.....	95
BIBLIOGRAPHY .....	97
VITA.....	102

## LIST OF TABLES

Table 2.1: Conducted Disturbances from 150 kHz to 30 MHz using a 50-ohm / 50- $\mu$ H AMN.....	17
Table 2.2: Expanded Uncertainties calculated from Table 2.1 .....	22
Table 2.3: Methods for characterizing conducted emissions measurement uncertainty.....	23
Table 3.1: LISN EUT Port L & C Matrices .....	34
Table 5.1: Test Instrumentation Setup for Uncertainty Measurements.....	64
Table 5.2: Measured Standard Deviations of ERR[f] .....	76
Table 5.3: CISPR 16-4 Uncertainty components and their respective measurements.....	77
Table 5.4: Measurement uncertainty due to noise floor (dB) for a given detector .....	82
Table 5.5: Measurement uncertainty due to LISN EUT input impedance mismatch (dB) .....	84
Table 5.6: Final measurement uncertainty values (dB) .....	85
Table 6.1: Uncertainty Factors (dB) for the Quasi-Peak Detector.....	87
Table 6.2: Uncertainty Factors (dB) for the Average Detector .....	88
Table 6.3: Uncertainty Factors (dB) for the Peak Detector .....	89
Table 6.4: Effect of LISN Correction Factors on ERR[f] (dB).....	92

## LIST OF FIGURES

Figure 2.1(a): Tabletop equipment test configuration [15] .....	7
Figure 2.1(b): Floor-standing equipment test configuration [15] .....	7
Figure 2.1(c): Floor-standing and tabletop equipment test configuration [15].....	8
Figure 2.2(a): ANSI C63.4 AMN network designed for 150kHz to 30MHz [16].....	9
Figure 2.2(b): ANSI C63.4 AMN network designed for 9kHz to 30MHz [16].....	10
Figure 2.2(c): CISPR 16 AMN network designed for 150kHz to 30MHz [13].....	10
Figure 2.3(a): ANSI C63.4 AMN input impedance characteristic for 9kHz to 30MHz [16].....	11
Figure 2.3(b): CISPR 16 AMN input impedance characteristic for 150kHz to 30MHz [13].....	11
Figure 2.4: Calculated input impedances of the circuits of Figure 2.2 overlaid with the standards and tolerances of Figure 2.3.....	12
Figure 2.5: ANSI C63.4 AMN insertion loss measurement setup [16] .....	15
Figure 3.1: SPICE circuit describing recommended LISN calibration equivalent circuit.....	26
Figure 3.2: Insertion loss of LISN in dB showing “perceived insertion loss” for frequencies below 1-MHz.....	28
Figure 3.3: (a) NEMA 5-15 plug, (b) NEMA 5-15 outlet, (c) CEE 7/7 plug, (d) CEE 7/7 outlet (all dimensions in millimeters) [23].....	32
Figure 3.4: LISN EUT Port geometries & equipotential electric field lines .....	33

Figure 3.5: SPICE circuit of Figure 3.1 with transmission line inserted at EUT port, representing the characteristics of EUT plugs from Table 3.1 .....	35
Figure 3.6: Three-conductor transmission line problem setup for solving LISN calibration .....	36
Figure 3.7: Transfer function H for worst-case EUT plug (CEE 7/7) .....	39
Figure 3.8: Combined Insertion Loss for worst-case EUT plug (CEE 7/7) .....	40
Figure 3.9: LISN insertion loss calibration using ANSI C63.4 “T” method, using a network analyzer (left), “T” EUT plug fixture (center), and LISN (right) .....	43
Figure 3.10: “T” EUT plug with ideally short leads on LISN side, and fixture compensation standards using EUT receptacle geometry .....	44
Figure 4.1: LISN measurement uncertainty test setup .....	47
Figure 4.2: Coupling Box Schematic .....	50
Figure 4.3(a): Completed coupling box, constructed from Solar 8012 LISN .....	51
Figure 4.3(b): Completed coupling box, showing internal wiring optimized for impedance control .....	52
Figure 4.4: Coupling box impedances for (a) input port and (b) EUT port .....	55
Figure 4.5: Coupling box insertion loss (a) without and (b) with 20dB attenuator .....	56
Figure 4.6: SPICE schematic showing combined coupling box & LISN .....	58
Figure 4.7: Simulated amplitude at LISN measurement port resulting from the schematic of Figure 4.6. The amplitudes shown are based on the test setups that will be described in Chapter 5 .....	59

Figure 5.1: Frequencies measured for the uncertainty experiment. The heavier weighting of the frequency distribution to the lower end of the spectrum reflects typical EUT measurement experience .....	62
Figure 5.2: ERR[f], 220V phase conductor, sinusoidal source, QP .....	68
Figure 5.3: ERR[f], 220V neutral conductor, sinusoidal source, QP .....	68
Figure 5.4: ERR[f], 110V phase conductor, sinusoidal source, QP .....	69
Figure 5.5: ERR[f], 110V neutral conductor, sinusoidal source, QP .....	69
Figure 5.6: ERR[f], 220V phase conductor, pulsed source, QP.....	70
Figure 5.7: ERR[f], 220V neutral conductor, pulsed source, QP.....	70
Figure 5.8: ERR[f], 110V phase conductor, pulsed source, QP.....	71
Figure 5.9: ERR[f], 110V neutral conductor, pulsed source, QP.....	71
Figure 5.10: ERR[f], 220V phase conductor, pulsed source, AVG .....	72
Figure 5.11: ERR[f], 220V neutral conductor, pulsed source, AVG .....	72
Figure 5.12: ERR[f], 110V phase conductor, pulsed source, AVG .....	73
Figure 5.13: ERR[f], 110V neutral conductor, pulsed source, AVG .....	73
Figure 5.14: ERR[f], 220V phase conductor, pulsed source, PK.....	74
Figure 5.15: ERR[f], 220V neutral conductor, pulsed source, PK.....	74
Figure 5.16: ERR[f], 110V phase conductor, pulsed source, PK.....	75
Figure 5.17: ERR[f], 110V neutral conductor, pulsed source, PK.....	75
Figure 5.18: Measurement uncertainty of NRVD wattmeter used to characterize sinusoidal signal source .....	80
Figure 5.19: Measured noise floor for the various test configurations .....	82

Figure 5.20: Uncertainty due to LISN EUT input impedance mismatch (for a current source) .....	84
Figure 6.1: Histogram of ERR[f], sinusoidal source, QP detector .....	93
Figure 6.2: Histogram ERR[f], pulsed source, QP detector .....	93
Figure 6.3: Histogram ERR[f], pulsed source, AVG detector .....	94
Figure 6.4: Histogram of ERR[f], pulsed source, PK detector.....	94

## **CHAPTER 1: INTRODUCTION**

### **1.1 Introduction to EMC and Conducted Emissions Testing**

Electromagnetic Compatibility (EMC) describes the engineering discipline of designing, measuring, and manufacturing digital devices such that their electronic subsystems are “compatible” with the EM environment in which they are used. Motivated by government-mandated standards, EMC regulations are designed to ensure that (1) the emissions levels from a digital device do not exceed a level that could cause interference with the operation of other devices, and (2) a digital device is sufficiently immune to environmental electromagnetic sources to ensure proper operation. (The FCC defines a digital device as “an unintentional radiator (device or system) that generates and uses timing signals or pulses at a rate in excess of 9,000 pulses (cycles) per second and uses digital techniques.” [1])

The focus of this thesis is on the subset of EMC regulations that describe conducted emissions measurements. Again referring to the FCC regulations [1], for a digital device “that is designed to be connected to the public utility (AC) power line, the radio frequency voltage that is conducted back onto the AC power line... shall not exceed the limits” (as defined by standard). In essence, a digital device must comply with these emission limits in order to be sold in a geography where the limits apply (e.g. FCC Part 15 limits are required for a

digital device to be sold in the United States). Because of this requirement, those who design and manufacture digital devices are motivated to meet and maintain compliance with EMC standards. And thus, those who perform the compliance measurements are motivated to provide data that is precise, accurate, and reliable because the ability for the digital device to be sold to customers is dependent on this data.

## **1.2 Requirements for Measurement Uncertainty in EMC Standards**

Measurement uncertainty is generally defined by industry-recognized documents ([3], [4], [5]) as “a parameter, associated with the result of a measurement, that characterizes the dispersion of the values that could reasonably be attributed to the measurand” [3]. Characterization of measurement uncertainty can be required for EMC laboratories, especially when the laboratory is accredited to ISO 9001 [6] and/or ISO/IEC 17025 [7] through an accreditation body (e.g. A2LA or NVLAP in the United States, or UKAS in the United Kingdom). Specifically, for a laboratory performing a calibration, ISO/IEC 17025 states:

*“5.4.6.1 A calibration laboratory, or a testing laboratory performing its own calibrations, shall have and shall apply a procedure to estimate the uncertainty of measurement for all calibrations and types of calibrations.”*



Based on this requirement, historically EMC laboratories determined their uncertainty values by using the methodology of NIS 81 [9] (recently replaced by the UKAS as [10]). However, in May of 2002, a new standard was introduced: CISPR 16-4 “Uncertainty in EMC Measurements” [2]. This document is significant, because although it retains the key concepts of NIS 81, the document was authored by CISPR (the “International Special Committee on Radio Interference”), which is responsible for creating the EMC standards in the European Union. As of the writing of this thesis, CISPR 16-4 is a voluntary standard, but a future revision of EN 55022 [11] could make CISPR 16-4 a mandatory requirement.<sup>1</sup>

### **1.3 The Need for a Well-Defined Method for Determining Conducted Emissions Measurement Uncertainty**

Although CISPR 16-4 gives guidance for the expected values for measurement uncertainty for a “typical” test laboratory, the determination of this value is the responsibility of the lab’s operator. Existing literature has provided either generic measurement uncertainty procedures ([2] – [5]) or component calibration procedures ([13] – [16]), but not uncertainty procedures specifically tailored for conducted emissions measurements. EMC industry research has begun to

---

<sup>1</sup> *The intent of this thesis is to discuss the technical details of the uncertainty characterization process, not to survey all international EMC standards and their adoption of measurement uncertainty requirements. The above references to standards are provided to give context to what is required of a typical EMC test laboratory. For a*

approach this topic (see [26] & [27]), however, these studies still rely heavily on equipment manufacturer's recommended uncertainty values and not direct characterizations of their equipment. This thesis intends to provide a method for directly characterizing a conducted emissions measurement system and thereby determine its true uncertainty value.

To this end, this thesis is divided into the following chapters: Chapter 2 gives a description of the test instrumentation used to perform conducted emissions measurements, defines measurement uncertainty as it applies to these measurements, and identifies possible sources of uncertainty. Chapter 3 describes the calibration method for a line impedance stabilization network (LISN) and refines it to be suitable for low uncertainty measurements. Chapter 4 describes the design, construction, and use of a device that enables full characterization of a measurement system. Chapter 5 details the data collected using such a device. Finally, Chapter 6 analyzes this data to provide a conclusive demonstration of the conducted emissions measurement system's measurement uncertainty.

© Robert A. Menke 2005

---

*more thorough discussion on the applicability of measurement uncertainty to EMC laboratories, see [8].*

## CHAPTER 2: BACKGROUND

### 2.1 Conducted Emissions Measurement Setup

The measurement of conducted emissions is generally defined by [15], [16] and [29]. These documents describe the equipment, test setup, and procedures required for these measurements. This thesis will specifically look at power line emissions for consumer electronics and computing equipment; these are the radio frequency (RF) voltages measured at the input terminals of the power cord of the equipment under test (EUT) occurring in the frequency range of 9kHz to 30MHz. A conducted emissions test setup consists of the following equipment:

- **Radio Noise Meter:** this device is tunable by frequency and measures RF voltage using peak, quasi-peak, or average detectors, as defined in [13] and [14]. Also referred to as a “receiver” in [15].
- **Impedance Stabilization Network (ISN):** this device provides electrical connections of the EUT with an outside source. The ISN typically provides a well-defined input impedance to its EUT terminals and a measurement port for connection to a radio noise meter.
- **Artificial Mains Network (AMN):** an ISN device specifically used for connecting the EUT to its power source (e.g. 120V-60Hz in North America).
- **Line Impedance Stabilization Network (LISN):** equivalent to AMN. ANSI C63.4 [16] uses the term LISN, and CISPR 22 [15] uses AMN.

- **Associated (or Auxiliary) Equipment (AE):** devices used to exercise the functions of the EUT. AE devices are not the subject of the emissions measurement, and if required, are typically connected to a separate AMN.
- **Other equipment:** this includes RF filters (isolates EUT measurement ports from externally-generated RF signals), coaxial cables & RF relays (connects the measurement devices to the various ISN's), and reference planes (large grounded metal plates defined by [15] or [16] as part of the test setup).

Figure 2.1 shows the configuration of the test equipment as shown in CISPR 22 (ANSI C63.4 figures are similar). Not shown are the AMN connections to the incoming power mains (including its associated RF filters) and AMN measurement port's connections to the measuring radio noise meter. The characteristics of the AMN are discussed in the next chapter.

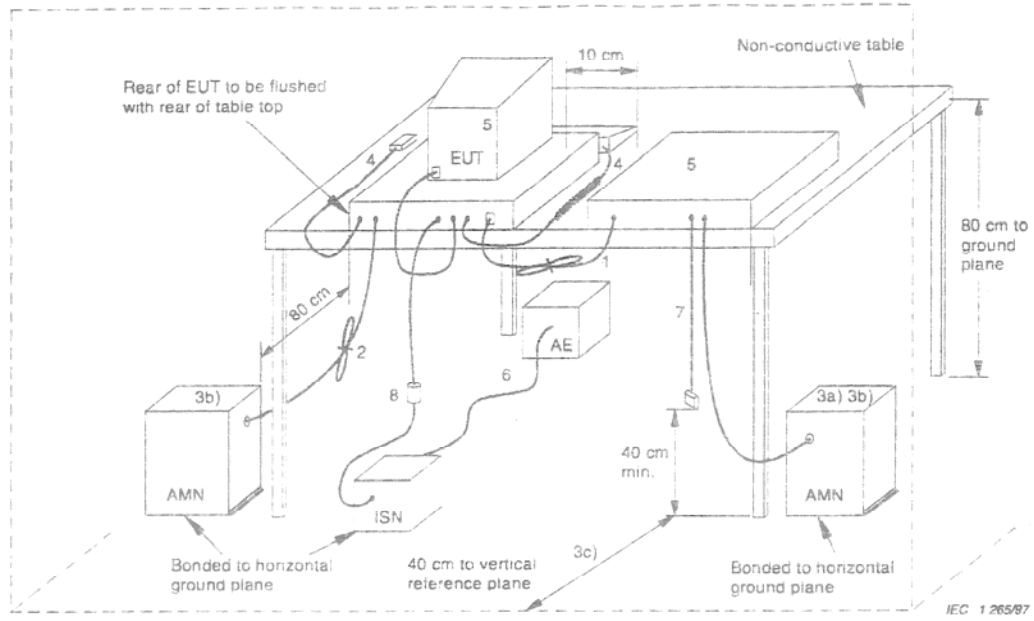


Figure 2.1(a): Tabletop equipment test configuration [15]

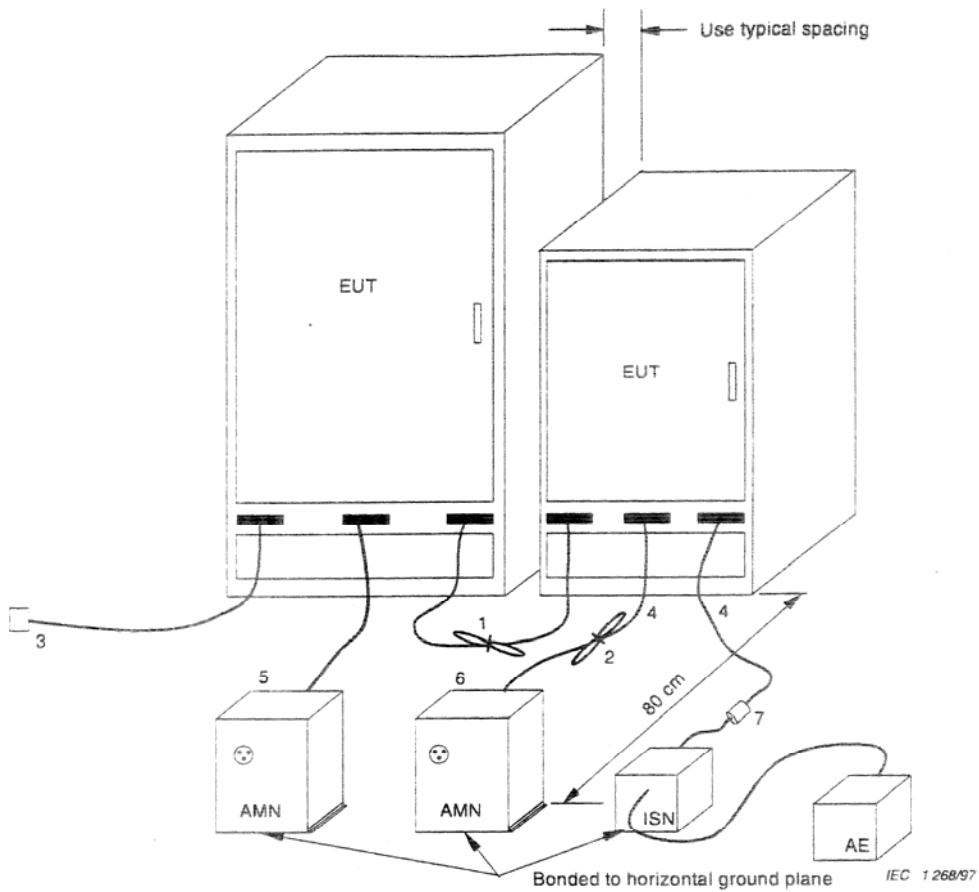


Figure 2.1(b): Floor-standing equipment test configuration [15]

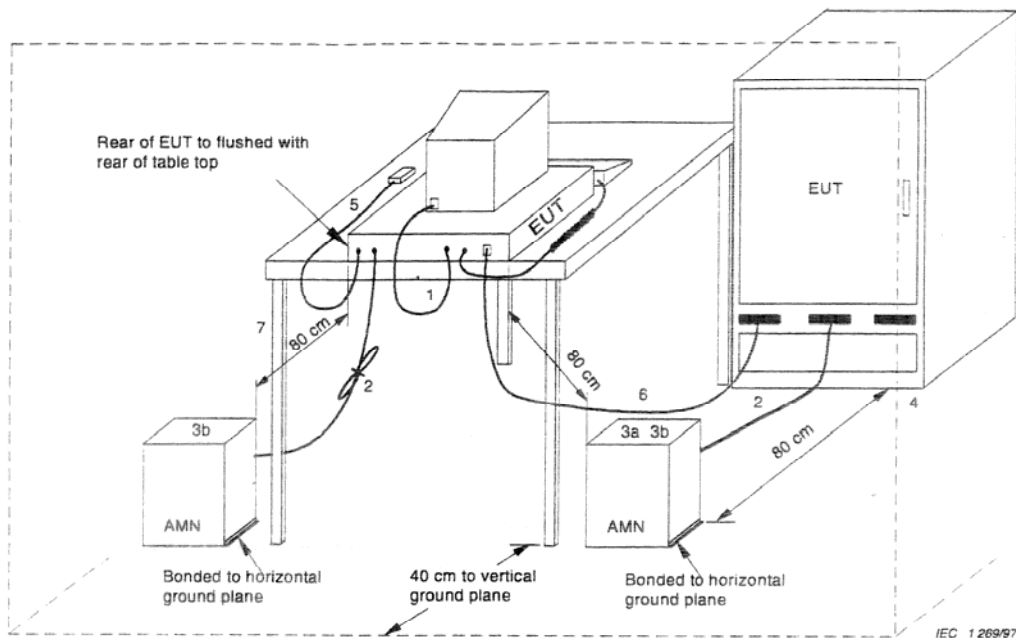
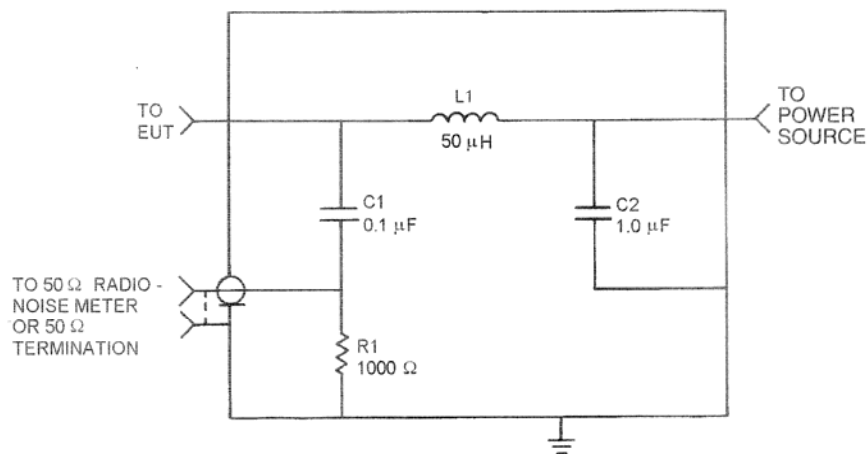


Figure 2.1(c): Floor-standing and tabletop equipment test configuration [15]

Regarding the receiver, it is capable of measuring the incoming signal with the various detectors defined in [13] & [14]. For conducted emissions, there are three detectors of importance: peak, quasi-peak, and average. With the peak detector active, the receiver will display the maximum voltage found at its input over a given sampling interval. The quasi-peak detector employs a signal filter with asymmetric rise and fall times, such that its output depends on the repetition rate of the signal. The average detector's result is based on the time-averaged amplitude of the signal. It is important to note that for a purely sinusoidal signal these three detectors will yield the exact same results. The reason: when tuned to a specific frequency, the receiver will detect a sinusoidal signal as having constant amplitude, thus rendering the differences between the time-responses of the three detectors irrelevant.

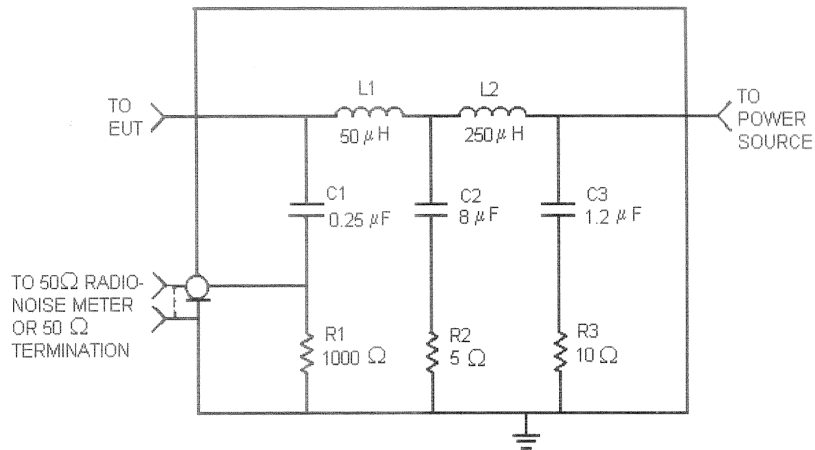
## 2.2 Artificial Mains Network (AMN) Characteristics

For AMN devices, there are three basic circuits used to describe the device's function. These are shown in Figure 2.2. Figure 2.3 shows the input impedance characteristic (defined as the impedance between the EUT port and ground), which is one of the most critical parameters in an AMN's design.



\*IN SOME LISNs, A SERIES RESISTANCE IS INCLUDED IN SERIES WITH CAPACITOR C2, E.G., CISPR PUBLICATION 16 - 1999

Figure 2.2(a): ANSI C63.4 AMN network designed for 150kHz to 30MHz [16]



\* IF CAREFULLY CONSTRUCTED, THIS NETWORK CAN BE USED ABOVE 150kHz TO AS HIGH AS 30 MHz.

Figure 2.2(b): ANSI C63.4 AMN network designed for 9kHz to 30MHz [16]

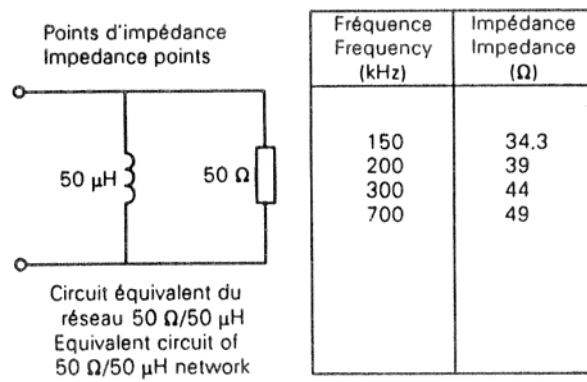


Figure 2.2(c): CISPR 16 AMN network designed for 150kHz to 30MHz [13] (measurement circuit only)



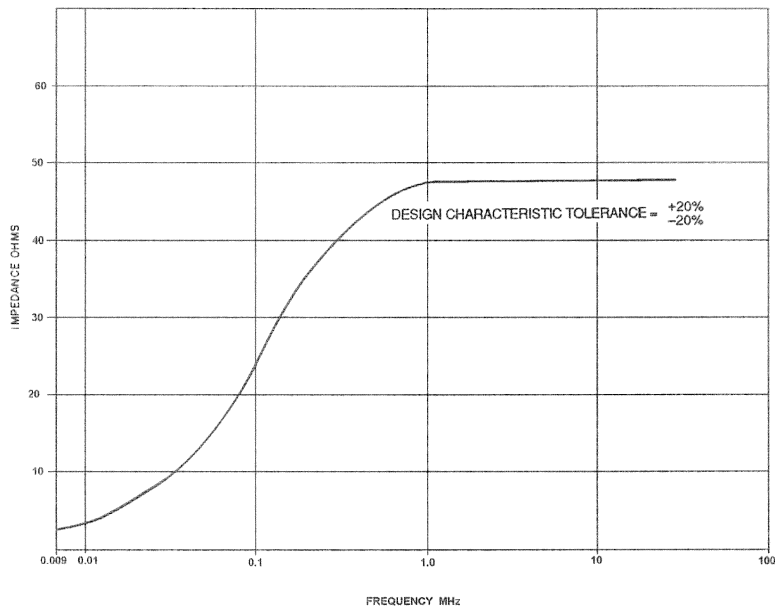


Figure 2.3(a): ANSI C63.4 AMN input impedance characteristic for 9kHz to 30MHz [16]

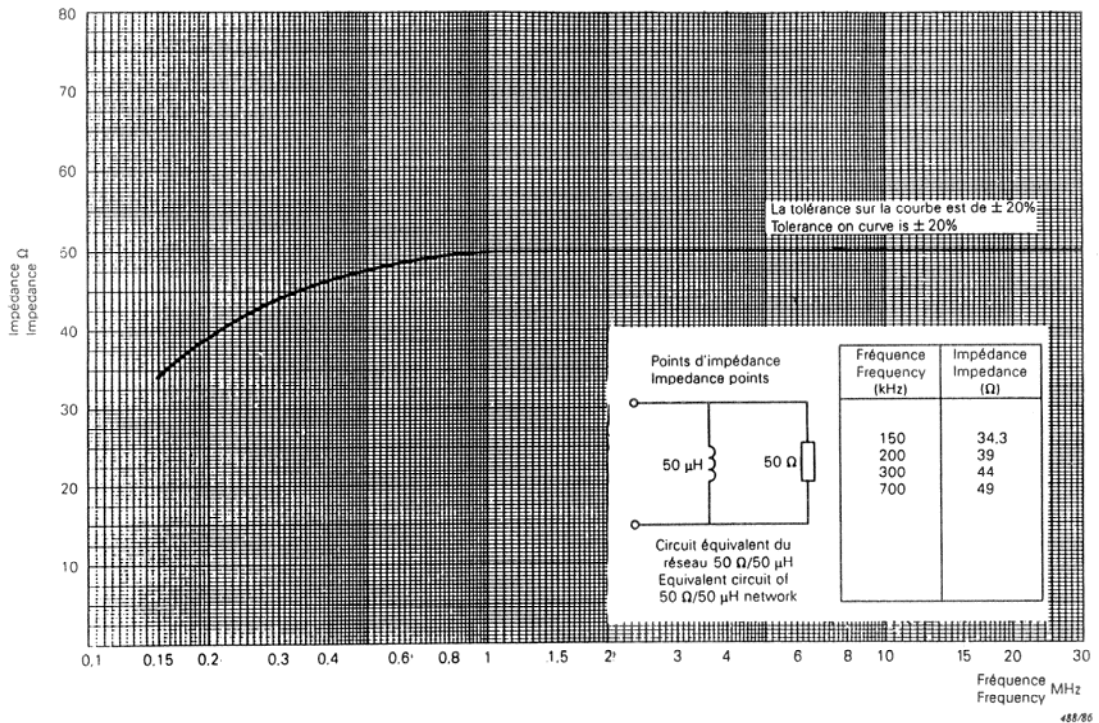


Figure 2.3(b): CISPR 16 AMN input impedance characteristic for 150kHz to 30MHz [13]

Note that Figure 2.3 shows acceptance tolerances of +20 to -20% for both ANSI C63.4 and CISPR 22 applications. If ANSI C63.4 1992 [21] is reviewed, it is found that the upper tolerance is a less strict +30%. This fact is of interest because the circuit of Figure 2.2(a), in its ideal form, does not meet the +20% tolerance requirement at 150kHz. Figure 2.2(c) is also deficient because it lacks a power port. Figure 2.4 shows the input impedances for the three circuits of Figure 2.2 overlaid with the standards and tolerances of Figure 2.3. (Note that Figure 2.3(a) is a hand-drawn graph with no tabulated values. The values of Figure 2.4 were hand-fitted to this graph using transparent overlays by the author.)

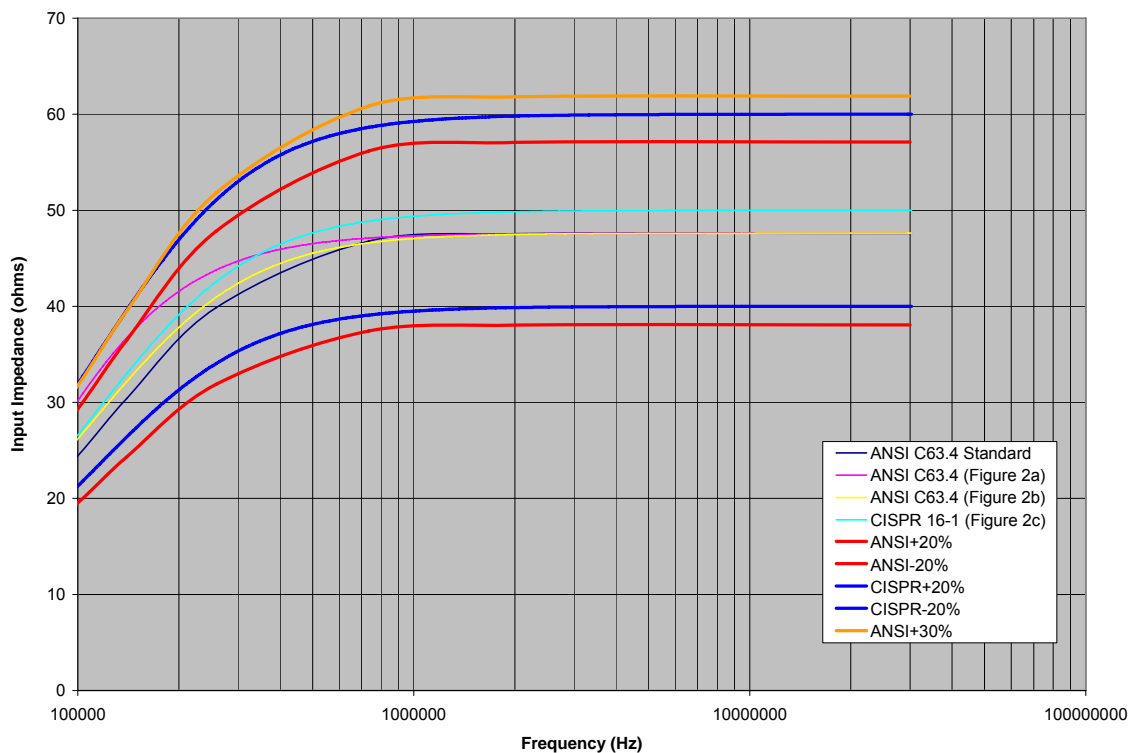


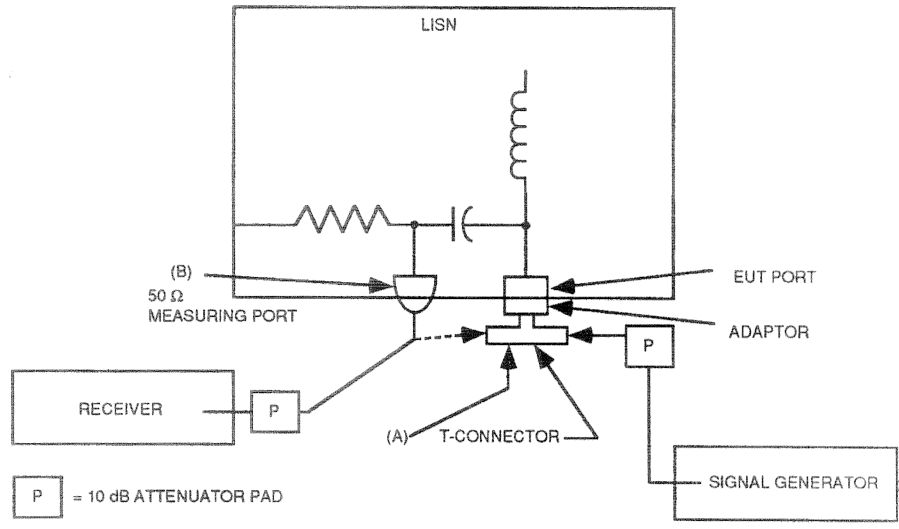
Figure 2.4: Calculated input impedances of the circuits of Figure 2.2 overlaid with the standards and tolerances of Figure 2.3

### **2.3 Calibration of an AMN**

Typically, laboratories accredited to ISO 9001 [6] or ISO/IEC 17025 [7] perform periodic calibration of their measurement equipment. For AMN devices, the interval for this calibration is defined either by standard or by manufacturer's recommendation, but is typically twelve months in industry practice. To perform the AMN calibration, the input impedance (defined as the impedance between the EUT port and ground) is measured as well as the insertion loss (the loss in volts measured between the EUT port and the measurement port). The input impedance must be within the tolerances of Figure 2.3. The insertion loss measured at calibration is used to generate correction factors for the AMN. Also included are the RF coaxial cable losses. These correction factors are then added to the radio noise meter's measurement, thus compensating for losses through the AMN, and yielding a total measurement equal to the actual voltage at the EUT terminals of the AMN. Therefore, it is in the test laboratory's best interest to perform this calibration with high accuracy because any calibration errors or AMN deficiencies will affect the final measurement value.

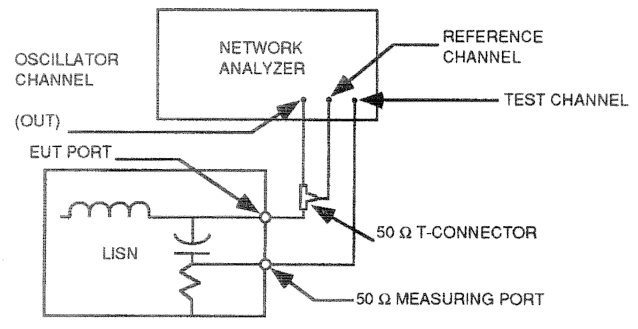
AMN input impedance is measured using a RF impedance analyzer to directly determine the impedance value at the EUT port. This device generates and sweeps a RF signal through the desired frequency range and measures the reflection coefficient ( $S_{11}$ ) to determine the RF impedance. To determine

insertion loss, ANSI C63.4 [16] prescribes the two methods shown in Figure 2.5. The two methods operate on the same principle: a signal is injected into the EUT port of the AMN, and the output is then measured at the AMN's measurement port. The measurement is then repeated with the AMN bypassed (or as in the network analyzer case, both paths are measured simultaneously). The ratio of these two measurements, typically expressed in decibels, is the insertion loss of the AMN with respect to frequency.



NOTE: If VSWR of receiver and signal generator is low, pads may not be needed or may be reduced to 6 dB or 3 dB.

(a) Method Using Receiver and Signal Generator



NOTE: Attenuator pads not used with network analyzer. Place T-connector as close to EUT port as possible. Use same length and type of cables between T-connector and reference channel input and 50 Ω measuring port and test channel input.

(b) Method Using Network Analyzer

Figure 2.5: ANSI C63.4 AMN insertion loss measurement setup [16]

## 2.4 Uncertainty Characterizations of EMC Measurements

Although the exact definition of measurement uncertainty varies between sources, in general, uncertainties are grouped into two categories:

Type A: Uncertainties derived from the statistical analysis of experimental data

Type B: Uncertainties that are not easily measured, and are therefore estimated based on past experience or taken from outside sources (such as manufacturer's specifications or calibration reports)

In general, Type A measurements are preferred because they are an actual measurement of the system's uncertainty, rather than the estimation of a Type B measurement. Also, Type A measurements typically yield a lower total uncertainty for complex measurement systems because Type B calculations must take into account *all possible* influences on uncertainty, whether or not they actually influence the measurement. (For example, the Type B study of CISPR 16-4 Annex A defines quantitative values for each uncertainty component that the standard's authors expected to influence EMC measurements. These are given in Table 2.1 as the total expanded uncertainty, and thus take into account all of the factors of Annex A.)

Table 2.1: Conducted Disturbances from 150 kHz to 30 MHz using a 50-ohm / 50- $\mu$ H AMN

Input Quantity ( $x_i$ )	Uncertainty of $x_i$ in dB	$c_i u(x_i)$ in dB
1. Receiver reading	+/- 0.1	0.10
2. Attenuation: AMN-receiver	+/- 0.1	0.05
3. AMN voltage division factor	+/- 0.2	0.10
4. Receiver corrections:		
a. Sine wave voltage	+/- 1.0	0.50
b. Pulse amplitude response	+/- 1.5	0.87
c. Pulse repetition rate response	+/- 1.5	0.87
d. Noise floor proximity	+/- 0.0	0.00
5. Mismatch: AMN-receiver	+0.7/-0.8	0.53
6. AMN impedance	+2.6/-2.7	1.08

(adapted from CISPR 16-4 Table A.2 [2])

In addition to defining values to uncertainty components, CISPR 16-4 also discusses a change in the method of determining the compliance of a digital device (derived from CISPR 16-4 Section 4.1), as described in (2.1):

$$\text{if } U_{\text{CISPR}} \geq U_{\text{lab}}: \quad (2.1)$$

$X > \text{limit}$ : emission is non-compliant

$X \leq \text{limit}$ : emission is compliant

$$\text{if } U_{\text{CISPR}} < U_{\text{lab}}:$$

$X + (U_{\text{lab}} - U_{\text{CISPR}}) > \text{limit}$ : emission is non-compliant

$X + (U_{\text{lab}} - U_{\text{CISPR}}) \leq \text{limit}$ : emission is compliant

where:

$U_{\text{CISPR}}$ : total expanded uncertainty given in CISPR 16-4 Table 1

$U_{\text{lab}}$ : total expanded uncertainty determined by the laboratory performing the measurement

$X$ : measured emission amplitude (voltage in dB( $\mu$ V), disturbance power in dB(pW), or electric field strength in dB( $\mu$ V/m), as applicable)

limit: maximum allowed emission amplitude defined by the applicable EMC standard

Without applying CISPR 16-4, a device could be measured per its applicable EMC standard and compliance could be determined solely based on comparing the emission's amplitude versus the applicable limit. If CISPR 16-4 is applied,

and if the  $U_{\text{lab}}$  exceeds  $U_{\text{CISPR}}$ , then the emission must be lowered by the difference between these two quantities in order to achieve compliance. Thus, for a test lab with higher uncertainties, a device deemed compliant without the use of CISPR 16-4 could become non-compliant when CISPR 16-4 is applied. This change in the compliance determination process is what has motivated the EMC community to investigate their measurement uncertainty thoroughly.<sup>2</sup>

## 2.5 Systematic Error and Corrections of EMC Measurements

Again referring to CISPR 16-4 [2], section A.5 discusses a measurement ‘correction’, which it defines as a “compensation for a systematic error.” In [4], ‘error’ is defined as “the measurement result minus the *true* value of the measurand.” Whether using the term ‘systematic error’, ‘error’, or ‘bias’[12], all uncertainty texts agree that this error (“if it is significant in size relative to the required accuracy of the measurement”[5]) is assumed to be corrected for before considering the measurement’s uncertainty. In other words, when making a measurement, any known error from a reference value needs to be “zeroed out” of a measurement, and uncertainty is then reported for this corrected value.

---

<sup>2</sup> Although (prior to the publication of CISPR 16-4) the UKAS in [3], [4], & [10] promoted the inability to determine compliance when a measured value is within the uncertainty range of the define limit, this has not been a requirement of laboratory accreditation. In fact, ISO/IEC 17025 Clause 5.4.6.2 states that “in those cases where a well-recognized test method specifies limits to the values of the major sources of uncertainty of measurement and specifies the form of presentation of calculated results, the laboratory is considered to have satisfied this clause by following the test method and reporting instructions.” Again, the applicability of uncertainty techniques to EMC compliance testing is discussed in more detail in [8].



The concept of errors and their corrections is important to EMC measurements for two reasons. First, an uncharacterized error can appear as measurement uncertainty if not properly considered. The reason: the person performing the uncertainty study uses their own engineering judgment to determine which factors are included in a Type A uncertainty experiment and/or Type B uncertainty calculation (example factors are given by CISPR 16-4 Annex A). CISPR 16-4 also states that “a correction that is not known, but is considered to be equally likely to be positive or negative, is taken to be zero.” Thus, if the study incorrectly assumes the influence of a correction, this error will instead be included in the measurement uncertainty.

The second reason for the importance of determining errors and their corrections is that these items contribute to the uncertainty of the final measurement.

“Because true values are never known exactly (else there is no need to make a measurement), corrections are always approximate and a residual error remains”[4]. This means that the experiment that determines the error and the method by which the correction is applied needs to be done in a very accurate manner. Also implicit in this statement is that the ‘true value’ (or ‘reference value’) must be well defined in order to make an accurate error determination.

## 2.6 Determination of Systematic Error, Corrections, and Uncertainty for a Conducted Emissions Measurement System

The focus of this thesis is on the application of measurement uncertainty characterizations to conducted emissions testing. To achieve this, an accurate measurement of systematic errors, corrections, and uncertainty variations must be done. As an introduction, a basic conducted emissions test setup consists of four components:<sup>3</sup>

1. *EUT* (equipment under test), whose emissions are to be measured
2. *AMN* (artificial mains network), which provides the proper impedances between the EUT, public utility power lines, and receiver (defined by [13] & [14])
3. *Receiver* which measures the RF voltage produced by the EUT at the AMN's terminals (defined by [15] & [16])
4. *Interconnect cabling* (typically 50-ohm coaxial cable), which provides the RF signal path between the AMN and receiver (this cabling may also include relays, pre-amplifiers, limiters, or attenuators)

---

<sup>3</sup> In addition to [13]-[16], which define test equipment for the United States and the European Union, standards exist for other geographies around the world. These include [17] & [18] for Australia/New Zealand, [19] for China, and [20] for Japan. In general, these national standards either refer directly to or derive from [13]-[16], especially with respect to test instrumentation and test methods. Therefore, the uncertainty techniques described in this thesis can be considered equally valid for EMC measurements for these geographies as well.

Each of these components have an associated measurement uncertainty. (Note that the uncertainty of the EUT is not considered here because the intent of this thesis is to characterize the measurement system, not the variations of the EUT itself.) Table 2.1 gives a list of the most common factors that influence conducted emissions measurements:

Descriptions of these quantities and the calculation of the uncertainty factors will be discussed in detail in Chapter 5 of this thesis. To begin the analysis of Table 2.1, the total expanded uncertainty is broken into two components in Table 2.2. (Note that the uncertainty due to the interconnect cables is typically small when compared to the AMN's characteristics, so item 2 is assumed solely influenced by the AMN.)

Although varying definitions for measurement uncertainty exist, this thesis assumes the method of CISPR 16-4 [2]. This assigns a near-normal distribution to measurement data, and the expanded uncertainty is the standard deviation for a 95% confidence level ( $k=2$ ). Accuracy is defined as the deviation from the mean value of this near-normal distribution from an ideal or known value.

Table 2.2: Expanded Uncertainties calculated from Table 2.1

Receiver (items 1 & 4a-d)	2.66 dB
AMN (items 2, 3, 5, & 6)	2.42 dB
Total (all items)	3.60 dB
<p>where expanded uncertainty is defined as:  <math display="block">2 u(X) = 2 \text{ SQRT}( \sum_i c_i^2 u^2(x_i) )</math> and:  <math>x_i</math> = uncertainty estimated for each quantity  <math>u(x_i)</math> = standard uncertainty in dB  <math>c_i</math> = sensitivity coefficient</p>	

As seen in Table 2.2, the receiver contributes the highest amount of uncertainty, although the AMN contributes an amount almost as large. Therefore, a reduction of the uncertainty of either of these two items can bring improvement to a conducted test laboratory's total expanded uncertainty.

As previously introduced, Type A uncertainty studies are from direct measurements for the test setup's uncertainties, and Type B are uncertainties estimated or derived from external sources. Table 2.3 describes the methods to be used for both Type A & B studies for receiver, AMN, and total system uncertainty characterizations.

*Table 2.3: Methods for characterizing conducted emissions measurement uncertainty*

<b>Type</b>	<b>Method</b>	<b>Reference</b>
Type A, receiver	Measure statistical variations of receiver readings given the range of input types and operating conditions expected to be measured when the unit is in service.	Included in total system method
Type A, AMN	Measure statistical variations of AMN impedances & attenuation given the range of operating conditions expected to be measured when the unit is in service.	Included in total system method
Type A, total system	Measure statistical variations of entire measurement system (receiver, AMN, and interconnect cables) given the range of input types and operating conditions expected to be measured when the unit is in service.	Chapter 5 (this thesis)
Type B, receiver	Choose a receiver with quality design and construction, low uncertainty reported in manufacturer's data sheet. Choose calibration laboratory with low uncertainty values and high accuracy.	manufacturer's data sheets and calibration laboratory's accreditation certificates
Type B, AMN	Choose an AMN with quality design and construction; one that closely matches the ideal AMN impedances per manufacturer's data sheet. Choose calibration laboratory with low uncertainty values and high accuracy.	manufacturer's data sheets and calibration laboratory's accreditation certificates

Note that for Type A studies, the methods for Type B studies still apply as general guidelines (using quality equipment and calibration services ensure the most accurate uncertainty characterizations). Based on the data in Tables 2.1, 2.2, & 2.3, the following conclusions can now be made about Type A uncertainty studies:

1. Reduction of the expanded uncertainty of the receiver, AMN, or both can reduce the total uncertainty of the measurement system.
2. The variations due to receiver readings are larger than the AMN's variations, thus if the receiver can be characterized to have a lower uncertainty in the conducted measurement test setup, the total expanded uncertainty will be reduced.
3. The AMN impedance is the single largest factor influencing conducted emissions uncertainty, thus the design of the AMN and calibration of this impedance are critical.
4. The mismatch between the AMN & receiver is also a significant factor, thus if their uncertainty can be characterized simultaneously, the total expanded uncertainty may be reduced (this is true because the impedances of these two units, and the resulting mismatch, are not necessarily independent or varying).
5. Systematic errors in the conducted emissions measurement system can be discovered and corrected for through the use of a total system Type A study.

These conclusions are investigated through the experiments and data described in this thesis.

## **CHAPTER 3: LISN CALIBRATION METHOD REFINEMENT**

### **3.1 Selection of Calibration Method and Circuit Model**

As discussed in the previous chapter, it is imperative that all systematic errors be corrected prior to any uncertainty studies. To that end, the author has made careful study of the LISN circuits and their calibration techniques as prescribed by the standard and compared these results to errors observed in actual calibration measurements. Only ANSI C63.4 [16] [21] specifically gives calibration procedures so these are to be considered the preferred method. Similarly, as shown in Figure 2.4 of the previous chapter, the Figure 2.2(b) LISN (9kHz to 30MHz LISN from ANSI C63.4) is the best match to the reference input impedances of CISPR 16 [13] and ANSI C63.4 [16]. Therefore, this LISN will be considered the reference design. An equivalent SPICE circuit of this LISN's calibration is given in Figure 3.1:

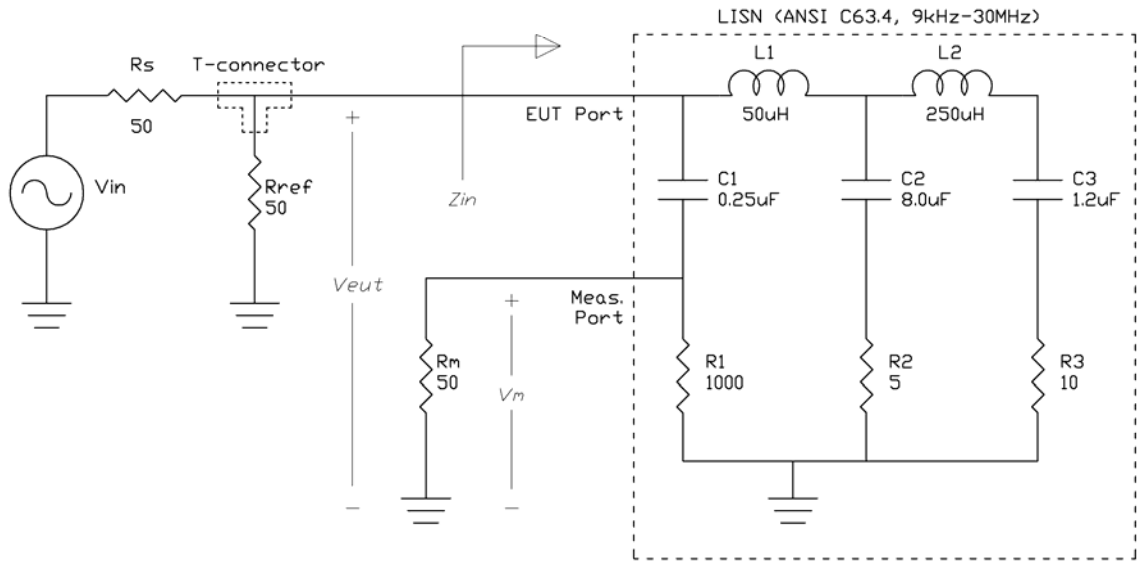


Figure 3.1: SPICE circuit describing recommended LISN calibration equivalent circuit

### 3.2 Low Frequency Calibration Errors

The insertion loss of the LISN is defined as the ratio of  $V_{IN}$  to  $V_{EUT}$  and is measured by comparing the voltage at the reference resistor  $R_{REF}$  with the voltage at the measuring resistor  $R_M$ . When the LISN impedance matches these resistors exactly, i.e. 50-ohms, then the system is perfectly balanced with a voltage ratio of unity. However, referring to the input impedance curves of Figure 2.4, the  $Z_{IN}$  of Figure 3.1 is not constant with respect to frequency. The mismatch caused by this intended impedance curve causes “perceived insertion



loss” in the LISN even if all components are ideally lossless. This loss can be empirically solved for by standard circuit analysis techniques:

$$\begin{aligned}
 V_{EUT} &= V_S - I_S \cdot R_S \\
 V_M &= V_{EUT} - \frac{I_{C1}}{j\omega \cdot C_1} \\
 I_{C1} &= I_M + I_{R1} \\
 I_{C1} &= \frac{V_M}{R_M} + \frac{V_M}{R_1} \\
 \Rightarrow V_M &= V_{EUT} - \frac{V_M}{j\omega \cdot C_1} \cdot \left( \frac{1}{R_M} + \frac{1}{R_1} \right) \\
 \Rightarrow \frac{V_M}{V_{EUT}} &= \left[ 1 + \frac{1}{j\omega \cdot C_1} \cdot \left( \frac{1}{R_M} + \frac{1}{R_1} \right) \right]^{-1} \tag{3.1}
 \end{aligned}$$

$$\text{Insertion Loss} \equiv 20 \cdot \log \left[ \frac{V_M}{V_{EUT}} \right] \quad (\text{in dB})$$

where:  $I_{C1}$  is the current through  $C1$ , defined in the positive  $V_{EUT}$  direction  
 $I_M$  is the current through  $R_M$ , defined in the positive  $V_M$  direction  
 $I_{R1}$  is the current through  $R1$ , defined in the positive  $V_M$  direction

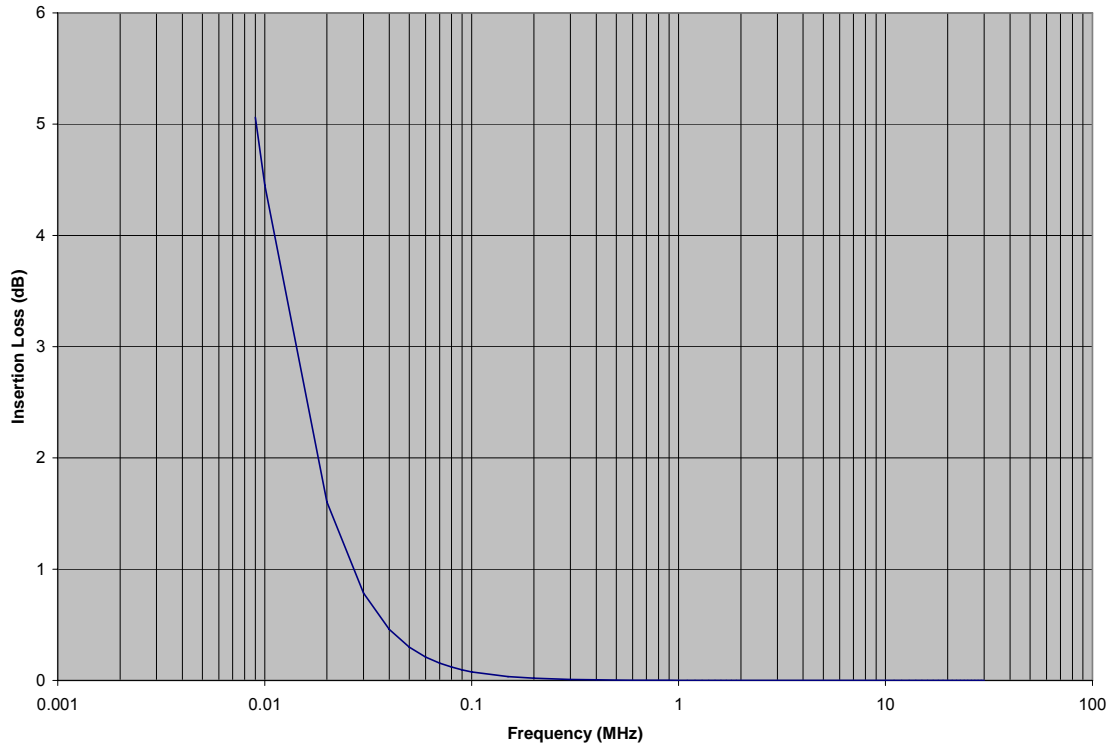


*Figure 3.2: Insertion loss of LISN in dB showing “perceived insertion loss” for frequencies below 1-MHz*

As a result of the impedance mismatch, the reference LISN gives an insertion loss of 5.06dB at 9kHz. At 150kHz the loss is reduced to 0.034dB, and is negligible at 30MHz. Another way of analyzing (3.1) is to consider the  $1/j\omega C$  leading term: for large  $\omega$ , the insertion loss correctly reduces to zero, but for smaller frequencies, this term leads to the large “perceived insertion loss” value.

### 3.3 High Frequency Calibration Errors

As shown in the low frequency case in (3.1), insertion loss correctly reduces to zero dB at high frequency when all LISN components are ideally lossless. A

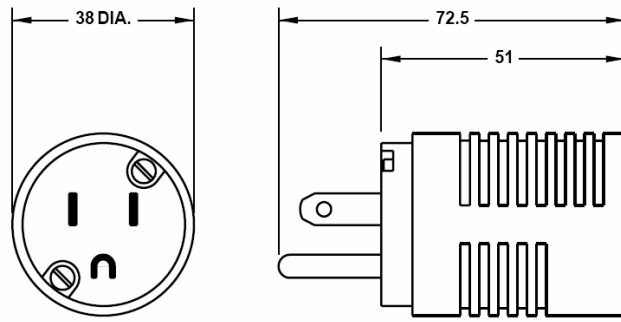
second critical assumption of the calibration process is that all components are electrically small compared to a wavelength. If the frequency becomes high enough where this is no longer true, then impedance discontinuities (i.e. transmission line effects) in the circuit will directly affect the measured insertion loss.

Referring to Figure 3.1, a thought experiment is considered by inserting transmission lines into various parts of the calibration circuit. (The voltage source, reference termination, and measuring termination are all considered to be ideal 50-ohm terminations. The LISN components will also be considered ideal circuit elements, as deficiencies in a LISN's construction contribute to the actual insertion loss of the device.) Since 50-ohm coaxial cables are typically used to connect RF test instrumentation, these will be considered first (also of ideal impedance and lossless). Given these constraints, one can make the following conclusions:

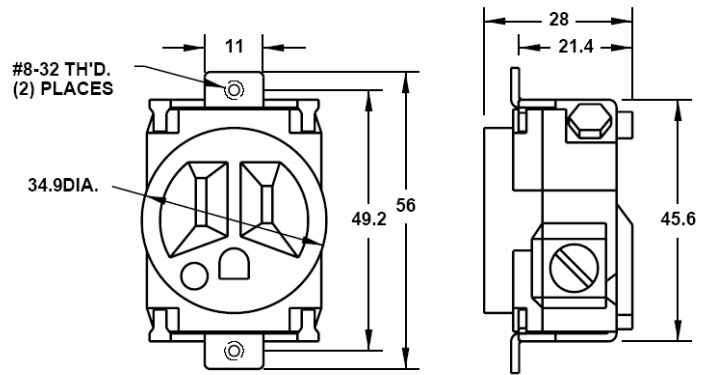
- a 50-ohm coax between  $R_s$  and the T-connector has no impact
- a 50-ohm coax between  $R_{ref}$  and the T-connector has no impact
- a 50-ohm coax between  $R_m$  and the LISN measurement port has no impact
- a 50-ohm coax between the T-connector and the LISN EUT port *will* have an impact because the parallel combination of  $R_s$  &  $R_{ref}$  (a 25-ohm Thevenin equivalent) gives rise to a mismatch to the 50-ohm coaxial cable

This mismatch at the LISN's EUT port was most likely anticipated by ANSI C63.4 [16] because as shown in Figure 2.5, instructions are given to "place T connector as close to EUT port as possible." Through experimentation, the author has found that the best method is to create a LISN calibration fixture that bonds the input and reference signal coaxes together directly at the LISN's EUT port (and thus zero length between the T-connection and the EUT port). However, one cannot eliminate the power plug that serves as the EUT port itself. Indeed, this plug is required to connect an EUT to the mains voltage for measurement, and these plugs were never intended to carry RF signals up to 30MHz. Two common types of these plugs are given in Figure 3.3: NEMA 5-15 for North America and CEE 7/4 (or "Schuko") for continental Europe [22] (CEE 7/7, used in France & Belgium, are similar, but have one less ground connection than the 7/4). Therefore, these plugs can be considered an integral and inseparable part of the LISN, and the unintended transmission line discontinuities they introduce must be accounted for.

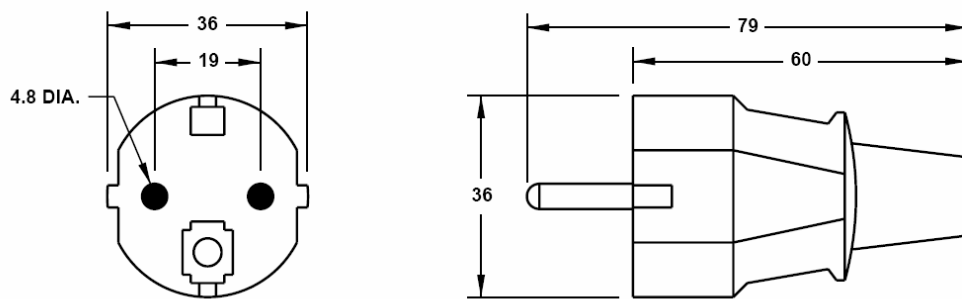
A 2-dimensional field solving program (XTK for Windows v6.8.0.1) was used to compute the characteristic inductance and capacitance matrices for these devices. The geometries used and the equipotential electric field plots are given in Figure 3.4, and the L & C matrices are given in Table 4.



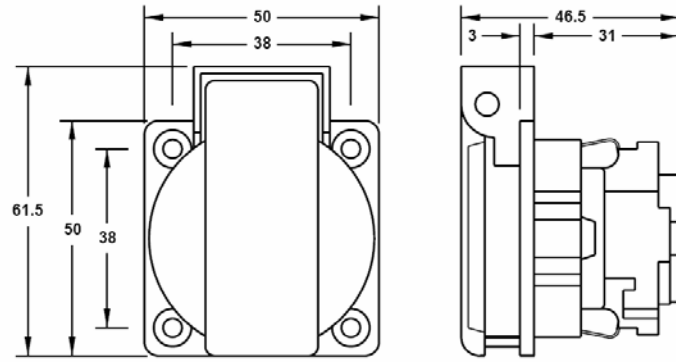
(a)



(b)



(c)

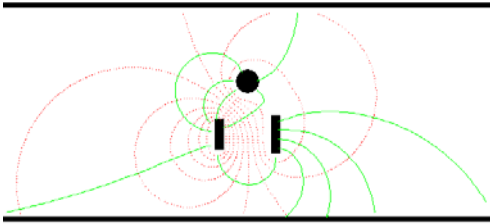


(d)

Figure 3.3: (a) NEMA 5-15 plug, (b) NEMA 5-15 outlet, (c) CEE 7/7 plug, (d) CEE 7/7 outlet (all dimensions in millimeters) [23]

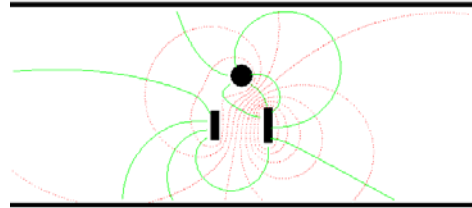
Configuration: nema\_5\_15p  
Conductor: 1 Mode: ELECTRIC  
X Range: 2193.750 2193.750  
Y Range: -1194.500 660.500

Page #1



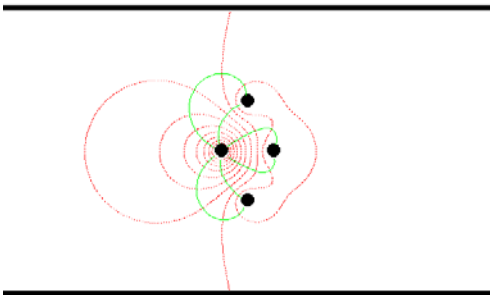
Configuration: nema\_5\_15p  
Conductor: 2 Mode: ELECTRIC  
X Range: -2193.750 2193.750  
Y Range: -1194.500 660.500

Page #2



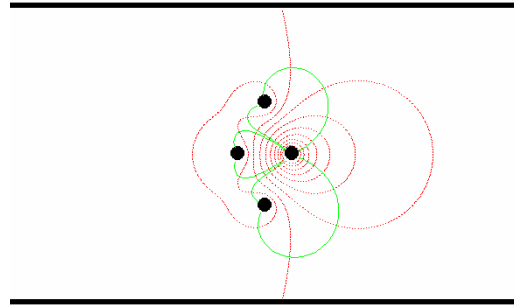
Configuration: schuko\_7\_4  
Conductor: 1 Mode: ELECTRIC  
X Range: 3513.750 3513.750  
Y Range: -2716.000 1299.000

Page #3



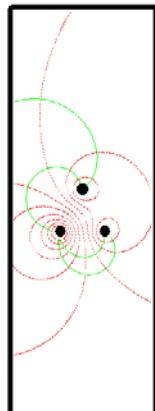
Configuration: schuko\_7\_4  
Conductor: 2 Mode: ELECTRIC  
X Range: -3513.750 3513.750  
Y Range: -2716.000 1299.000

Page #4



Configuration: schuko\_7\_7  
Conductor: 1 Mode: ELECTRIC  
X Range: 1171.250 1171.250  
Y Range: -3719.880 3011.380

Page #5



Configuration: schuko\_7\_7  
Conductor: 2 Mode: ELECTRIC  
X Range: -1171.250 1171.250  
Y Range: -3719.880 3011.380

Page #6

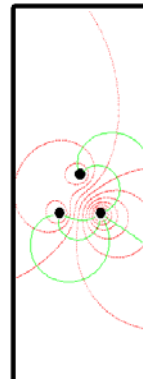


Figure 3.4: LISN EUT Port geometries & equipotential electric field lines

Table 3.1: LISN EUT Port L & C Matrices

*NEMA 5 – 15 : (North America)*

$$\bar{L} = \begin{bmatrix} 637.95 & 293.7 \\ 293.7 & 601.4 \end{bmatrix} nH / m, \quad \overline{Z_{even}} = \begin{bmatrix} 191.2 & 284.5 \\ 284.5 & 180.3 \end{bmatrix} ohms$$

$$\bar{C} = \begin{bmatrix} 22.52 & 10.98 \\ 10.98 & 23.86 \end{bmatrix} pF / m, \quad \overline{Z_{odd}} = 93.98 ohms, \quad Length = 72.5 mm$$

*CEE 7 / 4 : (Continental Europe)*

$$\bar{L} = \begin{bmatrix} 580.9 & 171.8 \\ 171.8 & 580.6 \end{bmatrix} nH / m, \quad \overline{Z_{even}} = \begin{bmatrix} 174.1 & 225.7 \\ 225.7 & 174.1 \end{bmatrix} ohms$$

$$\bar{C} = \begin{bmatrix} 20.98 & 6.22 \\ 6.22 & 20.98 \end{bmatrix} pF / m, \quad \overline{Z_{odd}} = 122.62 ohms, \quad Length = 79 mm$$

*CEE 7 / 7 : (France / Belgium)*

$$\bar{L} = \begin{bmatrix} 850.0 & 431.3 \\ 431.3 & 850.1 \end{bmatrix} nH / m, \quad \overline{Z_{even}} = \begin{bmatrix} 254.8 & 384.1 \\ 384.1 & 254.8 \end{bmatrix} ohms$$

$$\bar{C} = \begin{bmatrix} 17.6 & 8.94 \\ 8.94 & 17.6 \end{bmatrix} pF / m, \quad \overline{Z_{odd}} = 123.12 ohms, \quad Length = 79 mm$$



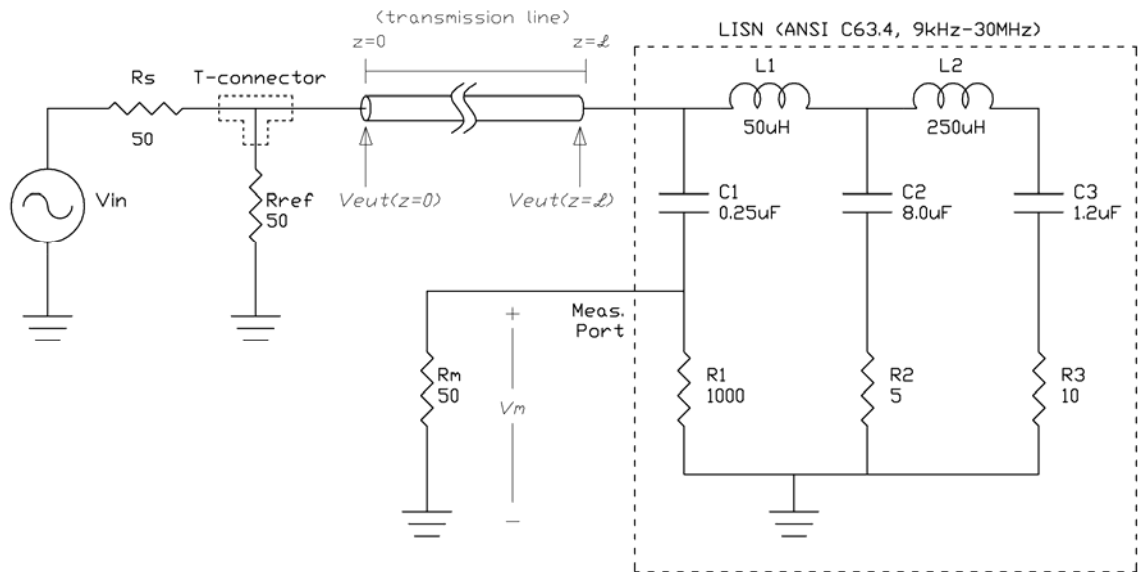


Figure 3.5: SPICE circuit of Figure 3.1 with transmission line inserted at EUT port, representing the characteristics of EUT plugs from Table 3.1

Figure 3.5 shows the SPICE circuit of Figure 3.1 with the addition of a transmission line at the EUT port. These transmission lines represent the electrical characteristics of Table 3.1 for the EUT plugs. This configuration can be solved analytically by setting up the LISN calibration as a three-conductor transmission line problem and solved using the chain parameter approach given by Paul [24]. (Paul's chain matrix approach is also used in [26] for conducted emissions analysis. In that work, the authors considered the effect of using electrically long cables (i.e. line cords) to connect an EUT to the measuring LISN.)

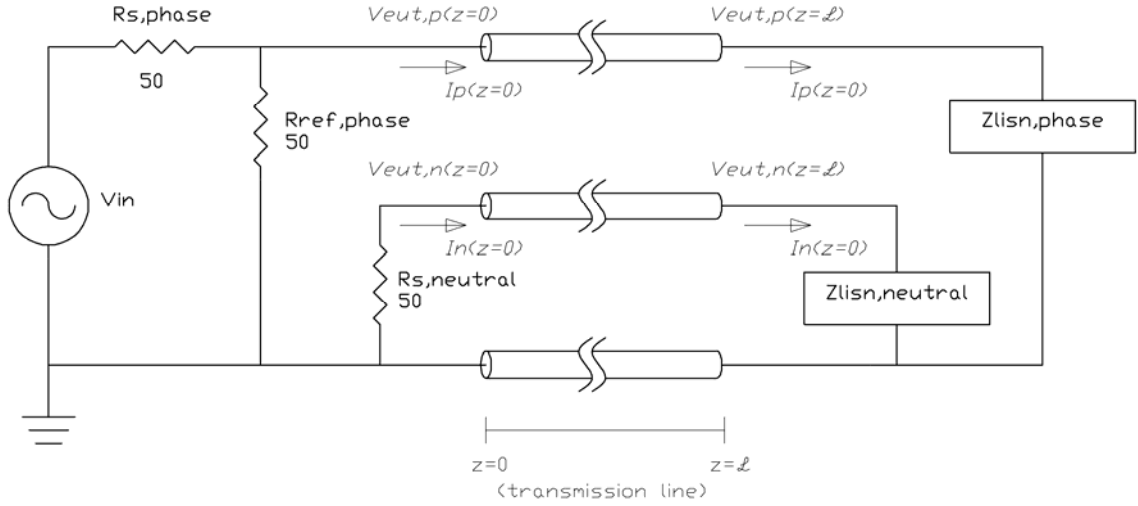


Figure 3.6: Three-conductor transmission line problem setup for solving LISN calibration

The low-frequency solution of (3.1) previously produced the ratio  $V_m/V_{EUT}$ . This is defined at the face of the LISN, as shown on the right hand side of Figure 3.6 at  $z=L$ . It is desired to determine the voltage at  $z=0$ , defined as the measurement point at the entry to the plug. The voltage and current is now modified by the chain parameter matrix  $\Phi(z=L)$  such that:

$$\begin{bmatrix} \bar{V}_{EUT}(z=L) \\ \bar{I}(z=L) \end{bmatrix} = \bar{\Phi}(z=L) \cdot \begin{bmatrix} \bar{V}_{EUT}(z=0) \\ \bar{I}(z=0) \end{bmatrix} \quad (3.2)$$

where:  $\bar{V}(z)_{EUT} = [V_{EUT,phase}(z) \ V_{EUT,neutral}(z)]$ ,  $\bar{I}(z) = [I_{phase}(z) \ I_{neutral}(z)]$

Which can be expanded into:

$$\bar{V}_{EUT}(\mathcal{L}) = \Phi_{11} \bar{V}_{EUT}(0) + \Phi_{12} \bar{I}(0) \quad (3.2a)$$

$$\bar{I}(\mathcal{L}) = \Phi_{21} \bar{V}_{EUT}(0) + \Phi_{22} \bar{I}(0) \quad (3.2b)$$

$$\text{and } \bar{I}(\mathcal{L}) \equiv \frac{\bar{V}_{EUT}(\mathcal{L})}{Z_{LISN}} \quad (3.2c)$$

Substituting (3.2c) into (3.2b) yields:

$$\bar{I}(0) = \Phi_{22}^{-1} \cdot \left[ \frac{\bar{V}_{EUT}(\mathcal{L})}{Z_{LISN}} - \Phi_{21} \bar{V}_{EUT}(0) \right] \quad (3.2d)$$

Then (3.2d) is substituted back into (3.2a):

$$\bar{V}_{EUT}(\mathcal{L}) = \Phi_{11} \bar{V}_{EUT}(0) + \Phi_{12} \Phi_{22}^{-1} \cdot \left[ \frac{\bar{V}_{EUT}(\mathcal{L})}{Z_{LISN}} - \Phi_{21} \bar{V}_{EUT}(0) \right] \quad (3.2e)$$

Which can be manipulated as follows:

$$\Phi_{22} \bar{V}_{EUT}(\mathcal{L}) = \Phi_{22} \Phi_{11} \bar{V}_{EUT}(0) + \Phi_{22} \Phi_{12} \Phi_{22}^{-1} \left[ \frac{\bar{V}_{EUT}(\mathcal{L})}{Z_{LISN}} - \Phi_{21} \bar{V}_{EUT}(0) \right] \quad (3.2f)$$

$$\Phi_{22} \bar{V}_{EUT}(\mathcal{L}) = \Phi_{11} \Phi_{22} \bar{V}_{EUT}(0) + \Phi_{12} \frac{\bar{V}_{EUT}(\mathcal{L})}{Z_{LISN}} - \Phi_{12} \Phi_{21} \bar{V}_{EUT}(0) \quad (3.2g)$$

$$\Phi_{22} \bar{V}_{EUT}(\mathcal{L}) - \Phi_{12} \frac{\bar{V}_{EUT}(\mathcal{L})}{Z_{LISN}} = [\Phi_{11} \Phi_{22} - \Phi_{12} \Phi_{21}] \cdot \bar{V}_{EUT}(0) \quad (3.2h)$$

$$\bar{V}_{EUT}(\mathcal{L}) \cdot \left[ \Phi_{22} - \frac{\Phi_{12}}{Z_{LISN}} \right] = [\Phi_{11} \Phi_{22} - \Phi_{12} \Phi_{21}] \cdot \bar{V}_{EUT}(0) \quad (3.2i)$$

$$\bar{V}_{EUT}(\mathcal{L}) = \left[ \Phi_{22} - \frac{\Phi_{12}}{Z_{LISN}} \right]^{-1} \cdot [\Phi_{11} \Phi_{22} - \Phi_{12} \Phi_{21}] \cdot \bar{V}_{EUT}(0) \quad (3.2j)$$

$$\text{and define } \bar{H} \equiv \left[ \Phi_{22} - \frac{\Phi_{12}}{Z_{LISN}} \right]^{-1} \cdot [\Phi_{11} \Phi_{22} - \Phi_{12} \Phi_{21}] \quad (3.2k)$$

Finally the insertion loss (IL) is derived as: (applies to  $V_{EUT,phase}$  or  $V_{EUT,neutral}$ )

$$V_{EUT}(z = \mathcal{L}) = \bar{H} \cdot V_{EUT}(z = 0)$$

$$\Rightarrow IL = \frac{V_m}{V_{EUT}(z = 0)} = \bar{H} \cdot \left( \frac{V_m}{V_{EUT}(z = \mathcal{L})} \right) \quad (3.3)$$

where:  $\frac{V_m}{V_{EUT}(z = \mathcal{L})} \equiv IL$  from equation (3.1)

The next step is to solve for the transfer function  $H$ . The simplest case to consider is when the medium is lossless and homogenous such that the chain matrix parameters are (from Paul [24]):

$$\Phi_{11} = \cos(\beta\mathcal{L}) \cdot \bar{I}_2, \quad \text{where: } \bar{I}_2 = \begin{bmatrix} 1 & 0 \\ 0 & 1 \end{bmatrix} \quad (3.4a)$$

$$\Phi_{12} = -j\omega\mathcal{L} \cdot \frac{\sin(\beta\mathcal{L})}{\beta\mathcal{L}} \cdot \bar{L}, \quad \text{where: } \bar{L} = \begin{bmatrix} l_G & l_m \\ l_m & l_R \end{bmatrix} \quad (3.4b)$$

$$\Phi_{21} = -j\omega\mathcal{L} \cdot \frac{\sin(\beta\mathcal{L})}{\beta\mathcal{L}} \cdot \bar{C}, \quad \text{where: } \bar{C} = \begin{bmatrix} c_G + c_m & -c_m \\ -c_m & c_R + c_m \end{bmatrix} \quad (3.4c)$$

$$\Phi_{22} = \Phi_{11} \quad (3.4d)$$

Using these values,  $H$  can be greatly simplified:

$$\bar{L} \cdot \bar{C} = \mu\epsilon \cdot \bar{I}_2$$

$$\Phi_{11}\Phi_{22} - \Phi_{21}\Phi_{12} = \cos^2(\beta\mathcal{L}) + \sin^2(\beta\mathcal{L}) = 1$$

$$\Rightarrow \bar{H} = -Z_{LISN} (\Phi_{12} - \Phi_{11} \cdot Z_{LISN})^{-1} \quad (3.4e)$$

With the final result as:

$$\bar{H} = Z_{LISN} \cdot \left[ j\omega\bar{L} \frac{\sin(\beta\mathcal{L})}{\beta\mathcal{L}} + \cos(\beta\mathcal{L}) \cdot \bar{I}_2 \cdot Z_{LISN} \right]^{-1} \quad (3.4f)$$

As a check, the transfer function correctly simplifies to the low-frequency case of  $|H|=1$  in the limit of  $\beta=\omega*\text{sqrt}(\mu\epsilon) \rightarrow 0$  and also the limit of  $\mathcal{L}\rightarrow 0$ . The matrices given in Table 3.1 can now be combined with (3.3) and (3.4) to compute the high-frequency IL. Results for the plug that exhibits the highest insertion loss, the CEE 7/7, are given graphically in Figures 3.7 and 3.8.

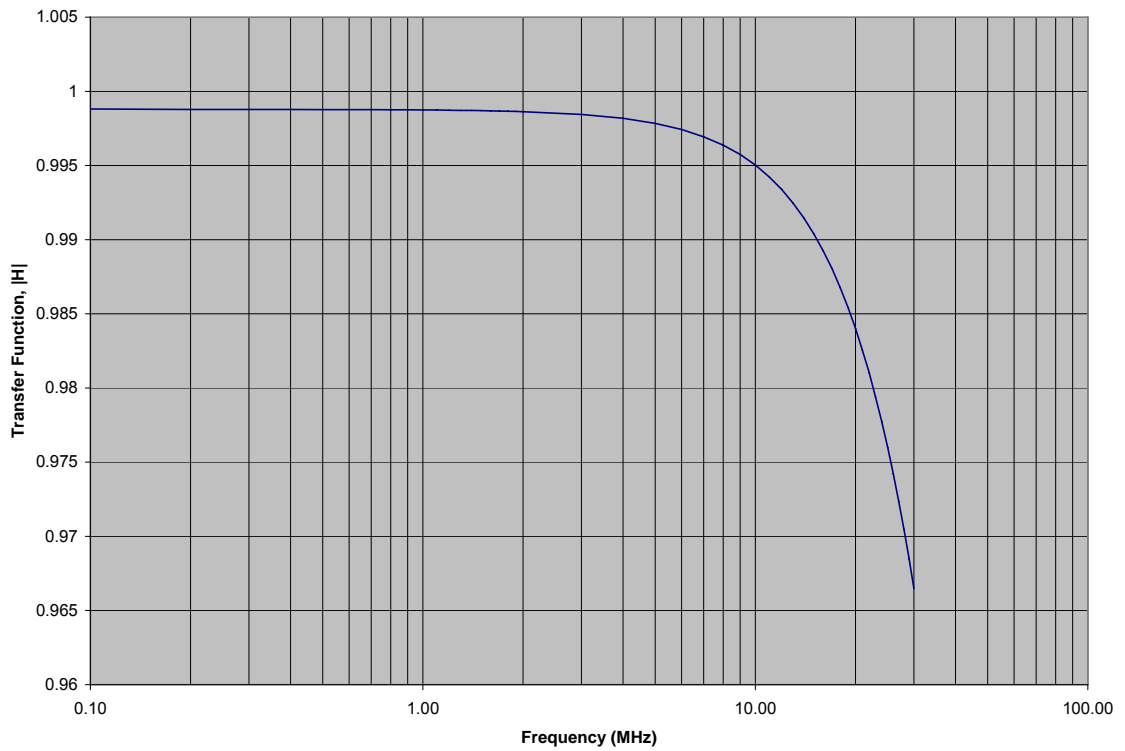


*Figure 3.7: Transfer function H for worst-case EUT plug (CEE 7/7)*

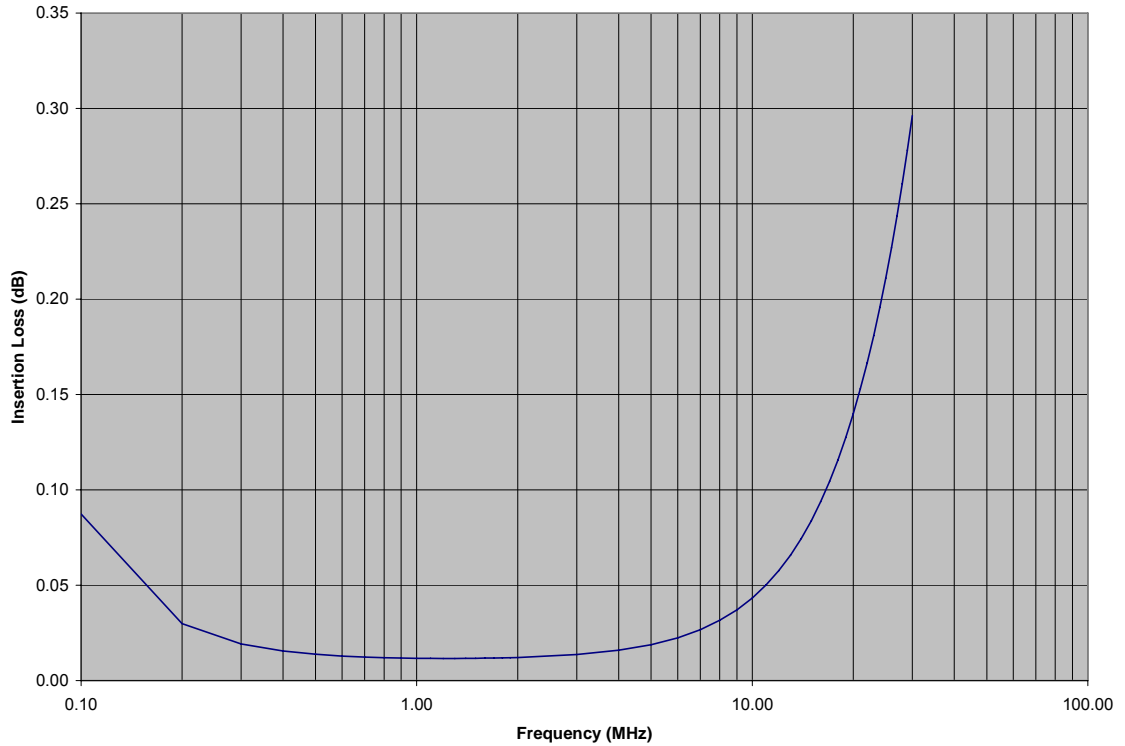


*Figure 3.8: Combined Insertion Loss for worst-case EUT plug (CEE 7/7)*

The plug with the highest inductance from Table 3.1 is the CEE 7/7, and its resulting worst-case insertion loss at 30MHz is computed to be 0.296dB. For the CEE 7/4, it is 0.138dB, and for the NEMA 5-15 is it 0.141dB. These are not insignificant values and have a non-trivial impact on the accuracy (and therefore uncertainty if corrections are not made) of the LISN measurement system. Furthermore, if the discontinuity is greater in magnitude or length (including the wiring that connects the EUT plug to the LISN circuits), then the effect can be even greater. The presence of discontinuities is a prime example of the quality of the LISN's construction having a direct impact on the final measurement.

### 3.4 Correction for LISN Calibration Systematic Errors

In the previous sections, systematic errors were shown in both the low and high frequency ranges of a LISN's calibration. For the low frequency case, it is insertion loss by design (i.e. an "ideal" LISN will show insertion loss for frequencies below 1MHz). For high frequencies, it is transmission line effects (impedance discontinuities whose lengths are not electrically short). In order to accurately determine a system's uncertainty, these errors need to be understood and corrected.

In the low frequency range (less than 1MHz), insertion loss is measured in the ideal LISN because its designed impedance deviates from the 50ohm references of the calibration instruments. For instance, at 9kHz the ideal LISN has an input impedance of 6.452ohms, and when calibrated in a 50ohm system, yields an insertion loss of 5.06dB. Based on (3.1), for frequency ranges where  $1/j\omega C$  is significantly large, the IL depends on the parallel combination of  $R_1$  (inside of the LISN) and  $R_m$  (the termination at the LISN's measurement port). Thus, IL can be greatly reduced by increasing  $R_m$ . One method of doing this is using a high impedance active probe, such as the Agilent 41800A [25]. This probe has a typical input impedance of 100kohm, and the resulting IL at 9kHz is a negligible 0.022dB. Therefore, this active probe method can reveal "true" IL in the LISN (i.e. IL due to lossy or parasitic elements within the LISN). But for the final

determination of IL for LISN calibration, a 50ohm termination must be used because this is the value specified in the ANSI C63.4 procedure [16].

In contrast with the low frequency range, systematic errors in the high frequency range can be corrected during a LISN's calibration. This is because the impedance discontinuity at the EUT port has a fixed geometry and because the plug itself is part of the calibration fixture. Utilizing the "fixture compensation" features of the modern network analyzer, the frequency response of the EUT plug and receptacle can be calibrated out of the insertion loss measurement. Figure 3.9 shows an example calibration setup, with the network analyzer connected to a LISN using a "T" adapter constructed from an EUT plug. Figure 3.10 shows details of the EUT plug and fixture compensation adapters used in this calibration.



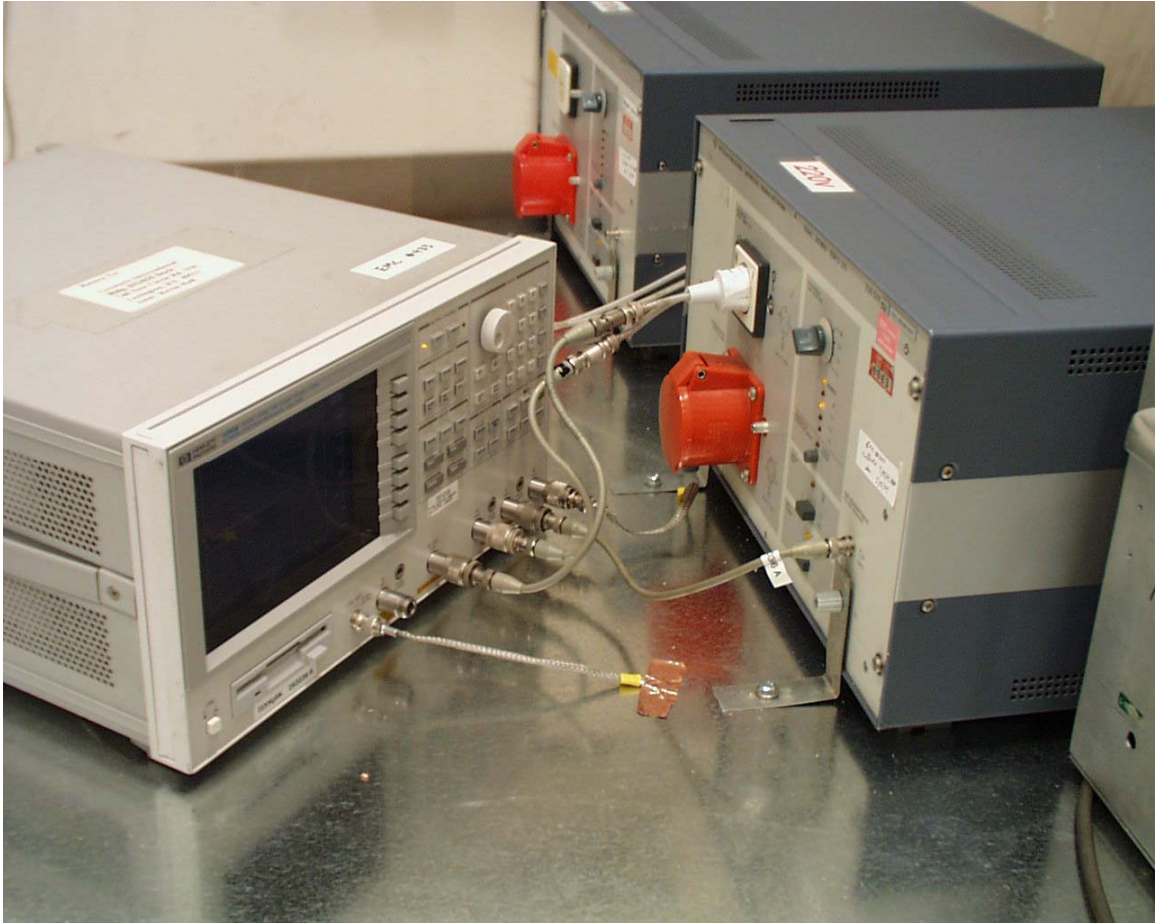


*Figure 3.9: LISN insertion loss calibration using ANSI C63.4 "T" method, using a network analyzer (left), "T" EUT plug fixture (center), and LISN (right)*



*Figure 3.10: “T” EUT plug with ideally short leads on LISN side, and fixture compensation standards using EUT receptacle geometry*

By using this set of EUT plug fixtures and the fixture compensation method, the network analyzer now compensates for the characteristics of the EUT plug as part of its measurement. In effect, this moves the measurement point in Figure 3.5 from  $V(z=0)$  to  $V(z=L)$ , which is often termed as shifting the measurement plane. It follows that the transfer function  $H$  from (3.4) returns to unity, and the resulting insertion loss reduces to the low frequency case—virtually zero loss for frequencies above 1MHz for the ideal LISN.

In conclusion, careful calibration of a LISN is required for accurate measurement of its insertion loss. This loss is then used as a correction factor in all measurements, thus “zeroing out” the systemic errors. With this complete, the next step is to study the measurement uncertainty of the system.

## **CHAPTER 4: TEST SETUP FOR TYPE A UNCERTAINTY MEASUREMENT OF A LISN**

### **4.1 Measurement Setup**

The previous chapter discussed, in detail, the techniques required for the best accuracy in LISN calibration. In addition, shortcomings of the current LISN calibration methodology were described. Now that the LISN and its calibration process have been fully investigated, the next step is to devise an experiment that will allow direct measurement of the uncertainty of the conducted emissions system (thus a Type A full-system study, demonstrated as the most accurate type in Chapter 2).

The key blocks of the proposed measurement are shown in Figure 4.1. Starting from the left-hand side of the figure, a signal generator is used to inject the RF signal into the system (this device should have a very accurate frequency and amplitude output because the uncertainty of the final measurement can be no better than this input). Next, a device designated as the “coupling box” allows the signal generator to be connected directly to the LISN’s EUT port. This is important because it allows the LISN to remain connected to the AC mains (thus leaving the measurement system intact) while protecting the output port of the signal generator. The remaining parts of the setup are the typical LISN

measurement system with an additional control line from the PC to the signal generator to allow for automated software control of the uncertainty measurement.

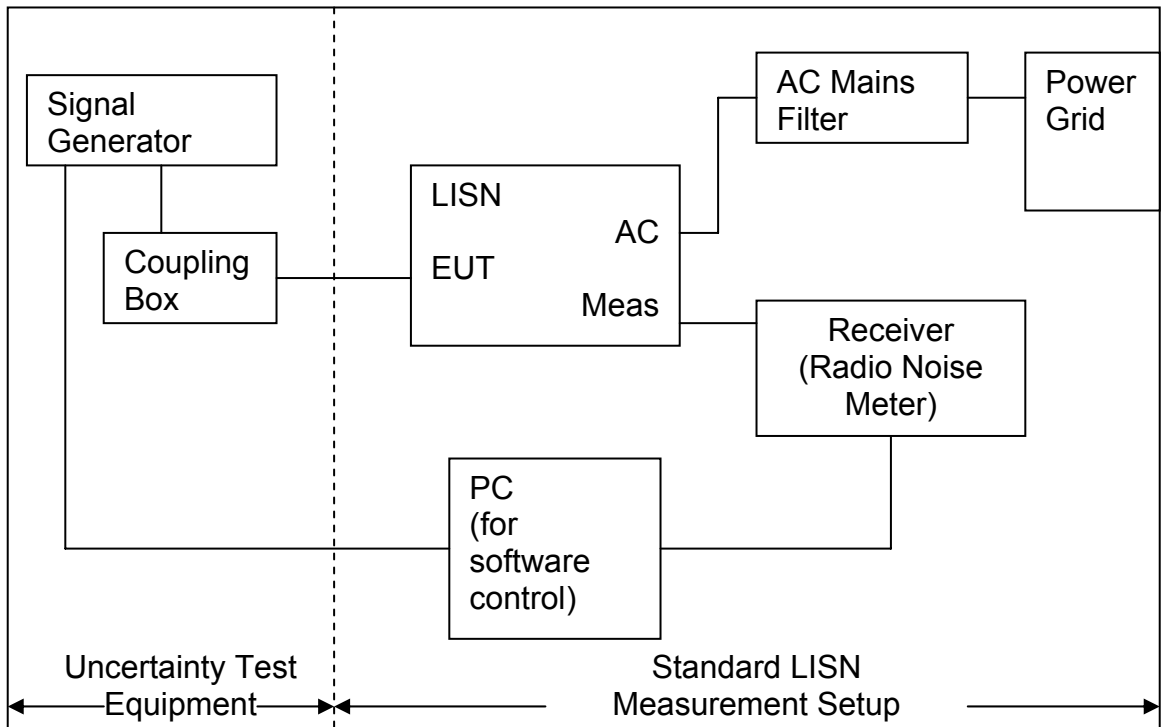


Figure 4.1: LISN measurement uncertainty test setup

As described previously in Chapter 2, the RF characteristics of the receiver are defined in [13]-[15], although these have been harmonized such that a single device can meet the requirements of all three of these regulations. Specifically, there are three types of detectors defined by these standards that are applicable to conducted emissions measurements: peak, quasi-peak, and average. Each has a different response to time-varying signals as defined in [13] and [14]. Therefore, in order to fully exercise the operating parameters of the measurement system, a signal generator or generators should be used to inject

the appropriate signals. For peak detection, a continuous wave (CW) sinusoidal signal source should be used because its RF amplitude should be independent of the type of measuring detector. For quasi-peak and average detection, a pulse generator that conforms to the specifications given in [13] should be used. This pulsed type of signal source will show the measuring system's response to transient (i.e. non-steady state) signals, such as those an actual EUT may present to the system.

## **4.2 Coupling Box Design Requirements**

Thus far all the components described in Figure 4.1 have been off-the-shelf or commercially available devices. The coupling box is not, however, so its design must be carefully described. Its primary purpose is to protect the signal generator from the high-voltage AC mains present at the EUT port so it must possess high-pass filter characteristics to block the AC mains voltage (typically 50 or 60Hz) but still pass the desired RF signals in the 150kHz to 30MHz range. Additionally, the coupling box must not distort the RF signals that it is intended to pass. Thus its frequency response should be ideally flat through the frequency range of interest. Finally, it should provide minimal loss of the RF signal it passes through to allow the widest dynamic range of the measuring system possible.

Figure 4.2 shows the schematic of the proposed coupling box. In this example, a 2 port LISN is used (a phase and neutral connection, per power industry terms). This concept could be easily extended to 3-phase (or higher) systems by duplication of the ports on the left-hand side of the figure. Essentially, the coupling box is a second-order LC high-pass filter. R1 was added to dampen a resonance between the stages of the filter. R1n and R1p represent a balanced 50ohm RF splitter: their purpose is to take the signal generator's input and equally divide it between the phase and neutral LISN circuits. The splitter has the advantage of not requiring manual switching of the injected signal between the EUT ports, but it does require connection to balanced downstream circuits to ensure accurate operation (i.e. an unbalance load will cause the voltages at the two output ports to not be identical). In the ideal case, the phase and neutral LISN ports will be balanced because their circuits and construction are identical. For the non-ideal case they will not be perfectly balanced, so the use of the splitter will show voltage variations between the two ports. In fact, this can be considered a desirable trait because this imbalance, which can be a factor in the system's measurement uncertainty, will be detectable by this coupling box's design.

An early prototype of the coupling box used a mechanical switch to select either the phase or neutral port of the LISN. However, it was found that a transient surge occurred if the switch was thrown while the coupling box was connected to the EUT's AC mains voltage, potentially damaging the output port of the

synthesizer. Based on the available dynamic range of the signal generator, it was determined that the 6-dB loss due to the R1n-R1p splitter did not affect accuracy. An additional 20-dB attenuator was also added at the signal generator's output port for further transient suppression.

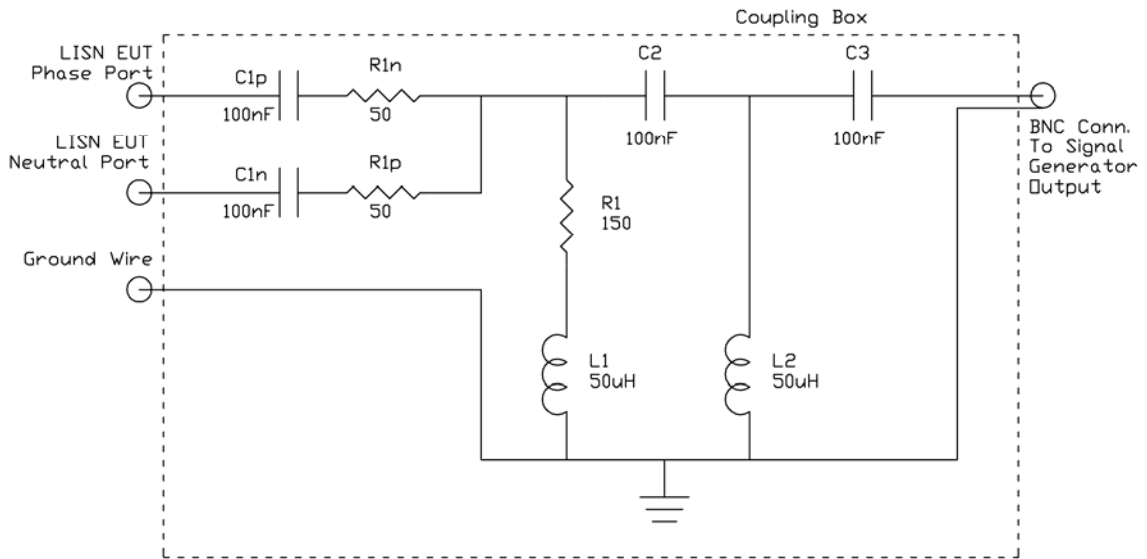


*Figure 4.2: Coupling Box Schematic*

The choice of using 50uH inductors and the 100nF capacitors was intentional. In order for the circuit to maintain a flat frequency response across the entire 150kHz to 30MHz frequency range, high quality components were required to construct the circuit. Referring back to Figure 2.2(a), these are the same values used in commercially available LISN's. Thus, the prototype coupling box was built from a discarded LISN, in this case, the Solar model 8012-50-R-24 pictured



in Figure 4.3. All the wiring was carefully routed to ensure impedance control in the critical signaling paths, with minimized loop areas for return currents to prevent parasitic mode conversion.

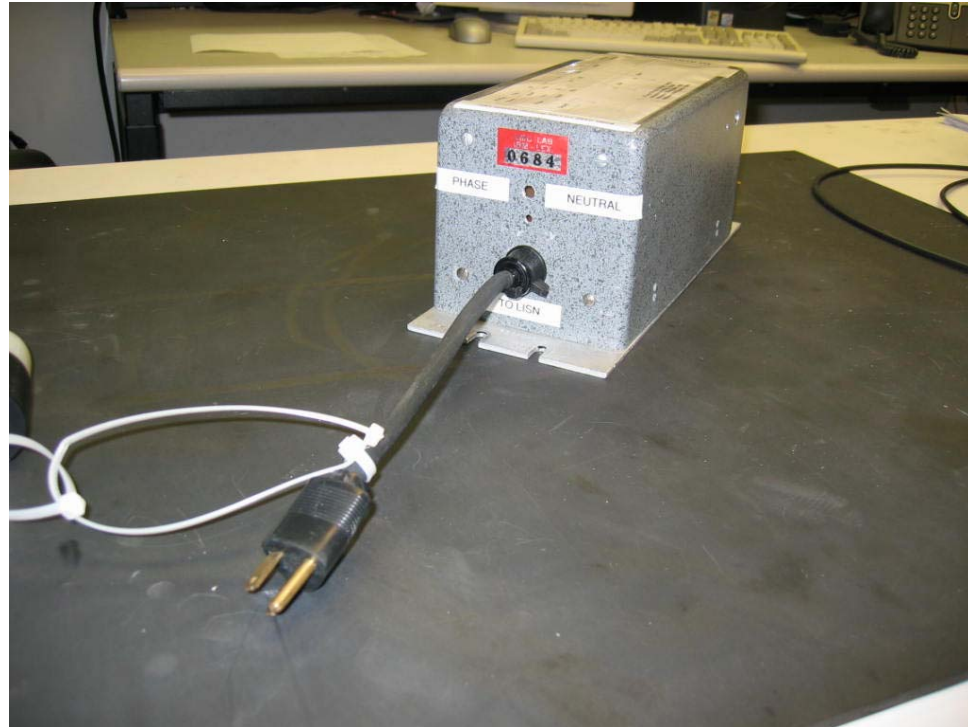


*Figure 4.3(a): Completed coupling box, constructed from Solar 8012 LISN*

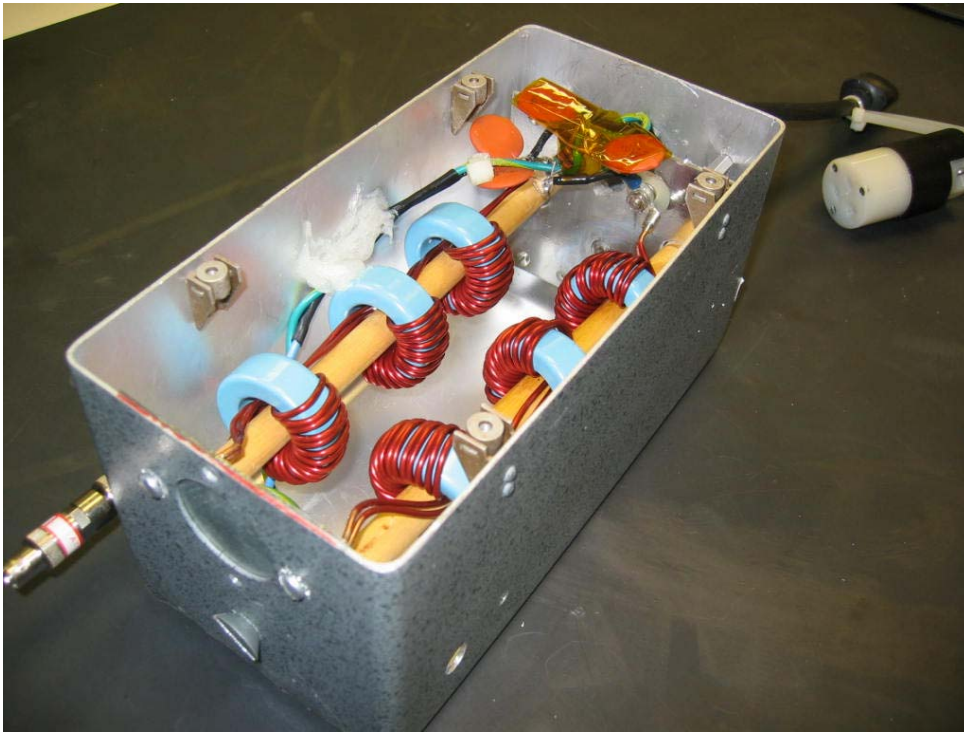


*Figure 4.3(b): Completed coupling box, showing internal wiring optimized for impedance control*

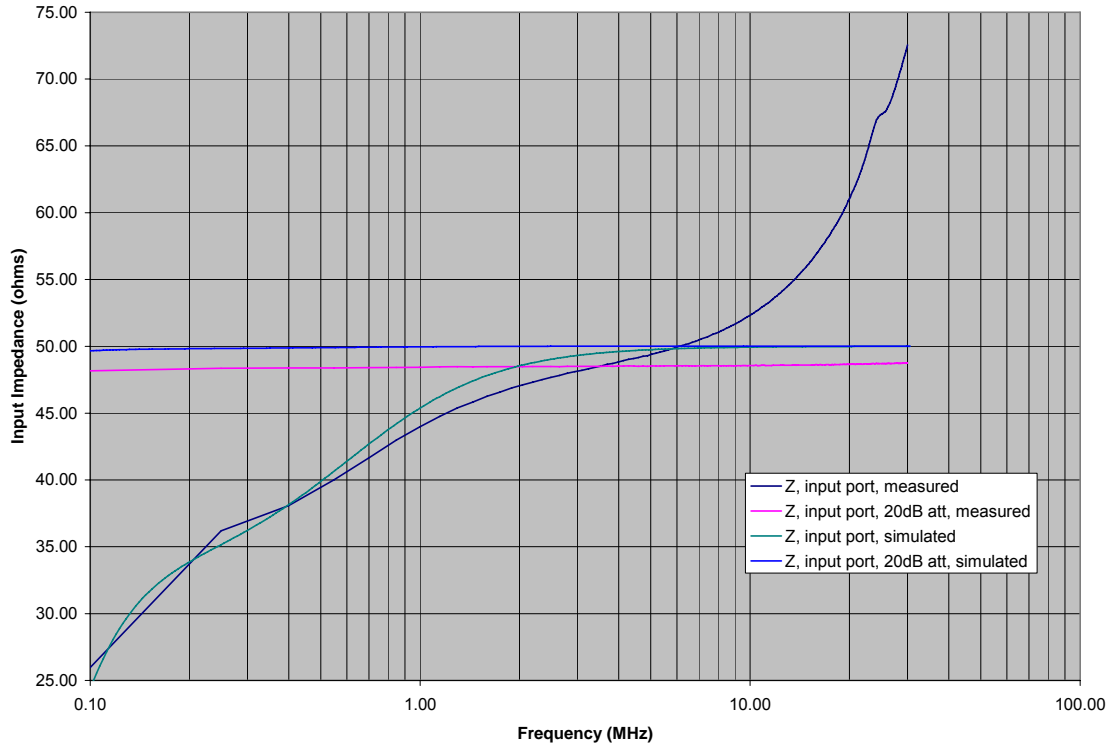
### **4.3 Simulated and Measured Coupling Box Characteristics**

Figures 4.4 and 4.5 show the impedances and insertion loss (IL) of the coupling box with respect to its ports. “Input” refers to the port that the signal generator used to connect to the LISN. “EUT” refers to the port that connects to the EUT terminals of the LISN, thus allowing the coupling box to connect to the LISN in the exactly the same manner as an actual EUT. Key features of these figures are as follows:

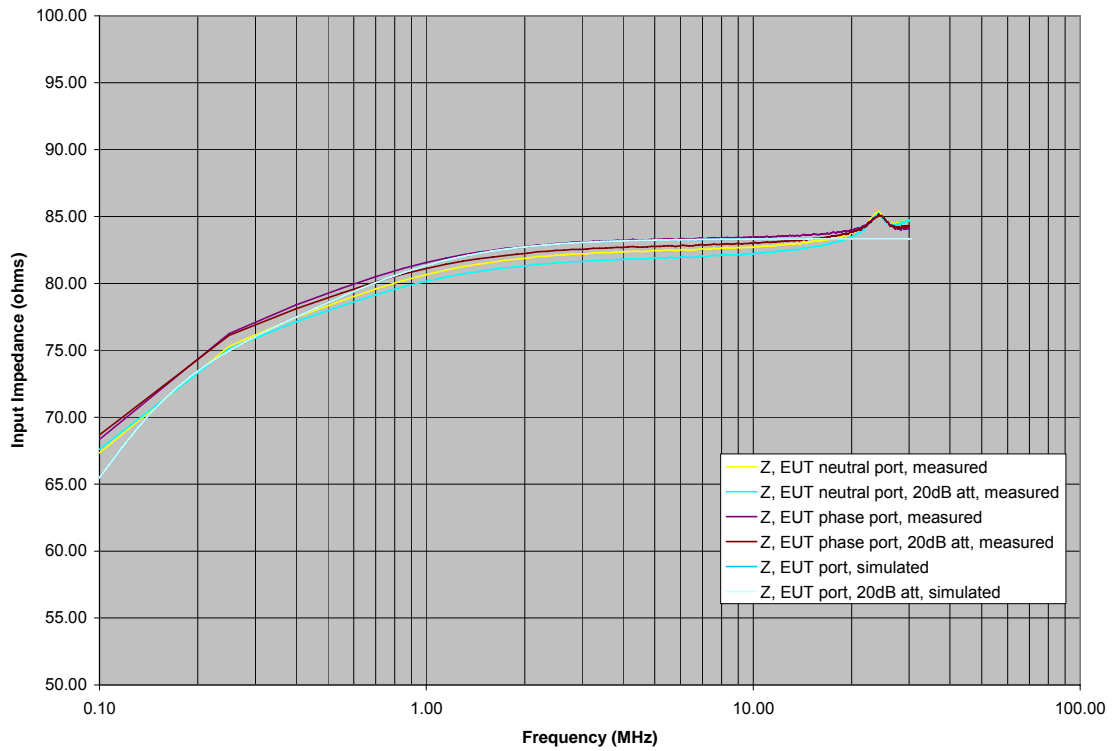
- Input port impedance correctly approaches 50ohms for frequencies greater than 1MHz; the addition of the 20dB attenuator allows an even better match for the signal generator’s 50ohm reference impedance.

- EUT port impedance is unaffected by the 20dB attenuator, thus isolation is shown between the coupling box's EUT and input ports.
- EUT port impedance is not 50ohms, however. An EUT is, by definition, a device with unknown RF characteristics and therefore has no requirement to match the LISN's input impedance. Therefore, as long as the impedance of the coupling box is well controlled (not varying over time, temperature, and small perturbations to the test setup) and allows for adequate system dynamic range, the EUT port impedance can be any value.
- IL between the input and EUT ports correctly changes by 20dB with the addition of the attenuator, demonstrating linearity.
- IL also approaches 6dB for frequencies greater than 1MHz, as expected due to the 2:1 splitter on the output.
- For frequencies less than 10kHz, the IL becomes very large (250dB at 50Hz) to protect the signal generator from the AC mains voltage (not shown).
- IL flattens with respect to frequency with the addition of the 20dB attenuator. This flatter frequency response reduces signal distortion.
- Without the 20dB attenuator, there is a 4dB difference between the measured IL and the simulated IL at 100kHz. For the measured data, there is a constant 20dB delta across all frequencies with the addition of the attenuator, so the measured data responds linearly and is considered accurate. On further investigation, the SPICE simulation shows a series resonance that occurs around 10kHz, so the dip in the IL graph of Figure 4.5 is the edge of that resonance. Because a potential for resonance has been shown in the

simulation, an attenuator will be included in all subsequent uncertainty measurements.

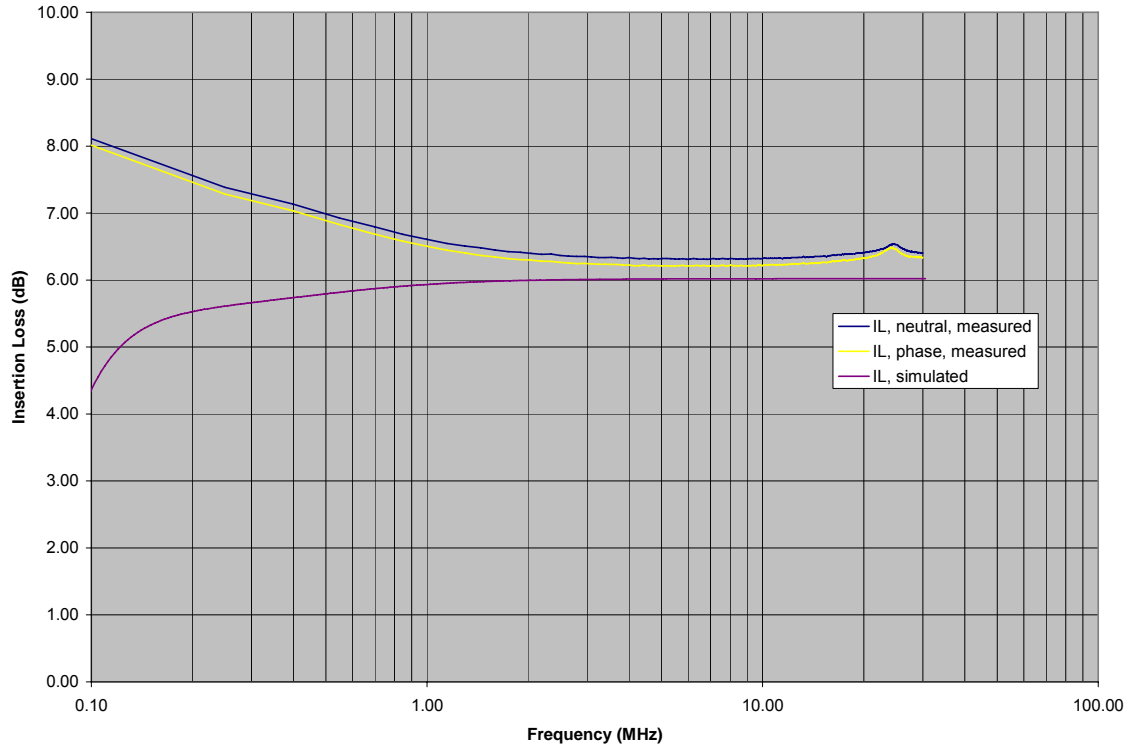


(a)

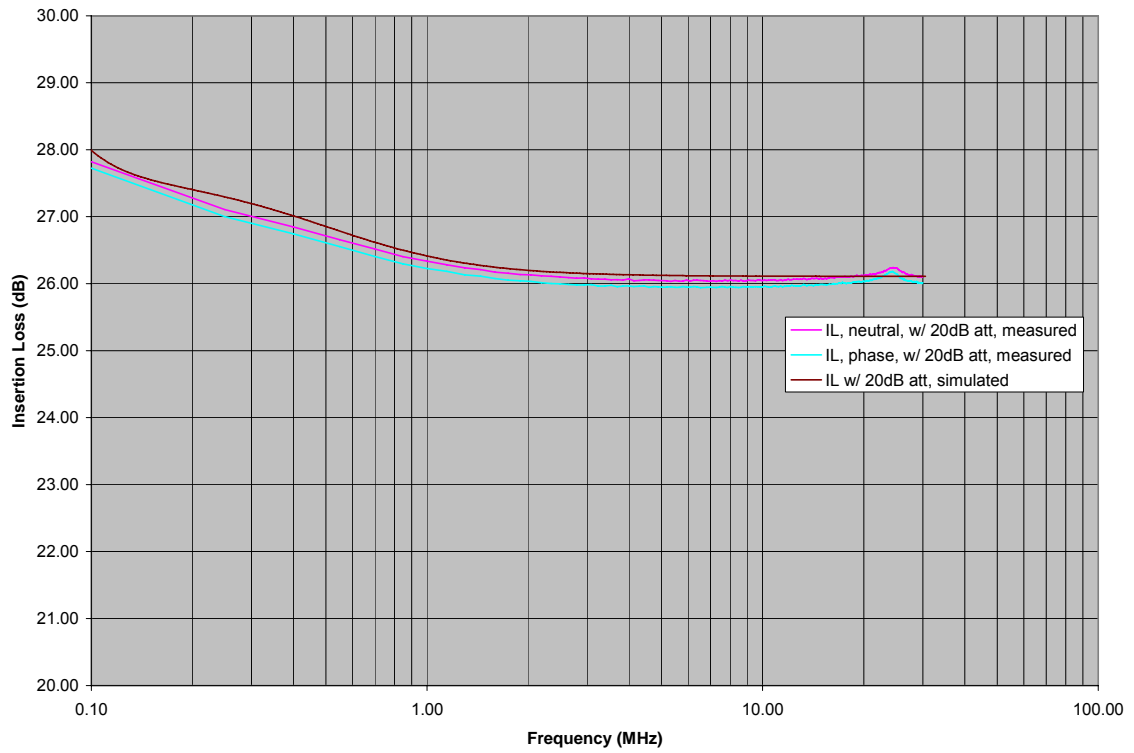


(b)

Figure 4.4: Coupling box impedances for (a) input port and (b) EUT port



(a)



(b)

Figure 4.5: Coupling box insertion loss (a) without and (b) with 20dB attenuator

#### **4.4 Coupling Box Interface with LISN**

Figure 4.6 shows the coupling box of Figure 4.2 combined with the LISN of Figure 2.2(b). For the SPICE simulation, an AC voltage source represents the signal generator. A segment of ideal (lossless) transmission line represents the interconnect between the coupling box and the LISN at the EUT port, and a 50-ohm resistive termination represents the measuring receiver. Figure 4.7 then shows the final amplitude seen at the LISN measurement port given the signal generator input levels defined in Chapter 5. As a preview of the results in Chapter 5, the LISN's measured were both Rohde & Schwarz models ESH3-Z5, and the simulated and measured results showed very good agreement: within 1dB at all frequencies.

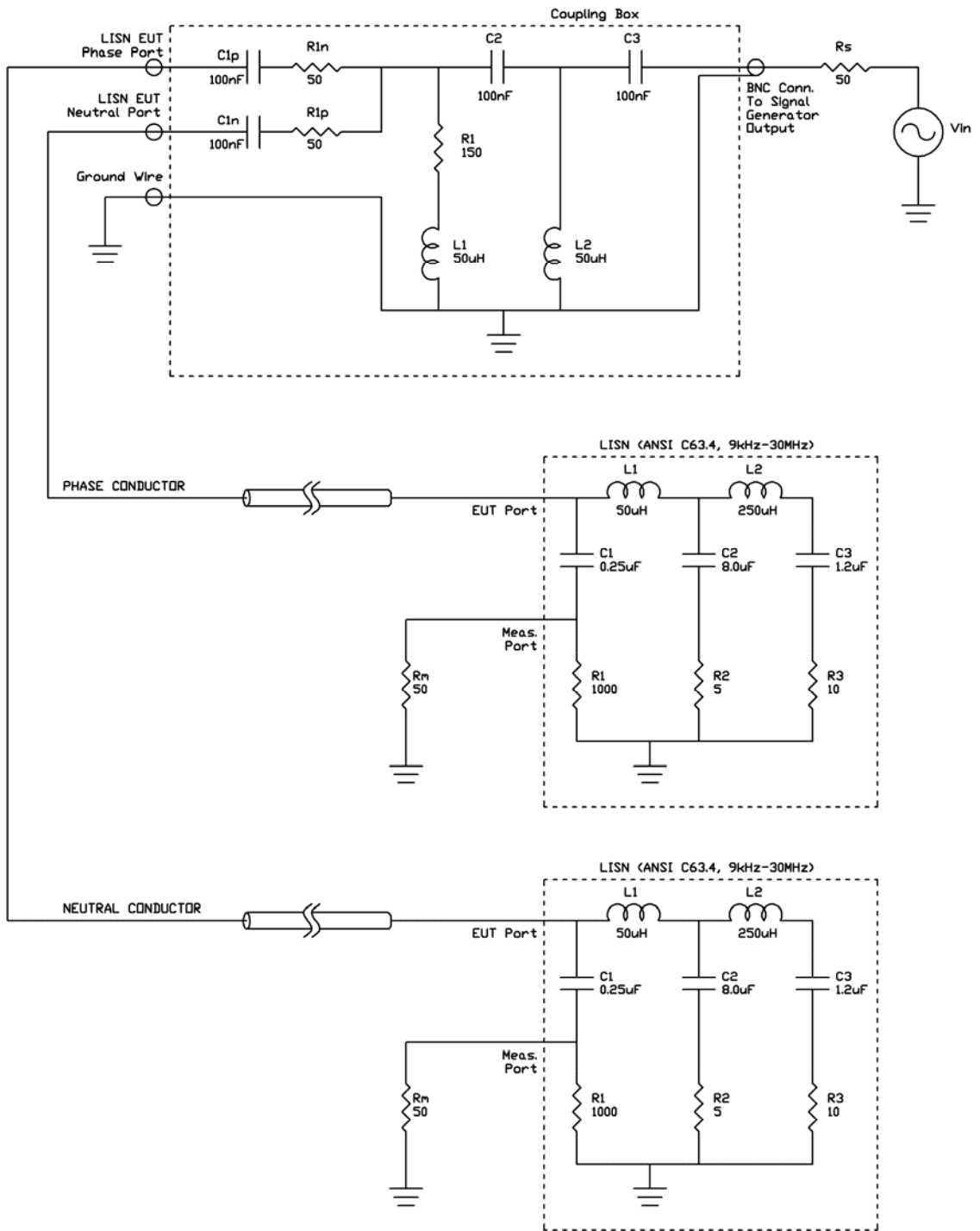
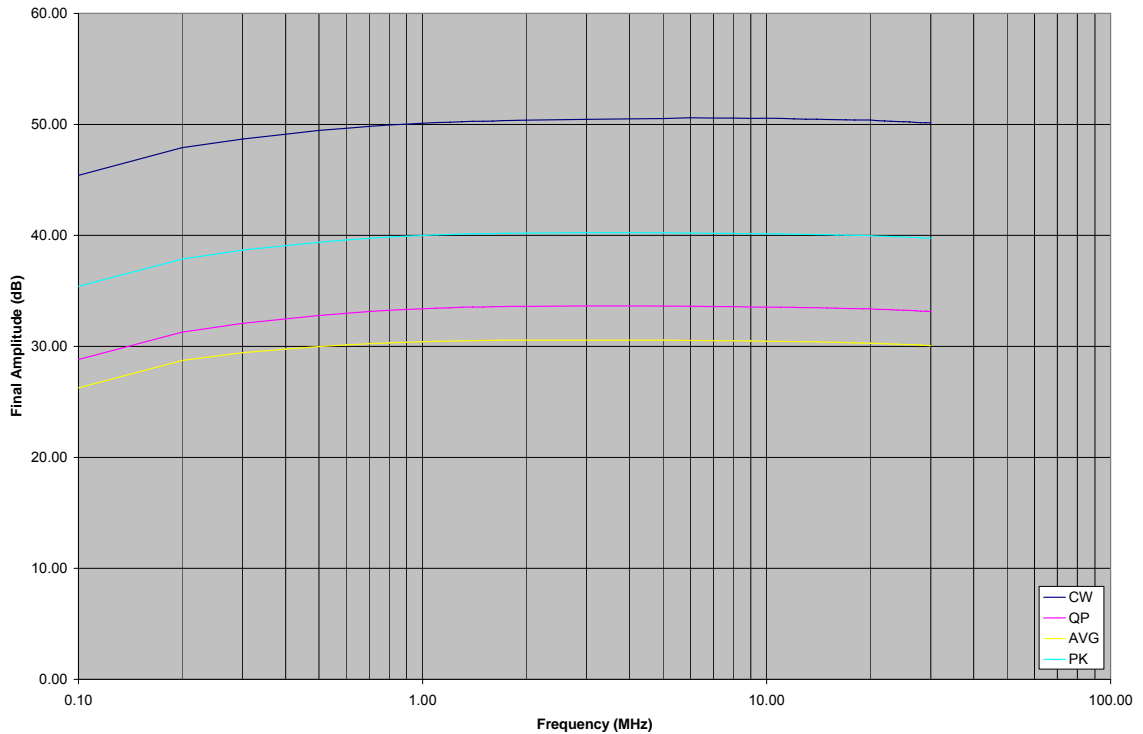


Figure 4.6: SPICE schematic showing combined coupling box & LISN





*Figure 4.7: Simulated amplitude at LISN measurement port resulting from the schematic of Figure 4.6. The amplitudes shown are based on the test setups that will be described in Chapter 5*

This setup will be used as the test vehicle to characterize the full system measurement uncertainty. Referring back to Figure 4.1, each of the blocks of the measuring system have been fully characterized with the exception of the signal generator. In terms of uncertainty, it is not possible to measure uncertainties smaller than the reference or standard used in the measurement, thus this procedure's uncertainty will be limited by the uncertainty of the signal generator's output. (And thus a highly accurate signal generator should be used.) The next chapter will show the measurements and resulting uncertainty calculations of the measurement system defined here.

## CHAPTER 5. UNCERTAINTY MEASUREMENTS

### 5.1 Measurement Test Setup

Figure 4.1 of the previous chapter described the test setup to be used for the uncertainty measurement. The equipment used for this particular test case is as follows:

Signal Generator:	Rohde & Schwarz SML01 (for sinusoidal measurements) Schwarzbeck IGUU 2916 (for pulsed signal measurements)
Coupling Box:	constructed from Solar 8012-50-R-24 LISN
LISN:	Rohde & Schwarz ESH2-Z5 (one each for 110V & 220V)
Receiver:	Rohde & Schwarz ESIB-7
AC Mains Filter:	Integrated with Lectroshield shielded room LSW1-11154
PC:	Dell Optiplex GX110 with custom GPIB control software

The procedure used to record the measured results is as follows (waiting for instrument settling time is assumed between each step):

1. Install coupling box per Figure 4.1 with the LISN to be tested. Turn on all equipment and allow to warm-up per manufacturer's recommended operating procedures.
2. Initialize the signal generator to a known frequency and amplitude.
3. Initialize the receiver to the desired detector type and input port.
4. Select the appropriate measurement path (e.g. the 110V LISN's phase conductor) for measurement using the associated RF relays (part of the automated conducted measurement system).
5. Load receiver's internal memory with appropriate correction factors (LISN IL & coaxial cable IL) appropriate to the measurement path.
6. Set the signal generator to the first frequency and amplitude to be measured.
7. Set the receiver to the same frequency as the signal generator, allow settling time, then record received amplitude.
8. Repeat steps 6 & 7 for each frequency to be measured.
9. Repeat steps 4 – 8 for each measurement path considered.
10. Repeat steps 1 – 9 for each detector type (peak, quasi-peak, and average) and signal generator (sinusoidal or pulsed signal).

For these measurements, each trial was repeated 16 times to provide statistical significance to the data. The list of frequencies that were measured is shown graphically in Figure 5.1. Starting at 100kHz, the test procedure increased the frequency in 100kHz steps up to 2MHz, then used 1MHz steps for the remaining

points up to 30MHz. These steps provided a total of 48 amplitude measurements per frequency sweep. Instead of using traditional linear or logarithmic steps sizes, this approach was used because it best represented the distribution of EUT noise emission spectrums based on engineering experience of this particular test laboratory. (The reason for this is that many conducted EMC emissions problems are generated by switching power supplies or regulators. These devices typically operate in the kilohertz range thus their emissions spectrum is strongest at the low end of the spectrum.)

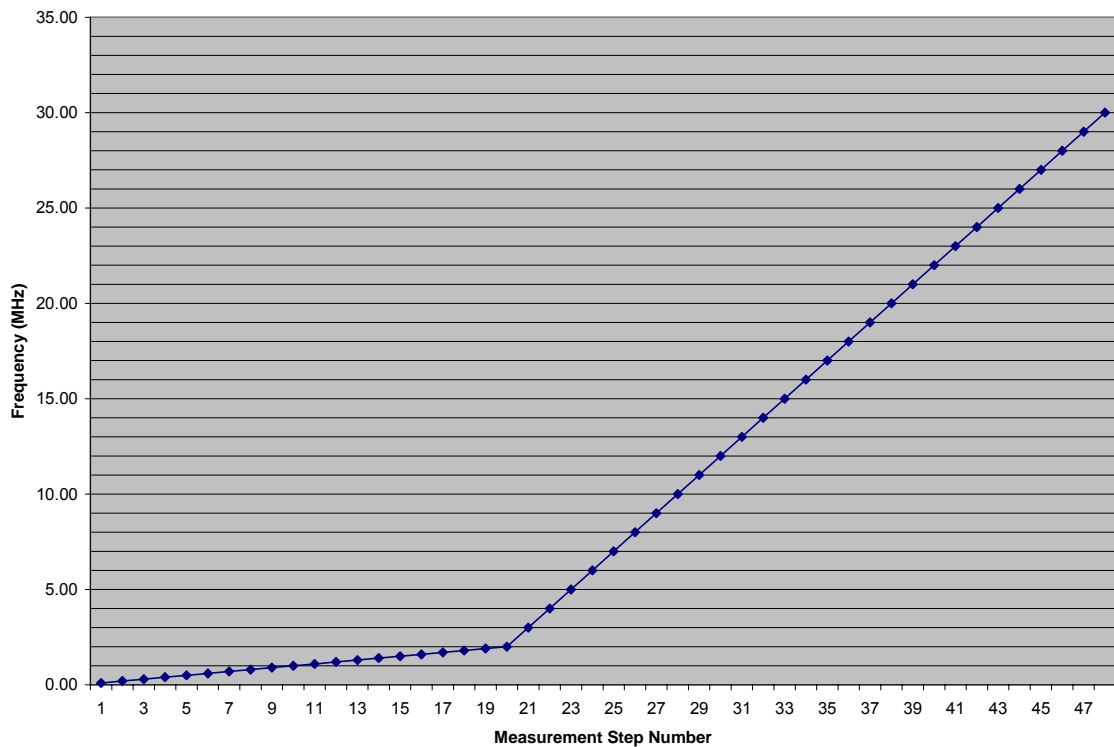


*Figure 5.1: Frequencies measured for the uncertainty experiment. The heavier weighting of the frequency distribution to the lower end of the spectrum reflects typical EUT measurement experience*

Based on the procedure outlined above, data was generated in the following combinations:

4 different conductors:

- 220V phase
- 220V neutral
- 110V phase
- 110V neutral

4 different measurement types:

- sinusoidal source, measured with quasi-peak detector
- pulsed source, measured with quasi-peak detector
- pulsed source, measured with average detector
- pulsed source, measured with peak detector

For conducted emissions measurements of an EUT, the values given in the final compliance test report are typically both quasi-peak and average amplitudes at a given frequency for a given conductor. The type of signal measured may be sinusoidal, pulsed (of varying repetition rates), or any combination of these two types. Therefore, the final uncertainty measurement result should be reported individually for each conductor, and individually for each detector, but the source types should be statistically combined because an EUT by definition has an unknown type of source. (Note that it is assumed that the peak, quasi-peak and average measurements of the sinusoidal signal will all be identical: because the

sinusoid does not vary with time, by definition the response of these three detectors will be the same. For this reason, the sinusoidal (or “CW”) result will be used in the uncertainty calculations for all three detector types.)

From Chapter 4, the simulated value of the total insertion loss from the input of the coupling box to the output of the LISN is known. Because of the output amplitudes available from the two different signal generators used for these measurements, and because of the sensitivities of the various detectors (versus their respective measurement noise floors), the final simulation was customized for each of the measurement setups as described in Table 5.1. (Note: “Attenuator” refers to the RF attenuator placed at the synthesizer input to the coupling box. The average measurement required a smaller attenuator because of the reduced dynamic range of the detector. Per the discussion in Section 4.3, the 6dB attenuator was sufficient to dampen the series resonance that may occur when no attenuator was used.)

*Table 5.1: Test Instrumentation Setup for Uncertainty Measurements*

	<b>Source Type</b>	<b>Detector</b>	<b>Amplitude</b>	<b>Attenuator</b>	<b>Rep. Rate</b>
1	Sinusoidal (CW)	QP	77dBuV	20dB	N/A
2	Pulsed	QP	60dBuV	20dB	100Hz
3	Pulsed	AVG	60dBuV	6dB	200Hz
4	Pulsed	PK	60dBuV	20dB	100Hz

Given the test setups defined in Table 5.1, the simulated values were generated using PSpice. However, all of the devices shown in Figure 4.1 cannot be assumed to have ideal or lossless responses. Thus, the simulation result was corrected per (5.1):

$$V_{sim,corr}[f] = V_{sim}[f] - H_{plug}[f] - CF[f] \quad (5.1)$$

$$CF[f] \equiv IL_{cable} + ERR_{attenuator} + ERR_{source\_amp} + DETECTOR\_ADJ$$

where:  $H_{plug}$  = insertion loss due to AC plug discontinuity  
 (see Table 5.1, NEMA 5-15 was used for 110V LISN,  
 CEE 7/7 was used for 220V LISN)  
 $CF$  = correction factor due to test setup  
 $IL_{cable}$  = insertion loss of cable from signal generator to  
 coupling box  
 $ERR_{attenuator}$  = error between ideal attenuator (as simulated)  
 and measured attenuation value  
 $ERR_{source\_amp}$  = error between ideal source amplitude (as  
 simulated) and measured amplitude  
 $DETECTOR\_ADJ$  = adjustment per CISPR 16-1 detector  
 type definition to account for pulse response of the  
 various detectors used (qp, avg, pk)

Note that the  $V[f]$  brackets indicate the result is frequency dependent, and is thus measured in discrete frequency steps ( $f$  in parenthesis would have indicated a continuous frequency domain). Finally, the error between the measured trials and the simulated value is computed per (5.2):

$$ERR^i[f] = V_{meas}^i[f] - V_{sim,corr}[f] \quad (5.2)$$

where:  $i$  indicates the  $i$ th measurement trial (of 16 total)

*Note that the  $V_{meas}$  value is measured per standard conducted emissions methods and thus includes the LISN and cable loss factors that are part of the measurement system.*

The standard deviation is computed across all samples in  $ERR$ , including the 16 trials ( $i$ ) and the 48 frequency steps ( $f$ ). This data represents the complete statistical variation of the measurement for these three supporting reasons:

1. The amplitudes chosen for the signal source are close to the Class B conducted emissions limit. Because this is the amplitude around which EUT pass/fail determinations are made, this is the amplitude of interest (thus varying amplitudes are not considered by this investigation).
2. The frequency steps chosen add additional weighting to the lower end of the spectrum, per EUT measurement experience. Using this scale, emissions are equally likely to occur anywhere in the measurement spectrum, so they are included in whole in the standard deviation calculation.
3. The 16 independent trials represent the variation of the measurement system over time and test setup, so they are all included in the statistical variation as well.

As described previously, this result will be reported once for each conductor (4 total) and measurement type (4 total), resulting in 16 unique statistical



measurements (each consisting of 16 trials with 48 unique frequencies steps) for the system. This brings the total number of measured data points in this study to 12288.

## **5.2 Measured Data**

Figures 5.2 to 5.17 show the measured results of the uncertainty study. Each line per figure represents one trial, for a total 16 trials per figure. This section reports the value of  $ERR[f]$  as defined in (5.2), and the following section will use this data to compute the full measurement uncertainty of the system. Table 5.2 then shows the standard deviations for each of the 16 unique statistical measurements.

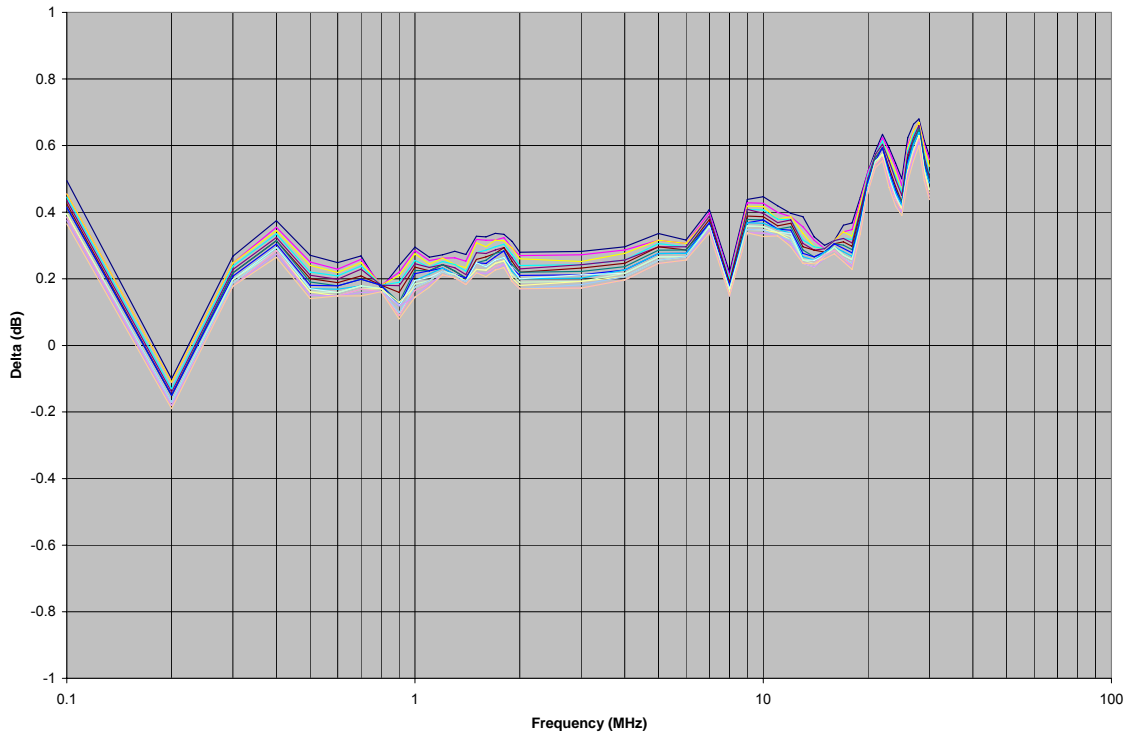


Figure 5.2:  $ERR[f]$ , 220V phase conductor, sinusoidal source, QP

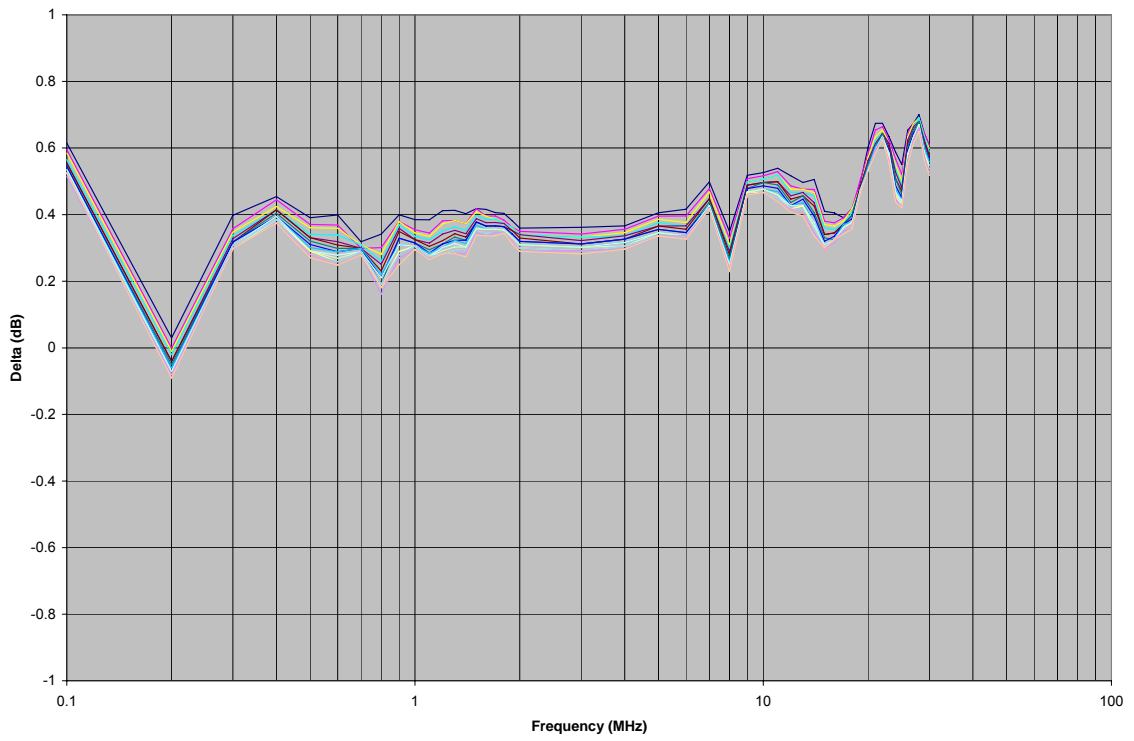


Figure 5.3:  $ERR[f]$ , 220V neutral conductor, sinusoidal source, QP

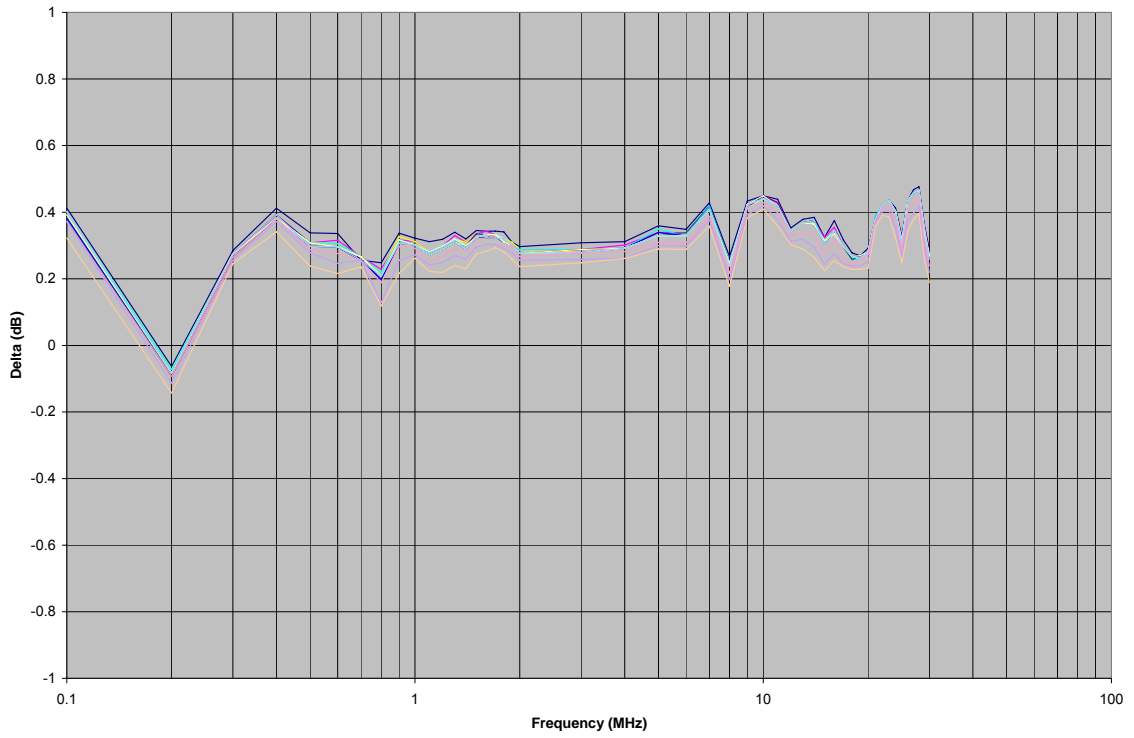


Figure 5.4:  $ERR[f]$ , 110V phase conductor, sinusoidal source, QP

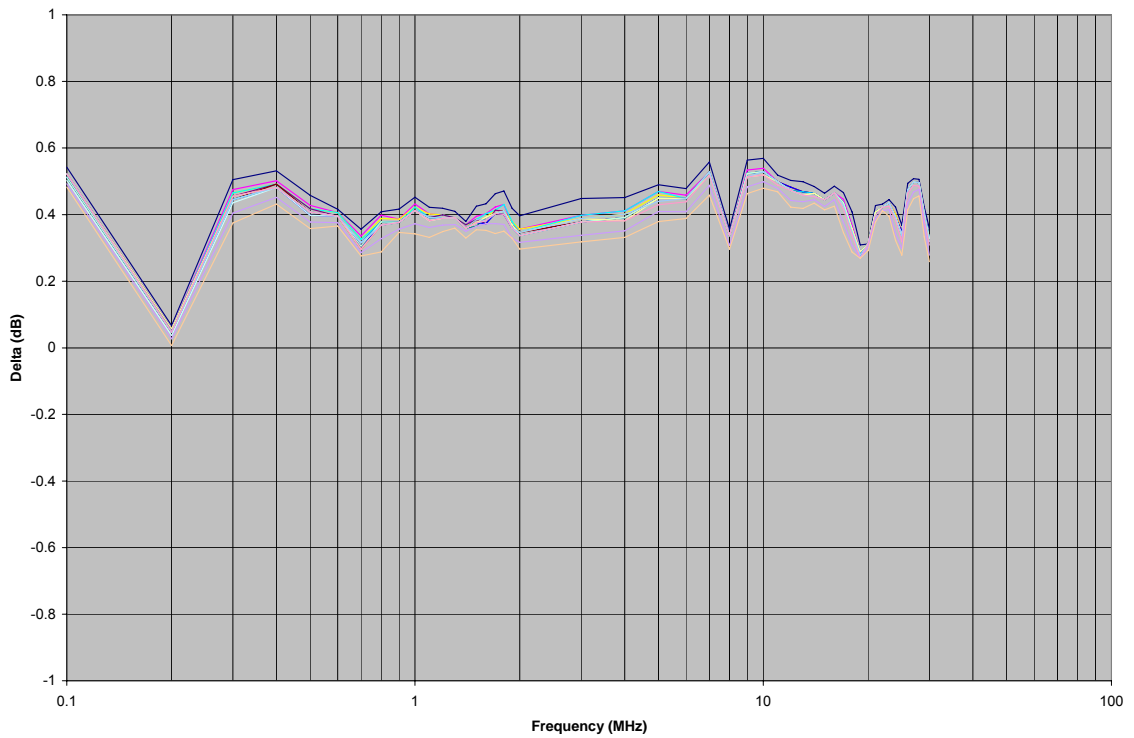


Figure 5.5:  $ERR[f]$ , 110V neutral conductor, sinusoidal source, QP

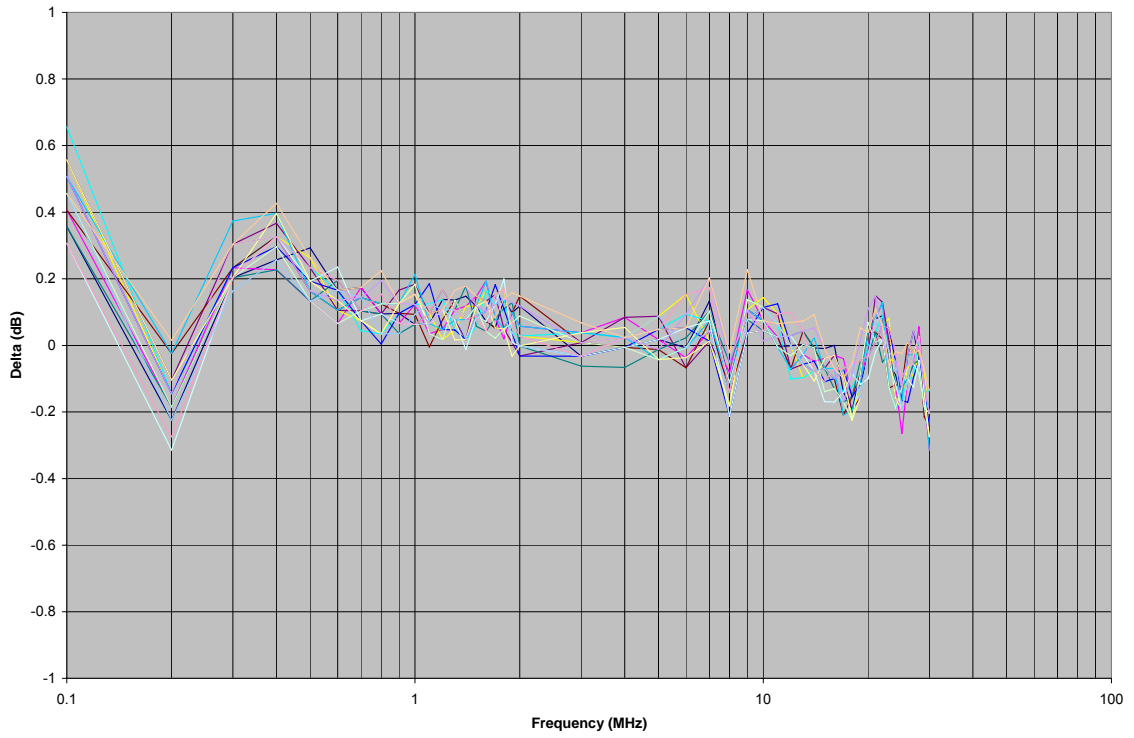


Figure 5.6:  $ERR[f]$ , 220V phase conductor, pulsed source, QP

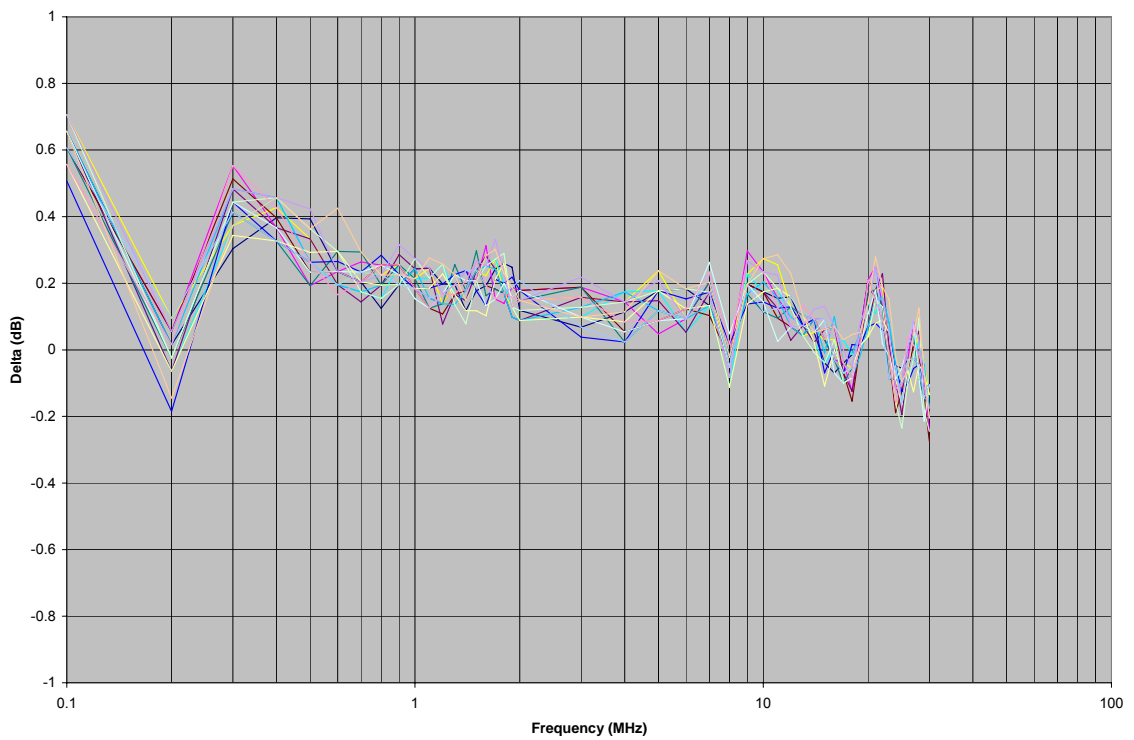


Figure 5.7:  $ERR[f]$ , 220V neutral conductor, pulsed source, QP

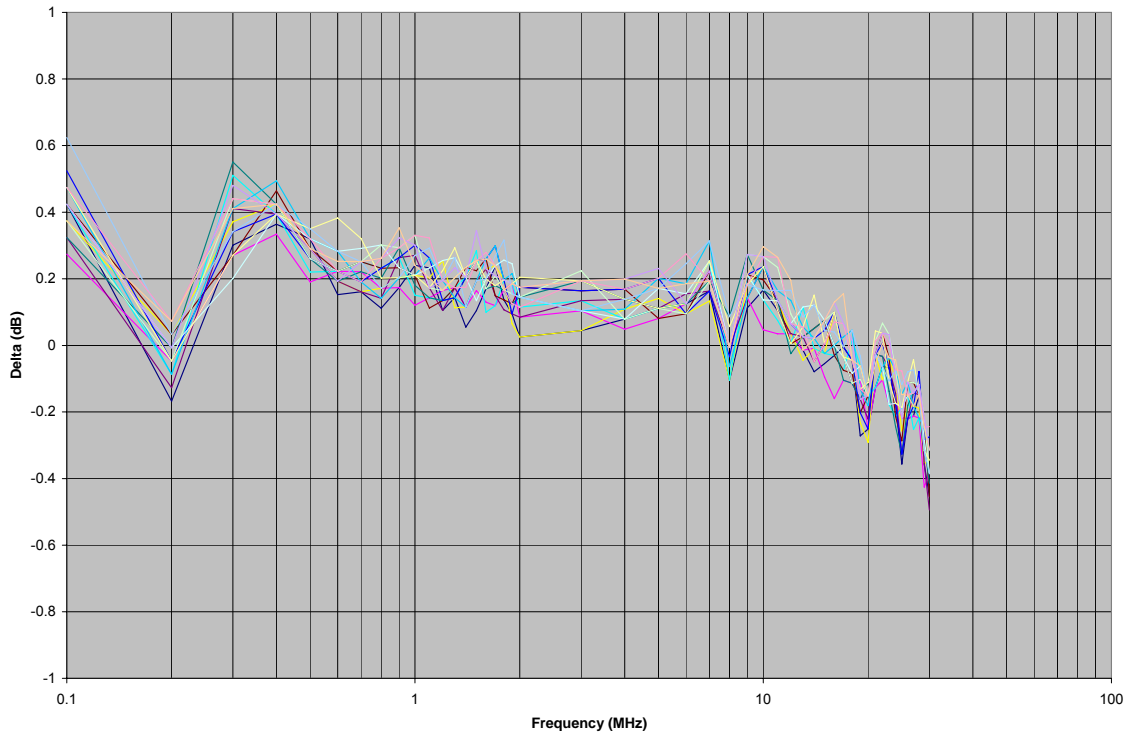


Figure 5.8:  $ERR[f]$ , 110V phase conductor, pulsed source, QP

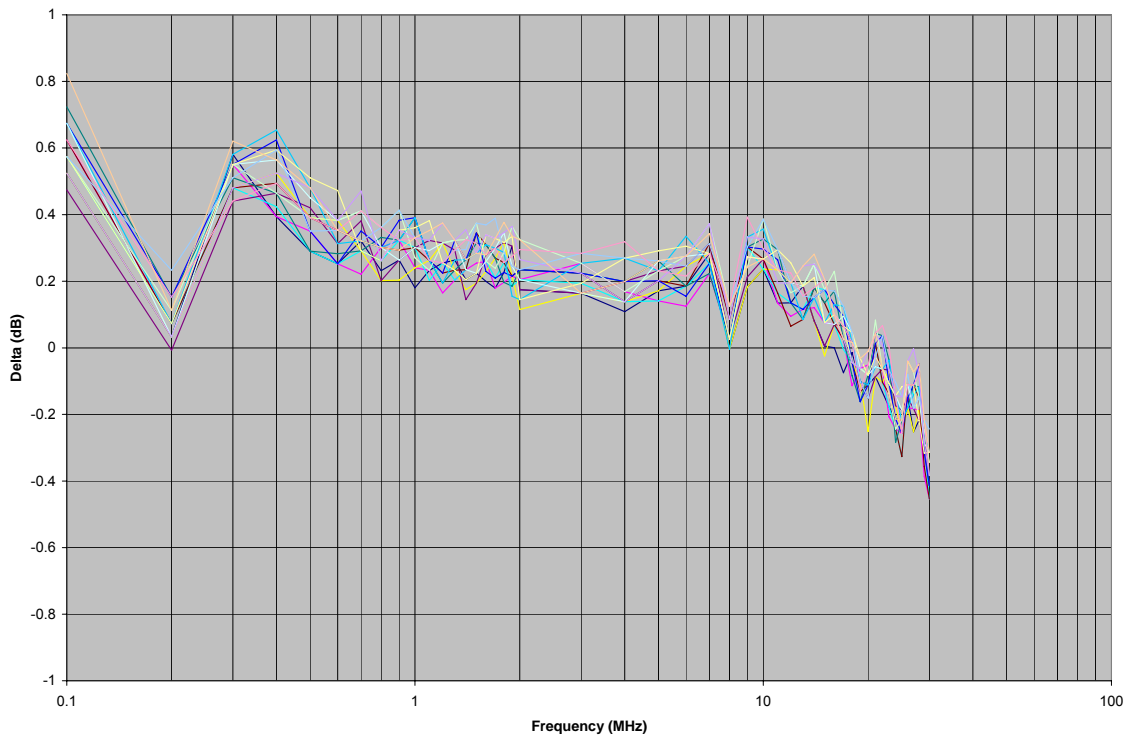


Figure 5.9:  $ERR[f]$ , 110V neutral conductor, pulsed source, QP

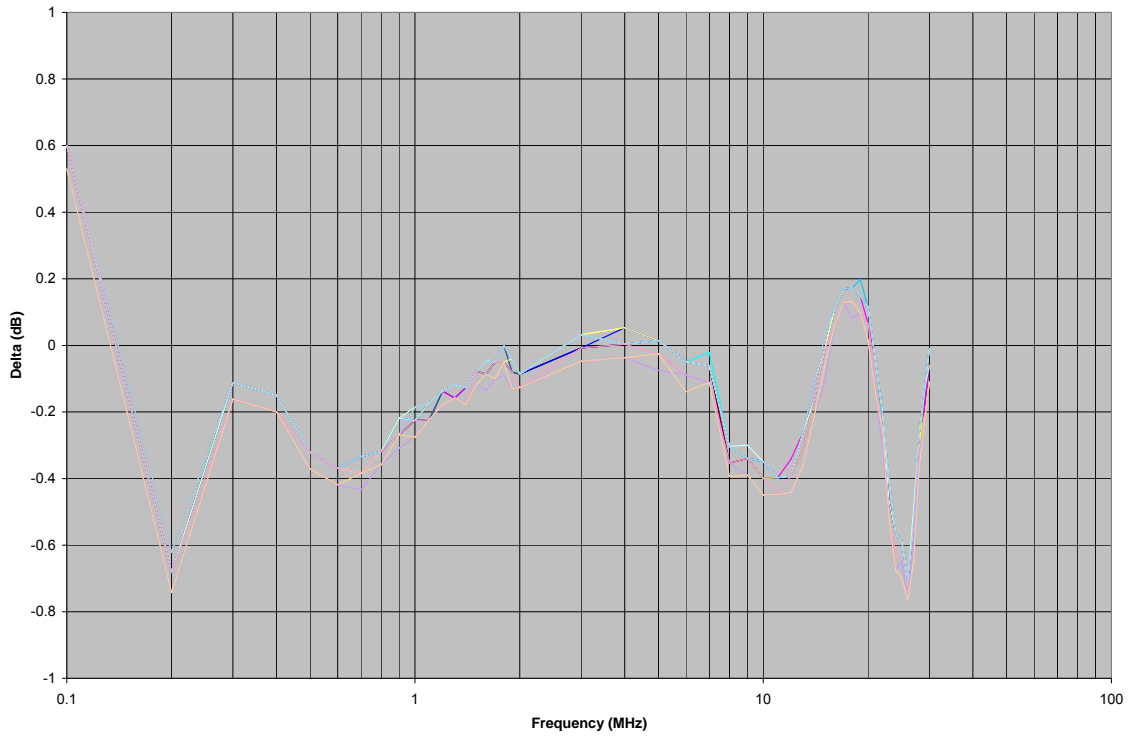


Figure 5.10: ERR[f], 220V phase conductor, pulsed source, AVG

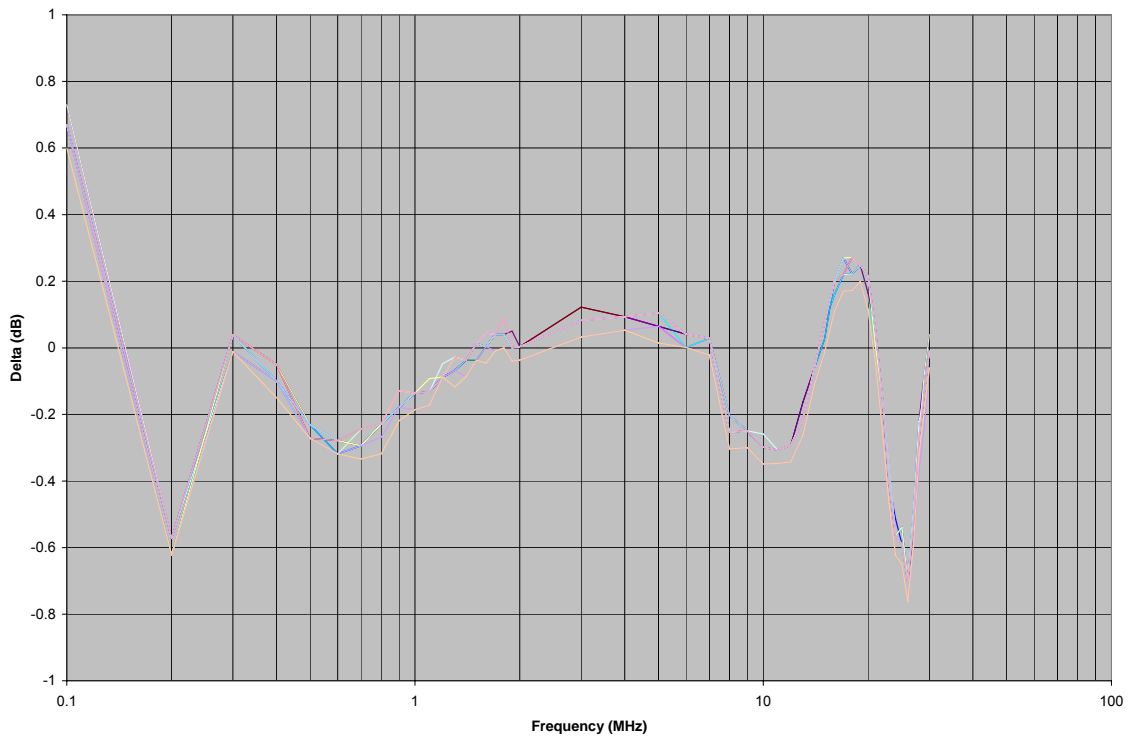


Figure 5.11: ERR[f], 220V neutral conductor, pulsed source, AVG

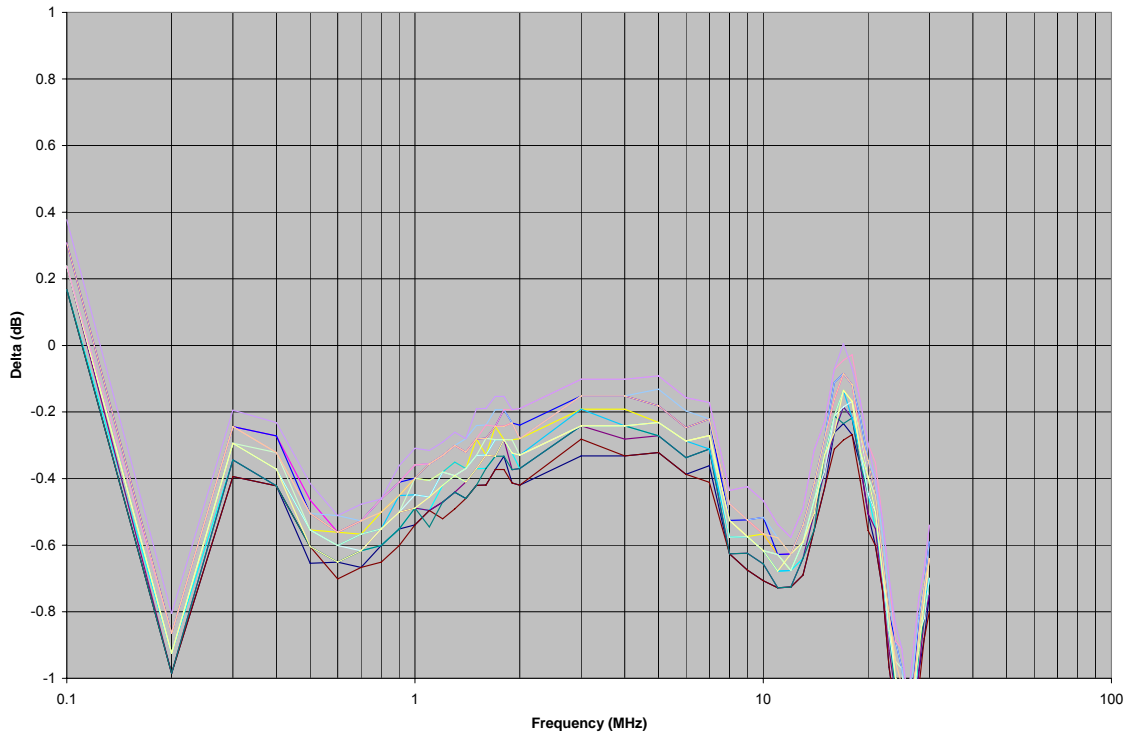


Figure 5.12:  $ERR[f]$ , 110V phase conductor, pulsed source, AVG

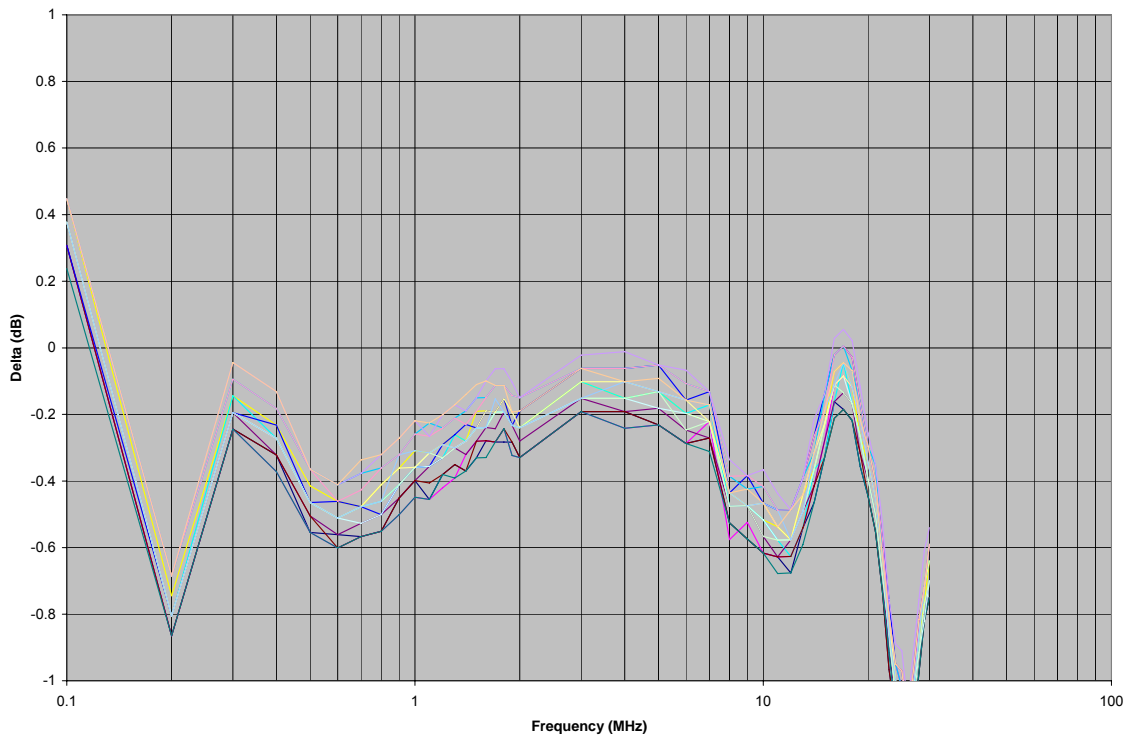


Figure 5.13:  $ERR[f]$ , 110V neutral conductor, pulsed source, AVG

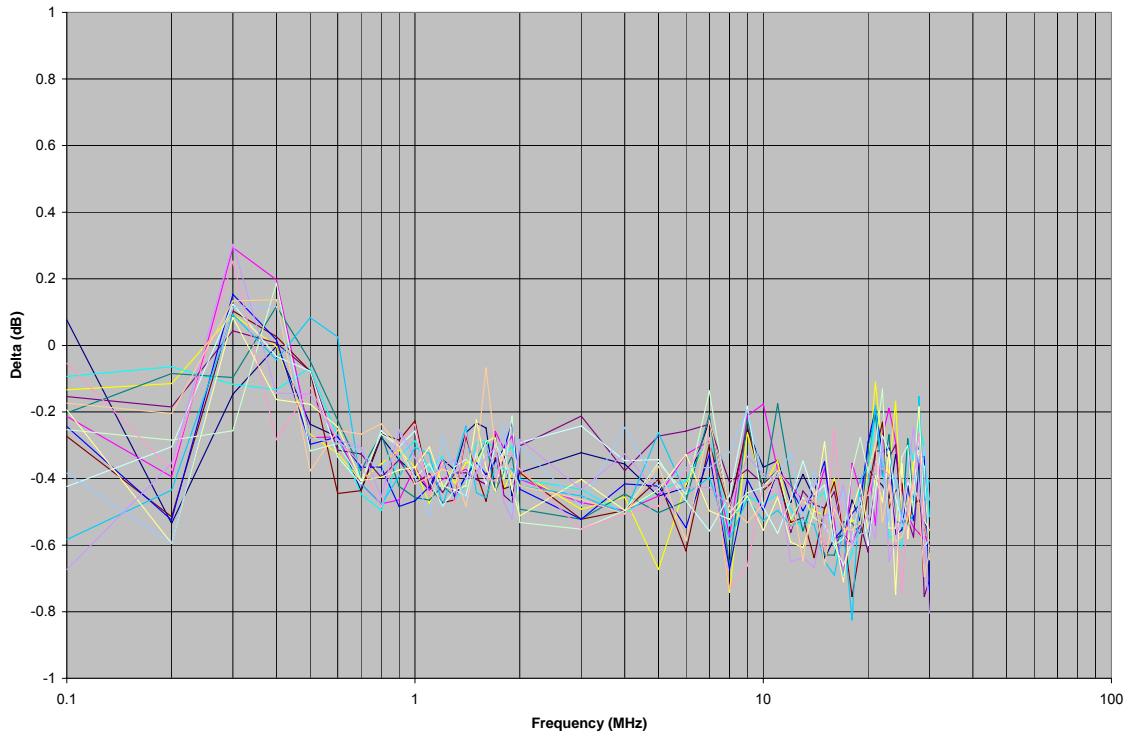


Figure 5.14: ERR[f], 220V phase conductor, pulsed source, PK

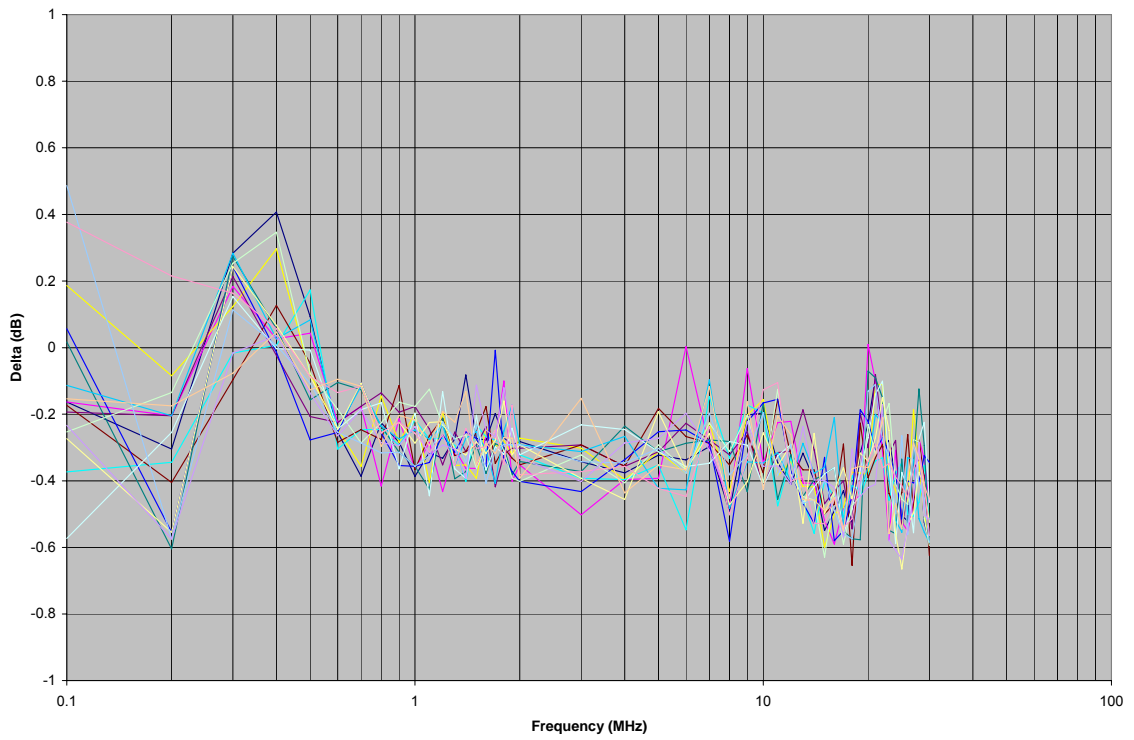


Figure 5.15: ERR[f], 220V neutral conductor, pulsed source, PK



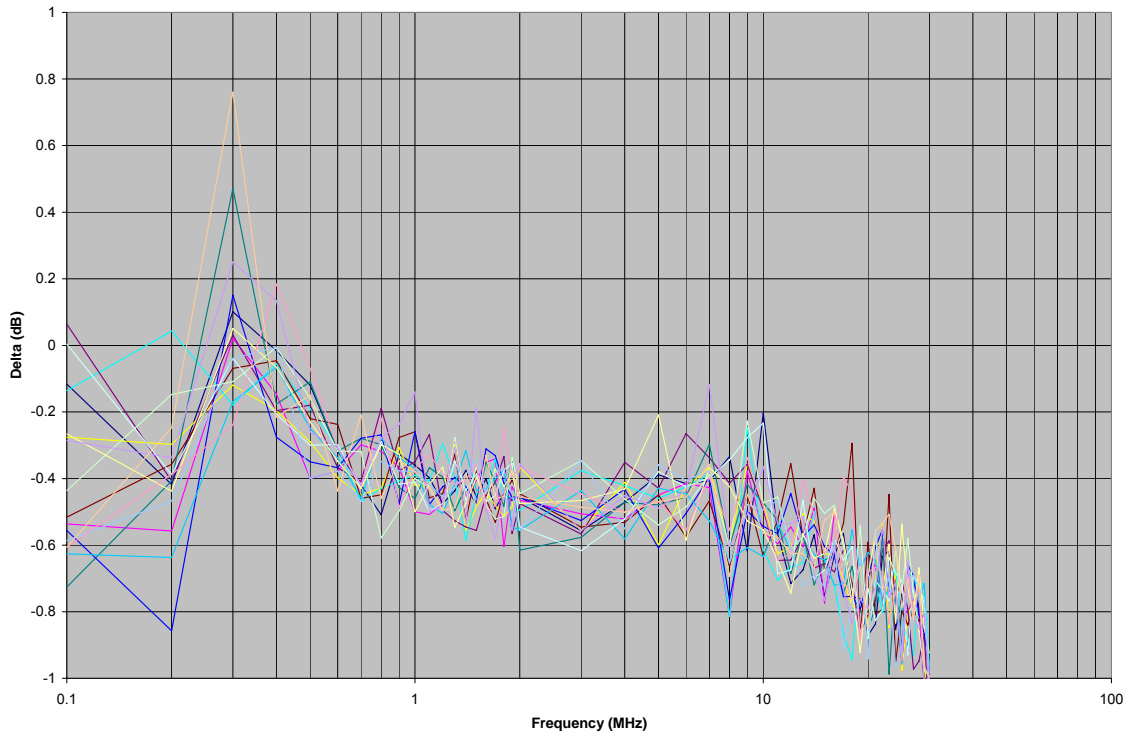


Figure 5.16: ERR[f], 110V phase conductor, pulsed source, PK

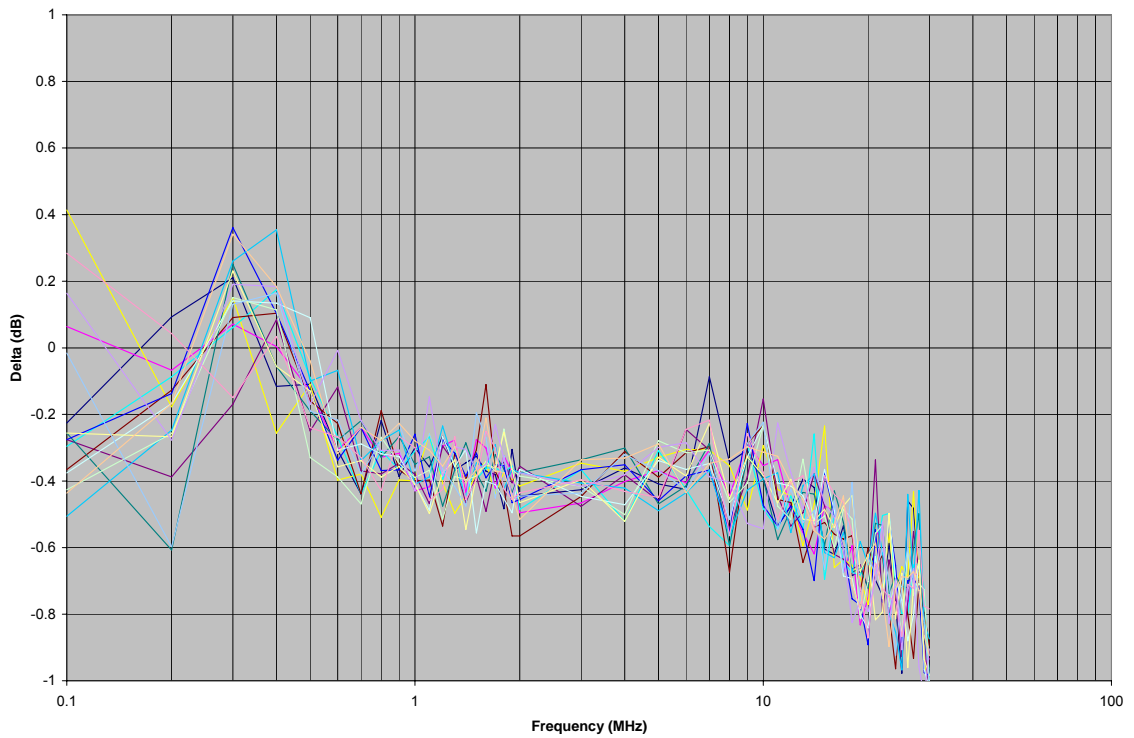


Figure 5.17: ERR[f], 110V neutral conductor, pulsed source, PK

Table 5.2: Measured Standard Deviations of ERR[f]

<b>Voltage</b>	<b>Conductor</b>	<b>Detector Type</b>	<b>Source Type</b>	<b>Standard Deviation (dB)</b>
110V	Neutral	QP	Sinusoidal (CW)	0.08158
110V	Neutral	QP	Pulsed-100Hz	0.219773
110V	Neutral	AVG	Pulsed-200Hz	0.305833
110V	Neutral	PK	Pulsed-100Hz	0.237431
110V	Phase	QP	Sinusoidal (CW)	0.087418
110V	Phase	QP	Pulsed-100Hz	0.186772
110V	Phase	AVG	Pulsed-200Hz	0.283668
110V	Phase	PK	Pulsed-100Hz	0.226048
220V	Neutral	QP	Sinusoidal (CW)	0.13509
220V	Neutral	QP	Pulsed-100Hz	0.155869
220V	Neutral	AVG	Pulsed-200Hz	0.253562
220V	Neutral	PK	Pulsed-100Hz	0.163999
220V	Phase	QP	Sinusoidal (CW)	0.150778
220V	Phase	QP	Pulsed-100Hz	0.136183
220V	Phase	AVG	Pulsed-200Hz	0.242239
220V	Phase	PK	Pulsed-100Hz	0.159514

### 5.3 Computation of Measurement Uncertainty

From Table 2.2 of Chapter 2, the total measurement uncertainty is the square root of the sum of the squares of each component of the uncertainty.

*Table 5.3: CISPR 16-4 Uncertainty components and their respective measurements*

<b>Input Quantity</b>	<b>Test Coverage</b>
1. Receiver reading	all measurements
2. Attenuation: AMN-receiver	all measurements
3. AMN voltage division factor	all measurements
4. Receiver corrections: a. Sine wave voltage b. Pulse amplitude response c. Pulse repetition rate response d. Noise floor proximity	sinusoidal (CW) signal measurement  pulsed measurements  pulsed measurements  noise floor measurement
5. Mismatch: AMN-receiver	all measurements
6. AMN impedance	LISN input impedance measurement

For each detector, the results for the sinusoidal source and the pulsed sources must be combined. It is assumed that these two factors are independent (unity coverage factors) as this provides a worst-case uncertainty determination. As

shown in Table 5.3, all components of the uncertainty (as defined in CISPR 16-4) have been accounted for by measurement, thus complete measurement uncertainty can now be calculated using (5.3):

$$U_{DET}^2 = U_{CW, SRC}^2 + U_{PLS, SRC}^2 + U_{CW, MEAS}^2 + U_{DET, MEAS}^2 + U_{CW, NF}^2 + U_{DET, NF}^2 + U_{Z, 0}^2 + U_{Z, \infty}^2 \quad (5.3)$$

where:

<b>Factor</b>	<b>Description</b>	<b>Reference</b>
$U_{DET}$	final calculated uncertainty of a given detector (QP, AVG, or PK)	Section 5.3.4
$U_{CW, SRC}$	uncertainty of the sinusoidal (CW) source	Section 5.3.1
$U_{PLS, SRC}$	uncertainty of the pulsed source	Section 5.3.1
$U_{CW, MEAS}$	measured stdev of the sinusoidal (CW) source	Table 5.2 (CW)
$U_{DET, MEAS}$	measured stdev of the pulsed source	Table 5.2 (QP, AVG, or PK)
$U_{CW, NF}$	uncertainty due to noise floor of the sinusoidal (CW) meas.	Section 5.3.2
$U_{DET, NF}$	uncertainty due to noise floor of the pulsed meas.	Section 5.3.2
$U_{Z, 0}$	uncertainty due to LISN impedance mismatch to voltage source at EUT port (zero impedance)	Section 5.3.3
$U_{Z, \infty}$	uncertainty due to LISN impedance mismatch to current source at EUT port (infinite impedance)	Section 5.3.3

### 5.3.1 Uncertainty of Sinusoidal and Pulsed Signal Sources

For the  $U_{CW, SRC}$  parameter, one could choose to use the manufacturer's datasheet or the instrument's calibration report to report the uncertainty of the sinusoidal source. However, these uncertainties would consider the entire range operating and environmental conditions for the instrument and thus would be much larger than the limited range of operation used in this test. For this case, the SML01 instrument is capable of generating frequencies up to 1.1GHz, but 30MHz is the maximum frequency used here. Therefore, statistical measurements were made of the output of the SML01 over the frequencies defined in Figure 5.1 and amplitudes in Table 5.1 using a highly accurate instrument: a Rohde & Schwarz NRVD watt-meter. The wattmeter includes software that determines the uncertainty of this measurement, which is shown in Figure 5.18:

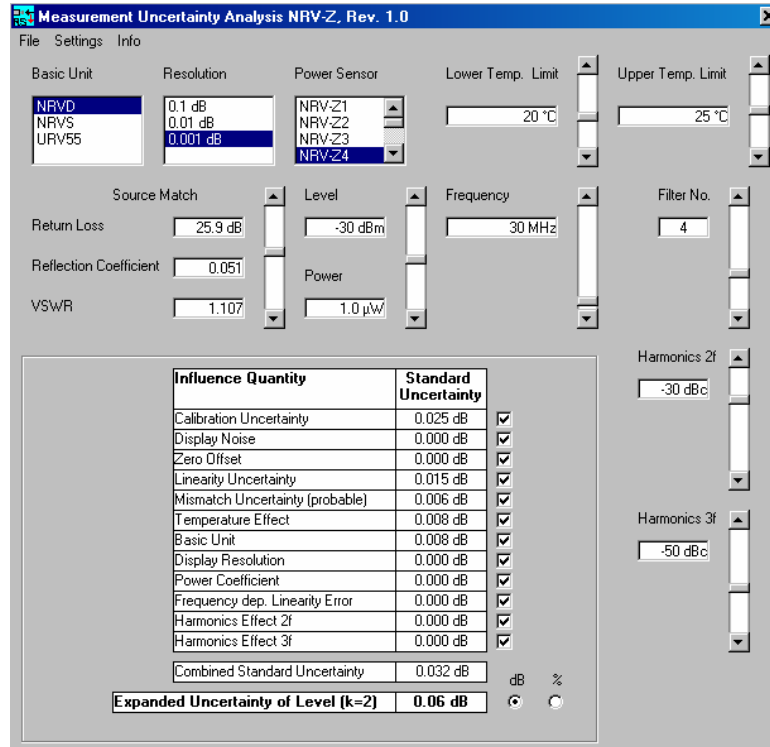


Figure 5.18: Measurement uncertainty of NRVD wattmeter used to characterize sinusoidal signal source

Based on these repeated measurements, the final uncertainty of the sinusoidal source is calculated as  $\sqrt{.032^2 + .0052^2} = .0324dB$  with expanded uncertainty (k=2) equal to 0.0648 dB.

For the  $U_{PLS, SRC}$  parameter, no instrument is available that can measure the output amplitude of the broad-banded pulse any more accurately than the manufacturer's reported uncertainty of 0.25 dB. Therefore, this is the value that will be used for the pulsed source uncertainty.

### 5.3.2 Uncertainty Due to Measuring Instrument Noise Floor

For the  $U_{CW,NF}$  and  $U_{DET,NF}$  parameters, the noise floor measurement is shown in Figure 5.19. The resulting noise floor uncertainties are reported in Table 5.4, and the measured noise floor of each detector were used in (5.4):

$$V_{NF,CW,total}^{linear}[f] = V_{sim,corr}^{linear}[f] + V_{NF,CW,meas}^{linear}[f]$$

$$U_{NF,CW} = stdev(V_{NF,CW,total}^{dB}[f] - V_{sim,corr}^{dB}) \quad (5.4a)$$

$$V_{NF,DET,total}^{linear}[f] = V_{sim,corr}^{linear}[f] + V_{NF,DET,meas}^{linear}[f]$$

$$U_{NF,DET} = stdev(V_{NF,DET,total}^{dB}[f] - V_{sim,corr}^{dB}) \quad (5.4b)$$

where:  $V_{NF,CW,meas}^{linear}[f]$  = the measured amplitude (in linear units) of the noise floor

for the sinusoidal (CW) signal measurement

$V_{NF,DET,meas}^{linear}[f]$  = the measured amplitude (in linear units) of the

noise floor for a given detector

$V_{sim,corr}^{linear}[f]$  = the corrected simulated amplitude (in linear units) of the

uncertainty measurement setup

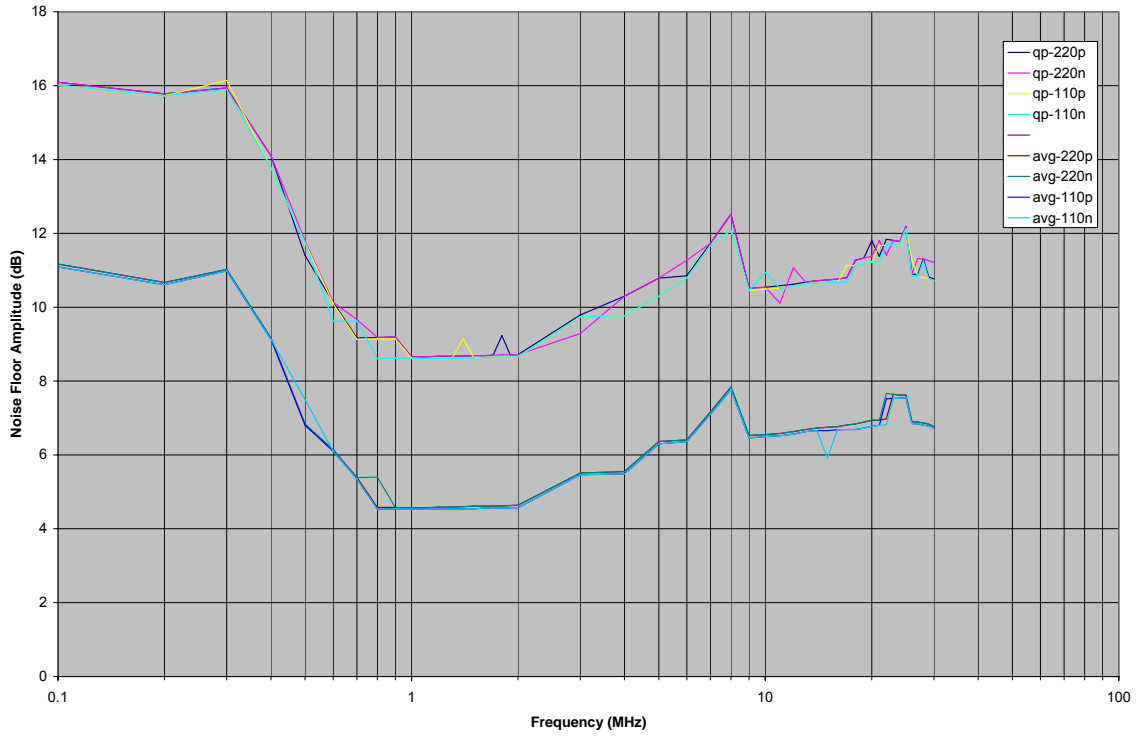


Figure 5.19: Measured noise floor for the various test configurations

Table 5.4: Measurement uncertainty due to noise floor (dB) for a given detector

Uncertainty	DET	Source Type	220	220	110	110
			Phase	Neutral	Phase	Neutral
$U_{NF,CW}$	QP	Sinusoidal (CW)	0.04	0.04	0.04	0.04
$U_{NF,QP}$	QP	Pulsed-100Hz	0.24	0.24	0.24	0.24
$U_{NF,AVG}$	AVG	Pulsed-200Hz	0.17	0.17	0.17	0.17
$U_{NF,PK}$	PK	Pulsed-100Hz	0.12	0.12	0.12	0.12



### 5.3.3 Uncertainty Due to LISN Input Impedance Mismatch

The final parameters to be found for (5.3) are  $U_{Z,0}$  and  $U_{Z,\infty}$ . These factors are due to the fact that the LISN input impedance (measured at the EUT port) is not ideal, causing non-ideal mismatches to an EUT of unknown impedance. To account for this, the two extreme cases are considered: an EUT that behaves as a voltage source (zero impedance), and an EUT that behaves as a current source (infinite impedance). These two are considered independent contributors to the measurement uncertainty, and since all real-world sources are equally likely to be either type, a 50% coverage factor is used for each. These parameters are calculated per (5.5), shown in Figure 5.20, and reported in Table 5.5:

$$ERR_Z[f] = Z_{meas}[f] - Z_{sim}[f] \quad (5.5)$$

$$U_{Z,\infty} = stdev \left[ 20 * \log_{10} \left( 1 - \frac{ERR_Z[f]}{Z_{sim}[f]} \right) \right]$$

$$U_{Z,0} = 0 \quad (\text{by definition, a voltage source's output does not vary by load impedance})$$

where:  $Z_{meas}[f]$  = the measured input impedance of the LISN (defined at the EUT port)

$Z_{sim}[f]$  = the simulated input impedance of the LISN per Figure 2.3(a)

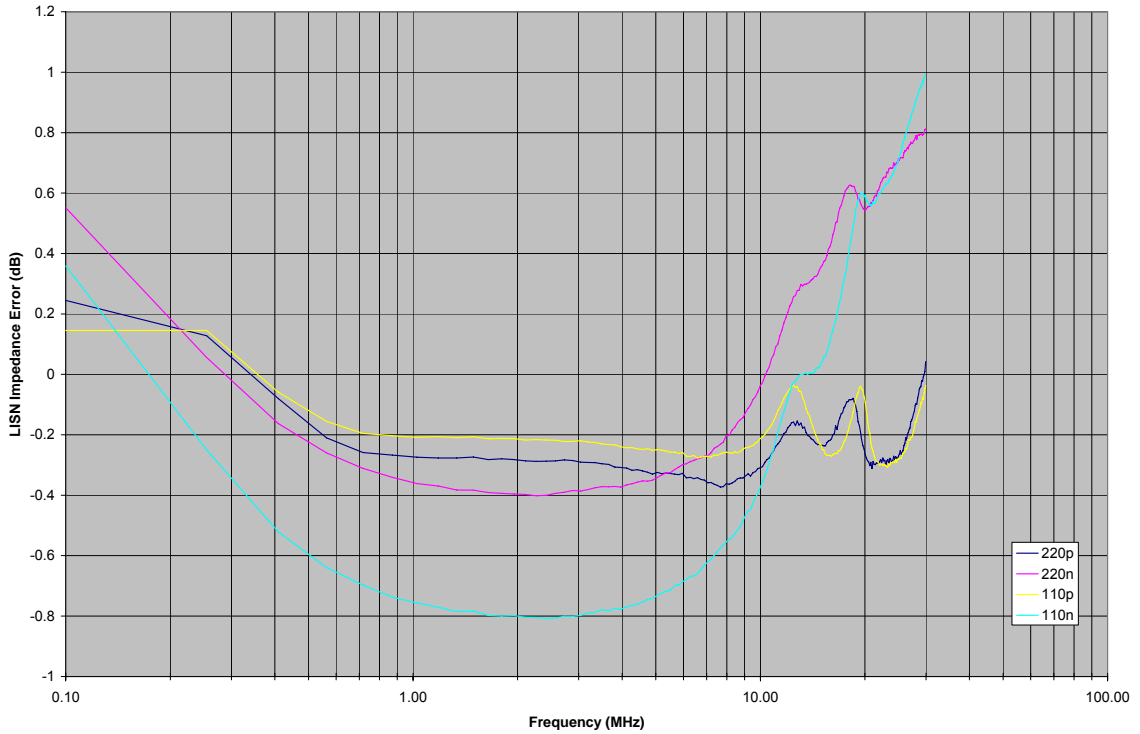


Figure 5.20: Uncertainty due to LISN EUT input impedance mismatch (for a current source)

Table 5.5: Measurement uncertainty due to LISN EUT input impedance mismatch (dB)

	<b>220 Phase</b>	<b>220 Neutral</b>	<b>110 Phase</b>	<b>110 Neutral</b>	<b>Notes</b>
$U_{Z,0}$ (Voltage Source)	0.00	0.00	0.00	0.00	lower bound of EUT mismatch, zero impedance
$U_{Z,\infty}$ (Current Source)	0.10	0.43	0.08	0.61	upper bound of EUT mismatch, infinite impedance

### 5.3.4 Final Calculated Measurement Uncertainty Values

Finally, based on all of these measured parameters, the total uncertainty can be calculated using (5.3). The results are given in Table 5.6, including coverage to the 95% confidence interval (the expanded uncertainty per CISPR 16-4 [2],  $k=2$ ).

*Table 5.6: Final measurement uncertainty values (dB)*

		<b>QP</b>	<b>k=2</b>	<b>AVG</b>	<b>k=2</b>	<b>PK</b>	<b>k=2</b>
<b>110V</b>	<b>Neutral</b>	0.52	1.04	0.53	1.07	0.48	0.96
<b>110V</b>	<b>Phase</b>	0.41	0.82	0.43	0.86	0.37	0.74
<b>220V</b>	<b>Neutral</b>	0.51	1.02	0.47	0.94	0.41	0.82
<b>220V</b>	<b>Phase</b>	0.41	0.82	0.42	0.84	0.36	0.72

As can be seen, the final worst-case expanded uncertainty, 1.07dB, is much less than the allowable value of 3.60dB defined in CISPR 16-4 (shown in Table 2.2 in this report). The immediate conclusion that can be drawn from this result is that this conducted measurement setup is acceptable for conducted emissions measurements, and high levels of accuracy can be expected.

## CHAPTER 6: ANALYSIS AND CONCLUSIONS

### 6.1 Dominant Uncertainty Factors

Equation (5.3) lists eight separate factors that contribute to the total uncertainty of the conducted emissions measurement system. Chapter 5 previously described the complete set of data for this system including each of these parameters for each possible measurement detector, conductor, and measurement frequency. If one desired to lower the uncertainty of their system, the largest impact could be realized by focusing on the dominant items, that is, those with the largest magnitude. Tables 6.1 – 6.3 summarize each of the factors found in Chapter 5 for the three types of detectors.

For the case of the quasi-peak detector (Table 6.1), the largest factors are the LISN impedance mismatch (0.30dB), uncertainty of the pulsed source (0.25dB), and the pulsed source noise floor (0.24dB). Based on these factors, the most effective way to lower the overall uncertainty of this measurement is to modify the LISN to improve its mismatch. Following that, the next item would be to use a more accurate pulse source for uncertainty measurement, and finally, to increase the signal-to-noise-floor margin of the uncertainty measurement. Determination of the dominant factors for the other two detectors types is done in the same manner using Tables 6.2 and 6.3.

Table 6.1: Uncertainty Factors (dB) for the Quasi-Peak Detector

Factor	Description	110V Neutral	110V Phase	220V Neutral	220V Phase	Aver- age
$U_{CW, SRC}$	uncertainty of the sinusoidal (CW) source	0.032	0.032	0.032	0.032	0.032
$U_{PLS, SRC}$	uncertainty of the pulsed source	0.25	0.25	0.25	0.25	0.25
$U_{CW, MEAS}$	measured stdev of the sinusoidal (CW) source	0.08	0.09	0.14	0.15	0.12
$U_{DET, MEAS}$	measured stdev of the pulsed source	0.22	0.19	0.16	0.14	0.18
$U_{CW, NF}$	uncertainty due to noise floor of the sinusoidal (CW) meas.	0.04	0.04	0.04	0.04	0.04
$U_{DET, NF}$	uncertainty due to noise floor of the pulsed meas.	0.24	0.24	0.24	0.24	0.24
$U_{Z,0}$	uncertainty due to LISN impedance mismatch to voltage source at EUT port (zero impedance)	0	0	0	0	0
$U_{Z,\infty}$	uncertainty due to LISN impedance mismatch to current source at EUT port (infinite impedance)	0.61	0.08	0.43	0.10	0.30
TOTAL (sum squares method)		0.52	0.41	0.51	0.41	0.51
<b>EXPANDED UC (k=2)</b>		<b>1.04</b>	<b>0.82</b>	<b>1.02</b>	<b>0.82</b>	<b>1.02</b>

Table 6.2: Uncertainty Factors (dB) for the Average Detector

Factor	Description	110V Neutral	110V Phase	220V Neutral	220V Phase	Aver- age
$U_{CW, SRC}$	uncertainty of the sinusoidal (CW) source	0.032	0.032	0.032	0.032	0.032
$U_{PLS, SRC}$	uncertainty of the pulsed source	0.25	0.25	0.25	0.25	0.25
$U_{CW, MEAS}$	measured stdev of the sinusoidal (CW) source	0.08	0.09	0.14	0.15	0.12
$U_{DET, MEAS}$	measured stdev of the pulsed source	0.31	0.28	0.25	0.24	0.27
$U_{CW, NF}$	uncertainty due to noise floor of the sinusoidal (CW) meas.	0.04	0.04	0.04	0.04	0.04
$U_{DET, NF}$	uncertainty due to noise floor of the pulsed meas.	0.17	0.17	0.17	0.17	0.17
$U_{Z,0}$	uncertainty due to LISN impedance mismatch to voltage source at EUT port (zero impedance)	0	0	0	0	0
$U_{Z,\infty}$	uncertainty due to LISN impedance mismatch to current source at EUT port (infinite impedance)	0.61	0.08	0.43	0.10	0.30
TOTAL (sum squares method)		0.53	0.43	0.47	0.42	0.46
<b>EXPANDED UC (k=2)</b>		<b>1.07</b>	<b>0.86</b>	<b>0.94</b>	<b>0.84</b>	<b>0.92</b>

Table 6.3: Uncertainty Factors (dB) for the Peak Detector

Factor	Description	110V Neutral	110V Phase	220V Neutral	220V Phase	Aver- age
$U_{CW, SRC}$	uncertainty of the sinusoidal (CW) source	0.032	0.032	0.032	0.032	0.032
$U_{PLS, SRC}$	uncertainty of the pulsed source	0.25	0.25	0.25	0.25	0.25
$U_{CW, MEAS}$	measured stdev of the sinusoidal (CW) source	0.08	0.09	0.14	0.15	0.12
$U_{DET, MEAS}$	measured stdev of the pulsed source	0.24	0.23	0.16	0.16	0.20
$U_{CW, NF}$	uncertainty due to noise floor of the sinusoidal (CW) meas.	0.04	0.04	0.04	0.04	0.04
$U_{DET, NF}$	uncertainty due to noise floor of the pulsed meas.	0.12	0.12	0.12	0.12	0.12
$U_{Z,0}$	uncertainty due to LISN impedance mismatch to voltage source at EUT port (zero impedance)	0	0	0	0	0
$U_{Z,\infty}$	uncertainty due to LISN impedance mismatch to current source at EUT port (infinite impedance)	0.61	0.08	0.43	0.10	0.30
	TOTAL (sum squares method)	0.48	0.37	0.41	0.36	0.40
	<b>EXPANDED UC (k=2)</b>	<b>0.96</b>	<b>0.74</b>	<b>0.82</b>	<b>0.72</b>	<b>0.81</b>

## 6.2 Effectiveness of LISN Correction Factors

In Section 2.5, it was discussed that true uncertainty is the measurement variation observed once all known systematic errors (bias) are removed. The primary method for removing these errors is by generating the LISN correction factors, but as shown in Chapter 3, this method may introduce unwanted errors into the system. This potential for error brings up an important question: given that LISN correction factors are on the same order of magnitude (in dB) as the uncertainty of the equipment measuring them, is there a net gain in system uncertainty when these factors are used?

This can be answered from the data collected in Chapter 5. First, Table 6.4 shows the means and standard deviations of the measured values versus the model for each conductor/detector combination. It shows that in all cases the standard deviation is lower with the corrections applied, and in the overall average, the correction factor is closer to the model by 0.35dB.

The distribution of the measured values can also provide insight into the usefulness of the LISN correction factors. Figures 6.1 – 6.4 show histograms of the measured values versus the model for each source & detector configuration. What can be seen graphically, and is indicated by the standard deviations in Table 6.4, is that the application of the correction factors “normalizes” the histograms. That is to say, in all four cases the corrected histogram more closely



resembles a normal (Gaussian) distribution, whereas the uncorrected histograms show artifacts such as bimodal or non-symmetric behaviors.

Based on these calculations and distributions, it can be concluded for this measurement system that the LISN correction factors do indeed improve the quality of the measurement system and lower its overall uncertainty. This correction has the added benefit of validating the method by which the correction factors are measured.

Table 6.4: Effect of LISN Correction Factors on ERR[f] (dB)

Conductor	Detector	Source	Standard Deviation		Average Error	
			w/ CF	w/o CF	w/ CF	w/o CF
110V Neutral	QP	Sinusoidal (CW)	0.08	0.16	0.41	0.10
110V Neutral	QP	Pulsed 100Hz	0.22	0.34	0.15	-0.15
110V Neutral	AVG	Pulsed 200Hz	0.31	0.39	-0.41	-0.71
110V Neutral	PK	Pulsed 100Hz	0.24	0.36	-0.45	-0.75
110V Phase	QP	Sinusoidal (CW)	0.09	0.16	0.36	-0.01
110V Phase	QP	Pulsed 100Hz	0.19	0.35	0.12	-0.25
110V Phase	AVG	Pulsed 200Hz	0.28	0.40	-0.45	-0.81
110V Phase	PK	Pulsed 100Hz	0.23	0.38	-0.49	-0.86
220V Neutral	QP	Sinusoidal (CW)	0.14	0.14	0.41	0.07
220V Neutral	QP	Pulsed 100Hz	0.16	0.30	0.13	-0.21
220V Neutral	AVG	Pulsed 200Hz	0.25	0.32	-0.11	-0.45
220V Neutral	PK	Pulsed 100Hz	0.16	0.29	-0.31	-0.65
220V Phase	QP	Sinusoidal (CW)	0.15	0.13	0.32	-0.05
220V Phase	QP	Pulsed 100Hz	0.14	0.29	0.03	-0.33
220V Phase	AVG	Pulsed 200Hz	0.24	0.32	-0.18	-0.54
220V Phase	PK	Pulsed 100Hz	0.16	0.29	-0.39	-0.76
				<b>Overall Average:</b>	<b>-0.05</b>	<b>-0.40</b>

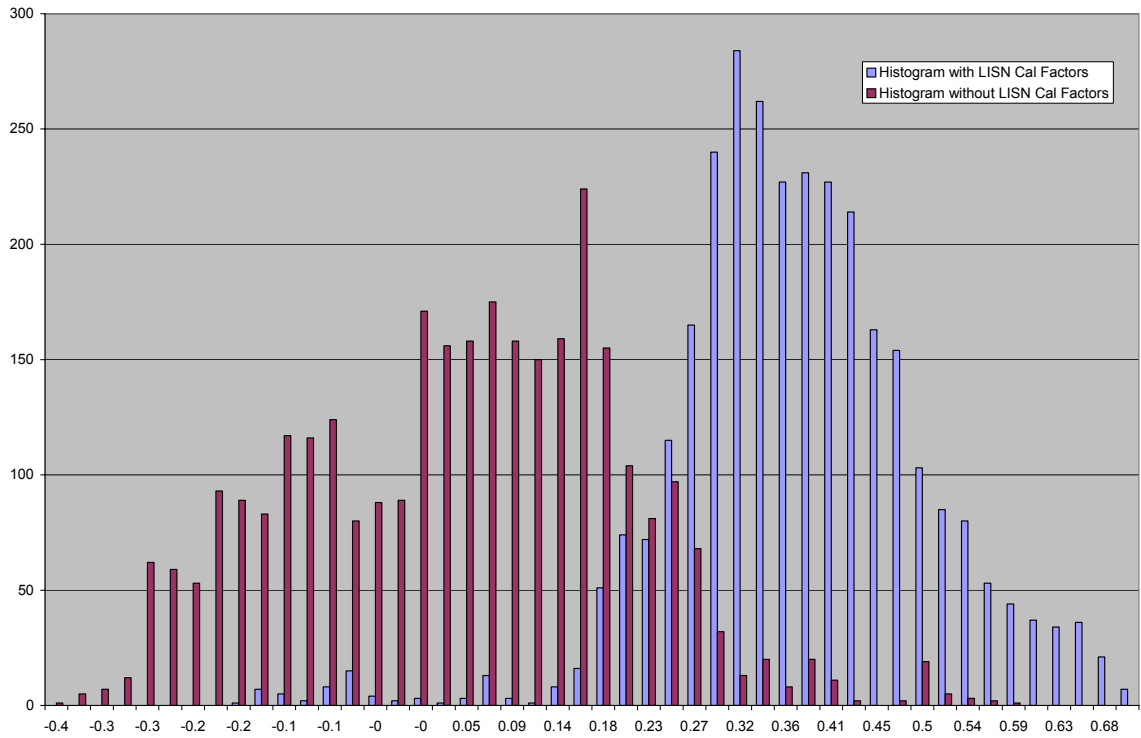


Figure 6.1: Histogram of  $ERR[f]$ , sinusoidal source, QP detector

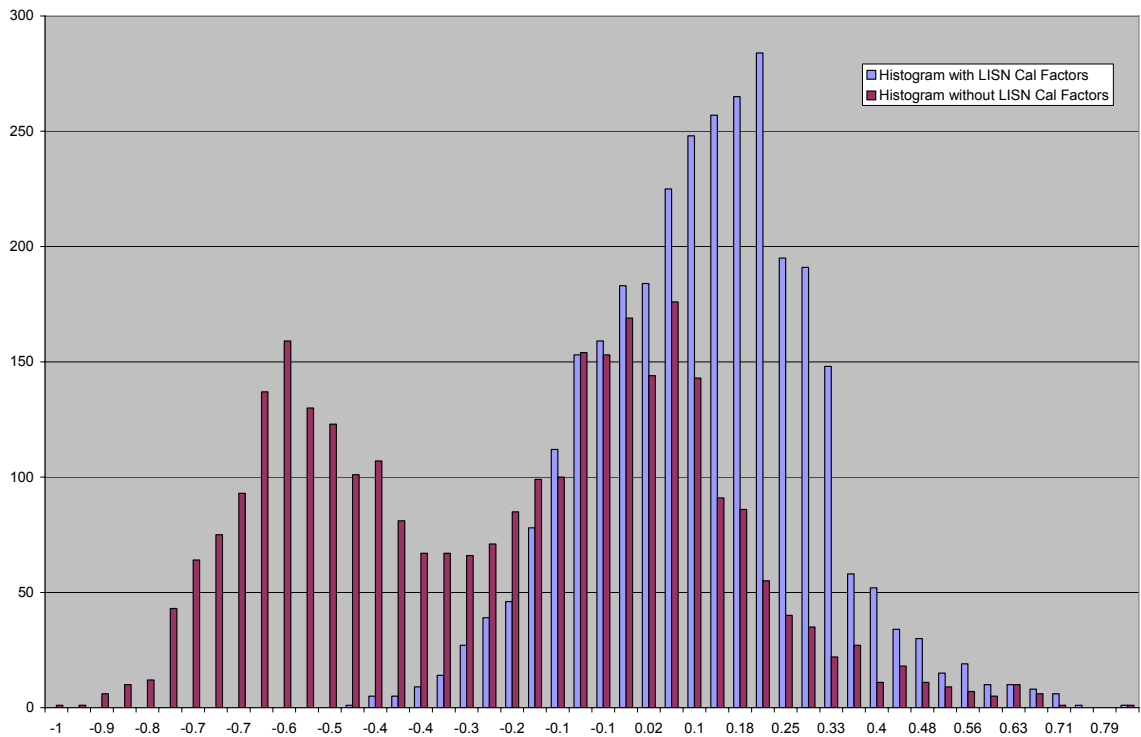


Figure 6.2: Histogram  $ERR[f]$ , pulsed source, QP detector

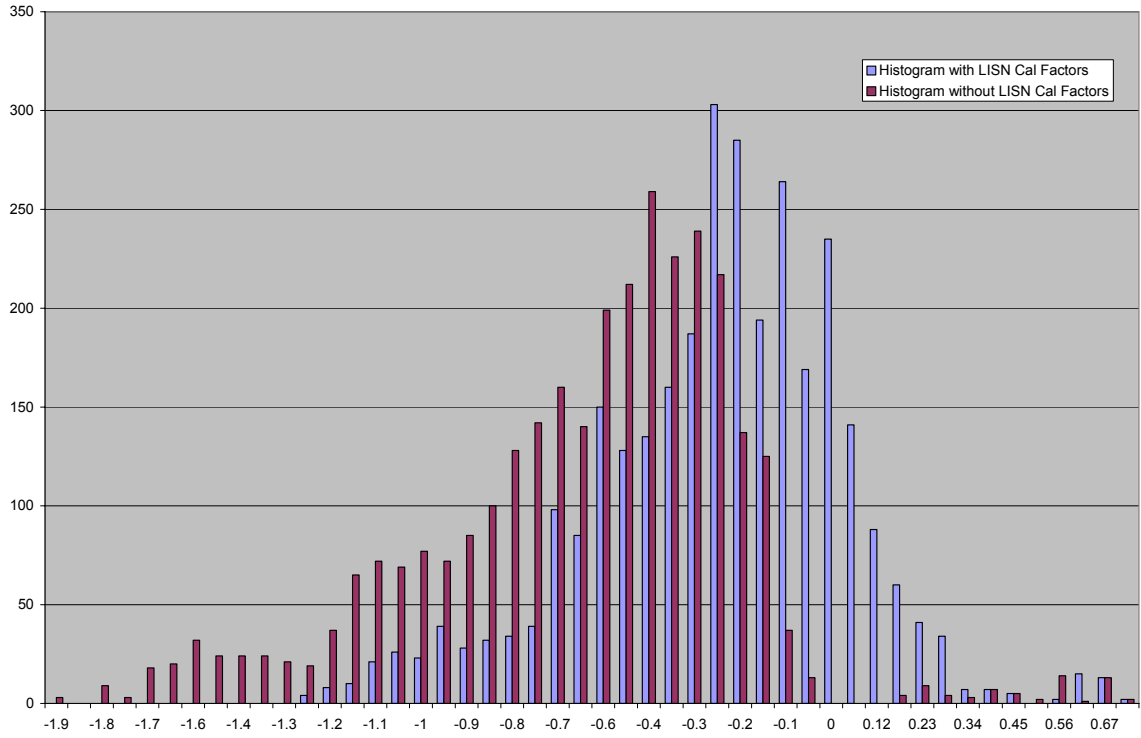


Figure 6.3: Histogram  $ERR[f]$ , pulsed source, AVG detector

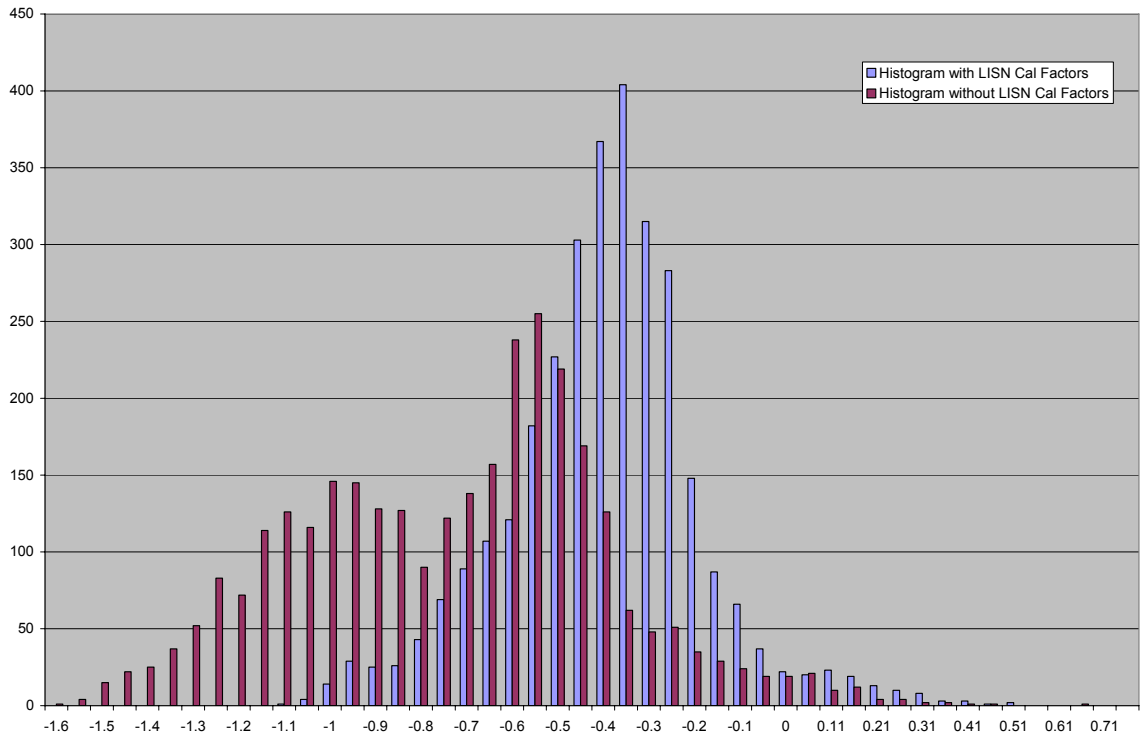


Figure 6.4: Histogram of  $ERR[f]$ , pulsed source, PK detector

### 6.3 Conclusions

A complete framework was created for characterizing the measurement uncertainty of a conducted emissions system. It has been shown that great care must be taken with each component that affects this uncertainty. This includes selection of measurement equipment, calibration of each piece of equipment, constructing proper uncertainty characterization procedures, and thorough analysis of the resulting data.

There are many advantages to such a system. The immediate benefit is meeting the minimum standards required by laboratory accreditation services (such as ISO, A2LA or NVLAP), or legal standards such as CISPR 16-4. But additionally, it allows the laboratory user to gain insight into the behavior of each part of the measurement system. One example is the validation of the LISN correction factors shown in Section 6.2, which proves accuracy versus an ideal model of the measurement system (this is shown in the reported ERR[f] of Figures 5.2 – 5.17, all approximately within 1 dB of the ideal simulated value). Also, the “coupling box” described in this document can be used to ensure on-going suitability of the measurement system. (For instance, a coupling box measurement at regular intervals can detect long-term drift or other influences that may affect measurements.) Finally, this framework determines quantitatively the factors influencing the uncertainty, so that efforts for uncertainty improvement can be maximized.

In conclusion, the measurement system characterized in this document has been proven to be suitable for highly accurate measurements with low uncertainty. Each factor influencing the uncertainty has been fully accounted for and included in the system characterization. This Type “A” uncertainty method provides the true uncertainty of the measurement system and allows the uncertainty value to be much lower overall.

## **BIBLIOGRAPHY**

FCC Code of Federal Regulations CFR 47, Parts 2 and 15, publicly available at <http://www.fcc.gov/oet/info/rules/part15/>

[1] CISPR Publication 16-4, "Uncertainty in EMC Measurements", April 2002

[2] United Kingdom Accreditation Service LAB 12, "The Expression of Uncertainty in Testing", September 1994

[3] United Kingdom Accreditation Service M 3003, "The Expression of Uncertainty and Confidence in Measurement", December 1997

[4] ANSI/SCSL Z540-2-1997, "U.S. Guide to the Expression of Uncertainty in Measurement", October 1997

[5] ISO 9001:2000, "Quality management systems – Requirements"

[6] ISO/IEC 17025:1999, "General requirements for the competence of testing and calibration laboratories"

[7] Kohler, J.L., Gradin, L.P., "Test laboratory position for expression of uncertainty and confidence in measurement", Electromagnetic Compatibility,

- 2003 IEEE International Symposium on , Volume: 1 , 18-22 Aug. 2003,  
Pages:292 - 297 vol.1
- [8] NAMAS NIS 81, “The Treatment of Uncertainty in EMC Measurements”,  
Edition 1, May 1994
- [9] United Kingdom Accreditation Service LAB 34, “The Expression of  
Uncertainty in EMC Testing”, Edition 1, August 2002
- [10] EN 55022 : 1998, “Limits and methods of measurement of radio  
disturbance characteristics of information technology equipment”
- [11] Adams, Thomas, “A2LA Guide for the Estimation of Measurement  
Uncertainty in Testing”, July 2002
- [12] CISPR 16-1: 1993-08, “Specification for radio disturbance and immunity  
measuring apparatus and methods – Part 1: Radio disturbance and immunity  
measuring apparatus”
- [13] ANSI C63.2-1987, “American National Standard for Instrumentation—  
Electromagnetic Noise and Field Strength, 10kHz to 40GHz—Specifications”



- [14] CISPR 22 : 1997, "Limits and methods of measurement of radio disturbance characteristics of information technology equipment"
- [15] ANSI C63.4-2003, "American National Standard for Methods of Measurement of Radio-Noise Emissions from Low-Voltage Electrical and Electronic Equipment in the Range of 9 kHz to 40 GHz"
- [16] AS/NZS 3548 : 1995, Australian/New Zealand Standard, "Limits and methods of measurement of radio disturbance characteristics of information technology equipment"
- [17] AS/NZS CISPR 22 : 2002, Australian/New Zealand Standard, "Limits and methods of measurement of radio disturbance characteristics of information technology equipment"
- [18] CNS 13438, Chinese National Standard, "Limits and methods of measurement of radio disturbance characteristics of information technology equipment"
- [19] Voluntary Control Council for Interference by Information Technology Equipment (VCCI), "Agreement of Voluntary Control Council for Interference by Information Technology Equipment", April, 2002.

- [20] ANSI C63.4-1992, "American National Standard for Methods of Measurement of Radio-Noise Emissions from Low-Voltage Electrical and Electronic Equipment in the Range of 9 kHz to 40 GHz"
- [21] "Panel Components - Guide to Worldwide Plug/Socket Patterns & Power Mains", <http://www.interpower.com/ic/guide.htm>
- [22] Dimensions of NEMA 5-15 and CEE 7/7 plugs and outlets derived from manufacturers datasheets found at <http://www.internationalconfig.com/Default.asp>; part numbers 5266-X, 8284-I, 70124, 70140.
- [23] Paul, C.R., Introduction to Electromagnetic Compatibility, Wiley Interscience, New York, 1992.
- [24] "Agilent 41800A Active Probe Technical Overview", <http://www.home.agilent.com/USeng/nav/-536895485.536879591/pd.html>
- [25] "Long-cable effects on conducted emissions levels", Pignari, S.A. Orlandi, A. ,Dipt. di Elettrotecnica, Politecnico di Milano, Italy; IEEE Transactions on Electromagnetic Compatibility, Publication Date: Feb 2003, On page(s): 43- 54

[26] “Undesired uncertainty in conducted full-compliance measurements: a proposal for verification of conformity of LISN parameters according to the requirements of CISPR16-1”, Tomasin, P. Zuccato, A. Florean, D., CREI Ven, Res. Consortium on Ind. Electron., Padova; 2001 IEEE International Symposium on Electromagnetic Compatibility, 2001. EMC, Meeting Date: 08/13/2001 -08/17/2001, Publication Date: 2001, Location: Montreal, Que. , Canada, On page(s): 7-12 vol.1

[27] “A method to calculate uncertainty of LISN conducted measurements”, Heise, E.R. Heise, R.E.W., Eastman Kodak Co., Rochester, NY; IEEE International Symposium on Electromagnetic Compatibility, 1998. 1998, Meeting Date: 08/24/1998 -08/28/1998, Publication Date: 24-28 Aug 1998, Location: Denver, CO , USA, On page(s): 253-258

[28] CISPR 16-2 : 2003: Specification for radio disturbance and immunity measuring apparatus and methods - Part 2: Methods of measurement of disturbances and immunity

## **VITA**

Name: Robert A. Menke

Date of Birth: 8/29/1976

Place of Birth: Springfield Ohio, USA

### Education:

The Ohio State University (Columbus Ohio), Bachelor of Science in  
Electrical Engineering, June 1999

### Professional Positions Held:

Hardware Engineer, Electromagnetic Compatibility, Lexmark International  
(Lexington Kentucky), July 1999 – January 2004

Signal Integrity Engineer, Controller Hardware Design, Lexmark  
International (Lexington Kentucky), February 2004 – July 2005

Electrical Engineer, New Product Development, Midmark Corporation  
(Versailles Ohio), August 2005 – present

Scholastic & Professions Honors:

Institute of Electrical & Electronics Engineers (IEEE), member since 1999

Member of IEEE Electromagnetic Compatibility and Microwave Theory &  
Techniques Societies

Prior Publications:

“Methods for Identifying Causes of EMI Emissions from Switched Mode  
Power Applications,” 2001 IEEE EMC Symposium

“High Frequency Spread Spectrum Clock Generation,” U.S. Patent  
Application, March 2003

“Modulated Clock Generator with Integrated MEMS Components,” U.S.  
Patent Application, December 2004

“Laboratory Measurement of Voltage Drop at an Integrated Circuit Core  
Due to Package Inductance,” 2005 IEEE EMC Symposium

Signed: Robert A. Menke

Date: November 29<sup>th</sup>, 2005